Cooling ions and molecules and thermodynamical equilibria in a 22-pole trap

Dissertation

zur Erlangung des akademischen Grades

doctor rerum naturalium

(Dr. rer. nat.)

vorgelegt
der Fakultät für Naturwissenschaften der Technischen Universität Chemnitz

von: Dipl. Phys. César Mogo

geboren am: 31.01.1976 in Faro, Portugal

Chemnitz,

To my supporting family, Maria do Carmo Cabrita Neves, Joaquim Gregório Cabrita Mogo, and specially to my dearest aunt Felizmina da Conceição Cabrita

Bilbliographische Beschreibung

Cooling ions and molecules and thermodynamical equilibria in a 22-pole trap

Dissertation an der Fakultät für Naturwissenschaften der Technischen Universität Chemnitz, Institut für Physik, von César Mogo

Chemnitz, 03.12.2010
102 Seiten
in Englischer Sprache mit 77 Zitaten, 3 Tabellen und 43 Abbildungen

Referat

Basierend auf Messungen in einer temperaturvariablen 22-Polspeicherapparatur werden im Folgenden zwei Gasphasen Ionen-Molekül-Reaktionssysteme vorgestellt. Im ersten Reaktionssystem wird mithilfe einer neuen Vorgehensweise zur Messung der Gleichgewichtskonstante der Reaktion $HCO_2^+ + CH_4 \rightleftarrows CH_5^+ + CO_2$ die Protonenaffinität von Methan bestimmt. Das zweite behandelt das $(Ar + N_2)^+$ Reaktionssystem, wobei die Temperaturabhängigkeit des Reaktionsratenkoeffizienten für sowohl die Hin- als auch die Rückreaktion mittels unterschiedlicher, sich ergänzender Methoden ermittelt wird. Diese Arbeit wurde ermöglicht durch eine sehr vielseitige Apparatur, die auf der HF-Ionenspeichertechnik basiert. Durch Hinzufügen eines Effusivstrahls zu dem Aufbau wird das Problem der Kondensation von Neutralgas an den Wänden umgangen und dadurch die Erweiterung des zugänglichen Temperaturbereichs bis unterhalb dessen Gefrierpunkts möglich. Die Einleitung (Kapitel 1) gibt einen kurzen überblick über die HF-Technik und andere verbreitete experimentelle Technologien. Es werden außerdem einige Aspekte der Bestimmung der Temperaturabhängigkeit der Reaktionsraten ebenso behandelt wie das thermodynamische Gleichgewicht im Laborkontext. Im Kapitel 2 werden der Apparaturaufbau und die verwendeten experimentellen Methoden dargestellt. Basierend

auf den Messungen der Gleichgewichtskonstanten, widmet sich Kapitel 3 der Protonenaffinität von Methan. Dieses Konzept hat Anwendungen in unterschiedlichen Gebieten, wie z.B. der Modellierung der Atmosphäre oder von Verbrennungprozessen sowie das Überprüfen von empirischen und *ab initio* Theorien der elektronischen Strukturen. Das in Kapitel 4 vorgestellte $(Ar - N_2)^+$ System ist ein gutes Beispiel für die Untersuchung der Rolle der Vibrationsanregung und das Vorhandensein von nicht-adiabatischer Kopplung in der Reaktionsdynamik. Die experimentellen Ergebnisse für die N_2^+ + Ar Reaktion zeigen, dass es möglich ist, den Ratenkoeffizienten ohne Beeinflussung durch vibrationsangeregten Stickstoff (N_2 ($\nu > 0$)) zu messen. Die Messungen der Rückreaktion bestätigen die Existenz eines Minimums der Reaktionsrate im Temperaturbereich von 30 bis 300 K, aufgrund des Vorhandenseins zweier Reaktionskanäle. Im Kapitel 5 erfolgt eine Zusammenfassung und ein Ausblick, wobei einige neue mögliche Wege für zukünftige Untersuchungen dargelegt werden.

Schlageworte

Ionen-Molekül-Reaktionen, HF-Multipol-Ionenfalle, thermodynamisches Gleichgewicht, Gleichgewichtskonstante, Protonenaffinität, Reaktionsenthalpie und -entropie, molekularer Schwingungszustand, HCO_2^+, CH_5^+, Ar^+, N_2^+.

Abstract

Two gas-phase ion-molecule reaction systems are presented here based on measurements done in a temperature variable 22-pole trapping machine. In the first case, the proton affinity of methane is determined based on a new technique for measuring the equilibrium constant of the $HCO_2^+ + CH_4 \rightleftarrows CH_5^+ + CO_2$ reaction. The second case reports to the $(Ar + N_2)^+$ reaction system, with reaction rate temperature dependencies measurements made both in the forward and reverse direction with different and complementary methods. The temperature variable 22-pole trapping machine allows one to determine equilibrium constants and reaction rate coefficients over a wide range of temperatures. The coupling of an effusive beam to the setup overcomes the problem of neutral gas wall condensation and extends the temperature range measurements beyond condensation point. The introduction (Chapter 1) gives a short overview about the rf technology and parallel experimental techniques developed in order to better characterize and understand the several mechanisms related to ion-molecule reactions. It also focuses some aspects of reaction rate temperature dependencies determination as well as thermodynamical equilibrium in laboratory environment. A short description of the setup and experimental methods are presented in Chapter 2. Based on equilibrium constant measurements, Chapter 3 is dedicated to the proton affinity of methane. This concept has applications on several fields such as atmospheric and combustion modeling, or testing empirical and *ab initio* theories for electronic structures. The $(Ar - N_2)^+$ system presented in Chapter 4, is known for being a good case study for inferring the role of vibrational excitation in reaction dynamics and to the existence of non-adiabatic coupling. The experimental results here presented for the $N_2^+ + Ar$ reaction demonstrate that it is possible to avoid parallel reactions with first vibrational excited state of nitrogen ($N_2(\nu = 1)$). On the other hand, the reverse reaction experiments confirm the existence of a minimum of the reaction rate in the 30 to 300 K range, due to the existence of two reaction channels. The question of the high rate coefficient towards lower temperatures being related to the N_2 rotational ground state population is raised. A summary and outlook are presented in Chapter 5, where some new possible paths of investigation are pointed out.

Key words

Ion-atom reactions, rf-multipole ion trap, thermodynamic equilibrium, equilibrium constant, proton affinity, reaction enthalpy and entropy, molecular vibrational states, HCO_2^+, CH_5^+, Ar^+, N_2^+.

Contents

Chapter 1

INTRODUCTION

1.1 The importance of ion-molecule reactions

Since they were discovered in the ionizers of mass spectrometers, approximately 100 years ago [tho11], gas-phase ion-molecule reactions have gained more and more importance.

Many of these reactions have no barriers, emerging as a preferred process if compared with a three-body or neutral-neutral system, in conditions where low densities and low temperatures prevail.

In earth atmosphere, absorption of light can produce O_2^+, N_2^+, O^+, N^+ and He^+, which then undergo various reactions. These chain reactions are of special significance in aerosol particle formation [apl00].

Ion-molecule reactions have also been the basis of the models developed in order to describe the behavior of interstellar molecular clouds, were ions are formed due to photo-ionization or cosmic ray ionization.

Other field where ion-chemistry plays a relevant part is in development of the early universe composition. As an example: although there are other possible mechanisms, the associative detachment reaction $H^- + H \rightarrow H_2 + e^-$ is a strong candidate through which the formation of H_2 in the Universe can be explained. Nevertheless, existing uncertainties with published values for the formation rate of H_2 varying within one order of magnitude is still an open question [glo06a, glo06b].

These kind of reactions have also technological applications, such as in temperature diagnostics in argon plasmas or cold environments [sch99, lin04, ger08b]. They are also an excellent base for testing fundamental research theories, as the numberless publications in *ab initio* calculations can testify for.

1.2 The contribution of 22-pole trap technology

One important question to be answered, is how to measure such reactions, with astrophysical interest, while closely simulating the conditions found in interstellar clouds [ger92c]. This led to a need for low temperature and pressure experiments, where complexes with very long lifetimes could be formed, and stabilization via ternary collisions could be neglected as a competing process to the radiative association. Differentiating between these processes means to cover a wide density range.

Flow afterglow (FA) [nor66] and selected ion flow tube (SIFT) [ada76] techniques are limited to their high pressure regime. Other limitation is the condensation of the neutral species at low temperatures. The development of techniques such as CRESU (Cinétique de Réaction en Ecoulement Supersonique Uniforme [row87]) or the free jet reactor [smi94, smi98] overcame this problem. But here, the minimum reaction rate is limited by the drift or flight time.

With trapping methods, ions can be retained for reaction for a much longer time, where ion cyclotron resonance (ICR) [mce89, dun90, mar98], and the Penning trap [bar84, lui85, bar86] play a relevant role. Still this last method is not sensitive enough to measure rate coefficients for extremely slow processes, due to uncertainties in the determination of the energy state of the neutral target gas. Although rf quadrupole ion traps can be used for measuring ion-neutral reactions [ved91], they still face problems in measuring low-energy association processes, mainly due to rf heating, which is the coupling of the rf motion into the random motion of the stored ions [blu89].

One solution is to use higher order field geometries, such as in the case of the 22-pole trap (22PT). Fundamental principles of ion confinement in inhomogeneous radio frequency fields were thoroughly discussed in recent years [ger92, ger95, ger08a]. Nowadays, the number and applications of 22PT have been consistently broadened such as: study of reaction dynamics while integrated with a beam of hydrogen atoms [bor09], laser induced reactions [sch05], as an ion source for preparing cold ions for the electrostatic storage ring in Aarhus or to cool H_3^+ ions for measuring state specific rate coefficients for dissociative recombination, at the ion storage ring TSR in Heidelberg [kre05]. In development stage is the next generation unit in the University of Tucson, where one of the main features is a expected broadened temperature range (10-1000 K).

1.3 Temperature determination

1.3.1 Temperature definition

The temperature T of an ideal gas is related to the average kinetic energy of the atoms $\overline{E}_k$ in the system by $\overline{E}_k = \frac{3}{2}k_B T$ (k_B - the Boltzmann constant), and were the distribution of energies of the particles are given by the Maxwell-Boltzmann distribution. The definition of the Kelvin temperature scale has already been defined*: the unit 1 Kelvin is based on the triple point of water leading to a uncertainty of k_B of 1.8 parts in 10^6 †. It is interesting to note that this definition is not a closed subject. It is expected in the next years for the Boltzmann constant k_B to be fixed, and temperature scale will be defined through the energy $k_B T$ [fell06]. Nevertheless, such precision is beyond the scope of this work, and the present definition is perfectly suitable for our purposes.

1.3.2 Temperature under the influence of rf fields

Depending on the system, at a molecular or atomic scale, energy may be referred, rather than temperature. Energy has different contributions, such as in the form of electronic, vibrational, rotational, or translational components. In the specific case of trapped particles, the boundary conditions imply a quantization of the translational degrees of freedom.

One example where the direct definition of temperature fails is in the laser cooling of ions into an ordered Coulomb crystal [rot06]. Such a structure is characteristic of a temperature in the sub-mK range, but the kinetic energies associated with the fast coherent motion due to the trap rf fields, where the ions are confined, are up to 7 orders of magnitude higher [sch00]. The low temperature is in accordance with the observation of the phase transition, and the Doppler width, as long as the laser is set perpendicular to the secular motion. But in the case of a collision between this ensemble of ions and a cold neutral target, the mean translational energy will correspond to a high temperature value, with the mean translational energy able to correspond to thousands of K [ger08a]. This problems are of special importance since at low collision energies, a collision complex tends to use the energy from all available degrees of freedom.

1.3.3 Temperature in a 22PT

One needs to know the reaction temperature when dealing with ion chemistry measurements. In the more specific case of rf traps the problem focuses on knowing the ions real temperatures and efficiently cooling them down. The same

Comité International des Poids et Mesures, 94th meeting (October 2005), p 235

†Recommended by the Committee on Data for Science and Technology (CODATA) [moh05].

applies to the target gas. Therefore, there is the need for development of proper methods for cooling and temperature measurement.

Thermalization and cooling of ions

In many experimental setups, cooling of ions is based on thermalization via buffer gas. Still, long storage times or many collisions may lead to equilibrium conditions, but not necessarily to the same temperature as the one from the buffer gas, or even to the one related to the black-body radiation field penetrating the ion cloud. Paul-traps are known for what is denominated as rf heating: ion-neutral collisions leading to a transfer of energy from the radio-frequency field to the ions. Here, the ion mean energy will tend to be higher when comparing with the neutral gas. This fact can be tested using reactions with suitable endothermicities. Also to take into to consideration, is the possibility of ions acquiring undesired micromotion (i.e. driven from the rf field), with several adverse effects (e.g. alterations of atomic transition line shapes, or limited confinement time in the absence of adequate cooling [ber98]).

Fortunately, this heating process can be almost neglected if experiments are carried on in traps with a wide field free region (such as ring electrodes [bah69] or 22-pole geometry), as shown by numerical simulations [pau94]. Collision between ions and buffer gas will happen mostly within the field-free region, as long as the ions are restrained by a wide, flat potential, with very steep repulsive walls.

In the case of larger molecules, there is an increase of the number of degrees of freedom to take in to consideration. This leads to an increased difficulty in cooling all these degrees down [row08]. This is the case of cooling down large biological molecules to a few K or below. Cooling of such ions is of large interest for studies of radiation damage of bio-molecules. It has relevance not only to structure and dynamics, related to the function of proteins, but also to the possibility to study effects of conformation changes as functions of temperature and (small) numbers of solvent ions.

It is expected, in an ideal situation, that trapped ions and buffer gas reach thermal equilibrium at a common temperature T, determined by the surrounding walls. In reality, translational temperature of the trapped ions and buffer gas tend to disagree. Nevertheless, if one approximates both ensembles by maxwellian functions with respective temperatures T_1 and T_2, then the collision temperature T is related to the mass weighted average of T_1 and T_2 by:

$$T = (m_1 T_2 + m_2 T_1)/(m_1 + m_2). \tag{1.1}$$

By allowing both ions and buffer gas molecules sufficient time to collide, it will be the collision temperature T to determine the internal temperatures of the stored ions, and not its initial translational temperature T_1. As a consequence, it is possible to efficiently cool down internal degrees of ions although

they are translationally hot, providing that the mass of the buffer gas is chosen to be smaller than the ions, and time is given for sufficient collisions to happen. Among other examples, is the work presented by Wang et al. where C_{60}^+ ions were cooled down to $T = 15.5\,K$ [wan05b]. The cooling efficiency through the use of buffer gas, and in comparison with other methods, such as laser cooling, has been recently and thoroughly discussed ([ger08b] and references therein).

Different ways to obtain a cold target gas

There are several options concerning the cooling of a neutral target gas. The first we make reference to is based on thermalization through collisions with surrounding walls. If in addition, one can make use of a cooling system such as cryogenic cooling, temperature dependent rates studies can be performed. As an example, such a setup was used to study a variety of ion-molecule reactions of interstellar interest, namely the chain of H-atom abstraction reactions, starting with the ion-molecule reaction $N^+ + H_2 \rightarrow NH^+ + H$ and ending with $NH_3^+ + H_2 \rightarrow NH_4^+ + H$, along with its deuterated analogue. Coefficients have been determined at temperatures between 15 and 300 K [ger93]. Other study was presented, were reactions of methane cations CH_4^+ with H_2, HD and D_2 (15 to 300 K temperature range) were measured [asv04a].

Other approach is to take advantage of trap's high sensitivity, in such way that at lower temperatures, the resulting vapour pressure is sufficiently high in order to allow measurements to be made [ger08a].

It is also possible to measure reaction rates based on atomic beam [bor08]. Results become different if the target gas beam is used instead of leaking the gas directly into the trap. In contrast to the homogeneous density in the trap, the beam diameter is smaller than the diameter of the ion cloud. In this case one has to characterize the flux and shape of the neutral beam or one uses a known chemical reaction for calibration purposes [luc05, bor09]. An interesting question is to know to what point all these methods and techniques applied to a 22PT apparatus agree with each other, when used on a single system. Section 4.3.2 will address this issue.

How to measure ions temperature

Several methods can be used or are under development in order to characterize the temperature of stored ions. One option is based on known temperature dependencies of collision processes such as weakly endothermic reactions or radiative association. This is the case of the direct use of a standard buffer gas helium in the reaction: $He^+ + 2He \rightarrow He_2^+ + He$ [ger92]. Measurements were made on a selected ion drift tube, ranging from 30 to 300 K [boh83], down to 10 K in a 22PT ([He] $\approx 10^{14}\,cm^{-3}$) [ger08a]. The temperature dependence for ternary association reaction rate was fitted with the function: $k_3 = 1.4 \times$

$10^{-31}(300\,K/T)^{0.6}\,cm^6\,s^{-1}$. This can be the base for temperature calibration above 10 K. Below this value, caution has to be taken due to interference of several effects: separation of ion temperature, density of the neutrals and the temperature dependence of the ternary association reaction. Also possible, is chemical probing with H_2. The reaction $C_2H_2^+ + H_2 \rightarrow C_2H_3^+ + H$ strongly depends on the ion temperature [ger94a].

Several other processes have been proposed, like following the production of $He - N_2^+$, a well-studied, weakly bound (12.5 meV) van der Waals molecule [pau94]. In this case it is possible by laser induced fragmentation of the van der Waals bond, to determine rotational temperatures. Other proposal is the combination of sub-K trapping with the GHz and THz techniques. Cold molecular ions such as CO^+, deuterated variants of H_3^+, or CH_5^+ are ideal test cases due to their rotational transitions [ger09a]. Suitable reactions or absorption spectroscopy could be used in their study.

Translational temperature of the ion cloud can also be determined, based on in situ determination of translational distributions (Doppler profile), once the spectral resolution is high enough [sch99]. Due to a slightly endothermic (179 meV) laser induced charge transfer $N_2^+ + Ar \rightarrow Ar^+ + N_2$, photoabsorption can be detected [pau93]. As ideal candidate, N_2^+ can be used because it can be excited with cheap but narrow bandwidth laser-diodes. Accomplished with success, this process consists in filling the ion trap with some Ar target gas. Unfortunately, condensation has been limiting the temperature range to stay above 35 K. For lower temperatures, the machine has to be integrated with skimmed Ar beam. In this context, Chapter 4 is dedicated to the study of the $(Ar\text{-}N_2)^+$ system. Measurements were made, based on several methods, including the use of an effusive beam for the reverse reaction: $Ar^+ + N_2 \rightarrow N_2^+ + Ar$.

1.4 Thermodynamical equilibrium

Thermodynamical equilibrium (TDE) is said to be achieved when a system is in mechanical, thermal and chemical equilibrium. Mechanical equilibrium is reached when the sum of all external forces is zero, and the sum of the moments of all external forces about any line is zero. Thermal equilibrium is achieved when there is no energy exchange between two systems in thermal contact with each other. In chemical process, equilibrium refers to the state where both reactants and products are present but have no further tendency to undergo net change. According to the kinetic gas theory, and neglecting quantum effects or non-relativistic speeds, all degrees of freedom of an ideal gas close or in a thermodynamic equilibrium can be described by Maxwell-Boltzmann distributions.

This outcome allows a single value of an intensive parameters such as temperature and pressure to be attributed to the whole system. Very important is the fact that TDE is characterized by a minimum in thermodynamic potential

such as, in the case of a system at constant pressure and temperature, the Gibbs free energy (G):

$$G = H - TS,$$

(where T is temperature, S entropy, and H is enthalpy of the system) [atk02]. This fact allows the determination of a reaction enthalpy and entropy as it will be shown in Chapter 3.

The process leading to a TDE is referred as thermalization, such as a system of interacting particles that is left unperturbed by exterior influences. They will interact and share among themselves the available energy and reach a state where the statistical distributions are constant in time. By describing a gas through a Maxwellian velocity distribution, this indicates that there was a sufficiently high number of elastic collisions, so that this equilibrium could be established.

1.4.1 TDE in interstellar medium

Since one the applications of the 22PT is in interstellar chemistry, one can ask if such suppositions, for the existence of TDE, can be applied in astrophysical conditions.

If radiation is emitted from a source in conditions of thermodynamic equilibrium, then temperature can be derived from spectral observations. When attributing a *temperature* to a certain location in space, this *temperature* is actually the one corresponding to the observed Maxwell-Boltzmann distribution, but corresponds to the assumption that the observed system is in TDE.

Problems arise if one wants to look at molecular composition, ionization, and excitation states of the gas [flo07]. The excitation, ionization, and molecular composition are often very different from TDE values at this temperature. This is mainly a consequence derived from the low pressures existing in interstellar medium (ISM). In reality, the observed interstellar radiation field is normally below the value which would be expected if in TDE. The expected thermalizing collisions between particles are not in sufficient number to compete with the faster radiative decay rates at atomic and molecular levels. Besides other factors, a constant presence of $\approx$ 100 MeV cosmic-ray particles keeps the ionization and chemical composition away from their expected equilibrium values [tie05].

One example, is the fact that in thermodynamic equilibrium the several energetic states should be described according to Boltzmann distributions. Nevertheless, is known that, ortho- and para-H_2 states population is not changed under such conditions [tro09].

A second example is the conversion of hydrogen and carbon monoxide into methane and water, as Klemperer [kle06] illustrates. Approximately 500 orders of magnitude differs between what is observed in ISM and the expected equilibrium ratio for $CO + 3H_2 \Leftrightarrow CH_4 + H_2O$ predicted by thermodynamics. These facts

leads, in certain circumstances, to relegate thermally averaged rate coefficients to a second plan, in favour of cold state specific cross sections studies.

1.4.2 Experimental determination of TDE

Although, the importance of TDE in interstellar medium is relatively small, as aforementioned, it is of high importance in other fields of research. Bond energies such as proton affinities can be derived from thermodynamic equilibrium measurements. They have an important role in describing chemical reactions, with applications ranging from synthetic to material chemistry, from atmospheric to combustion modelling or good tests for empirical and *ab initio* theories of electronic structure [ber94]. Several were the different laboratory approaches (e.g. FA or SIFT) and methodologies (direct or indirect measurement) with published work dedicated to this topic ([hun98] and references therein).

As already discussed, the assumptions to achieve ideal TDE are well defined. By transposing such conditions to a experimental point of view, it was argued by Paul and Gerlich that, if the attenuation rate for both primary ions and products becomes time independent, than one can assume that equilibrium conditions have been attained [pau94]. Chapter 3 will be dedicated to this issue, based on measurements and comparison with theoretical and experimental results obtained by other groups. The fact that temperatures can be easily varied, will allow us to obtain information about the enthalpy and entropy based on the equilibrium constant $K(T)$. Results indicate that relative TDE is achieved in a 22PT. Neutral gases pressures are maintained constant, a ratio between the ions is time independent, and if rf heating effects are minimized, ions and target gas are thermalized to the temperature of the surrounding walls via buffer gas collisions.

Chapter 2

EXPERIMENTAL

2.1 General concepts

The development of ion trap setups for studying ion-atom or ion-molecule reactions began in the 50's . The Paul trap [pau53], the Ion Cyclotron Resonance Cell (ICR) [mar98] or the Penning Ion Trap [lui85] are examples of this development. In the late 80's, Gerlich and colleagues presented a combination of an ion source, a mass filter, an rf ion trap, a quadrupole mass spectrometer, and an ion detector [ger92c, ger95].

This present work of is based on an highly versatile apparatus, having as a center unit a 22-pole trap (22PT). Measurements were made by coupling a N_2 Cold Effusive Beam (CEB)*. In its whole, this setup has been denominated CEB-22PT. Since rf-trap based apparatus have already been described in the literature [ger95, asv04a, sav05b, ger08a, meh09], only a brief description of the several units and measuring procedures from our setup will be presented here.

The CEB-22PT is depicted as a schematic drawing in Fig. 2.1. Generally the functioning principles of this family of ion trapping machines can be described as follows: a set of ions is generated in the ion source and selected in a first quadrupole mass spectrometer (QPI). Using a quadrupole bender, the primary ions are guided into the 22PT where they are trapped. During trapping, translational and internal degrees of freedom are cooled down to the temperature of the trap walls via inelastic collisions with buffer gas (usually helium is used due to its high efficiency and low reactivity). The neutral gas which is to react with the ions (target gas), can be leaked into the trap through a direct gas inlet and in the present case, in the form of a Cold Effusive Beam. During a given storage time, the reactions between the produced ions and neutral gases take place. The remaining primary and the product ions are then extracted, mass analyzed in the second quadrupole spectrometer (QPII), detected, and finally counted.

* For an updated description of the CEB please refer to [meh09]

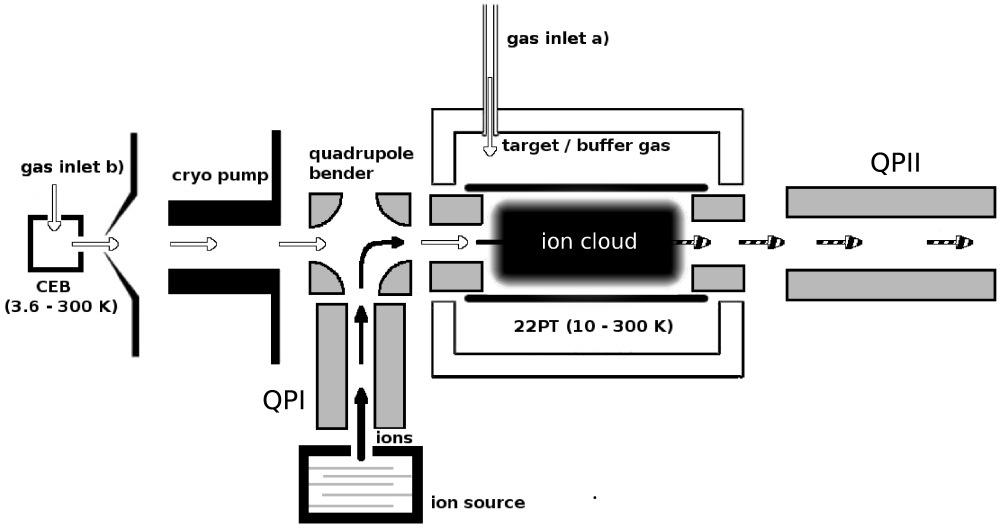

Fig. 2.1: Scheme of the CEB-22PT machine where the modules are: a source for ion production (lower part), a first quadrupole mass filter (QPI) for primary ion selection, a 22PT rf based ion trap where the ion-neutral gas reactions take place (center), followed by a second quadrupole (QPII). A Daly detector is used for analyzing the ions (not observed in the figure). The Cold Effusive Beam is located on the left side.

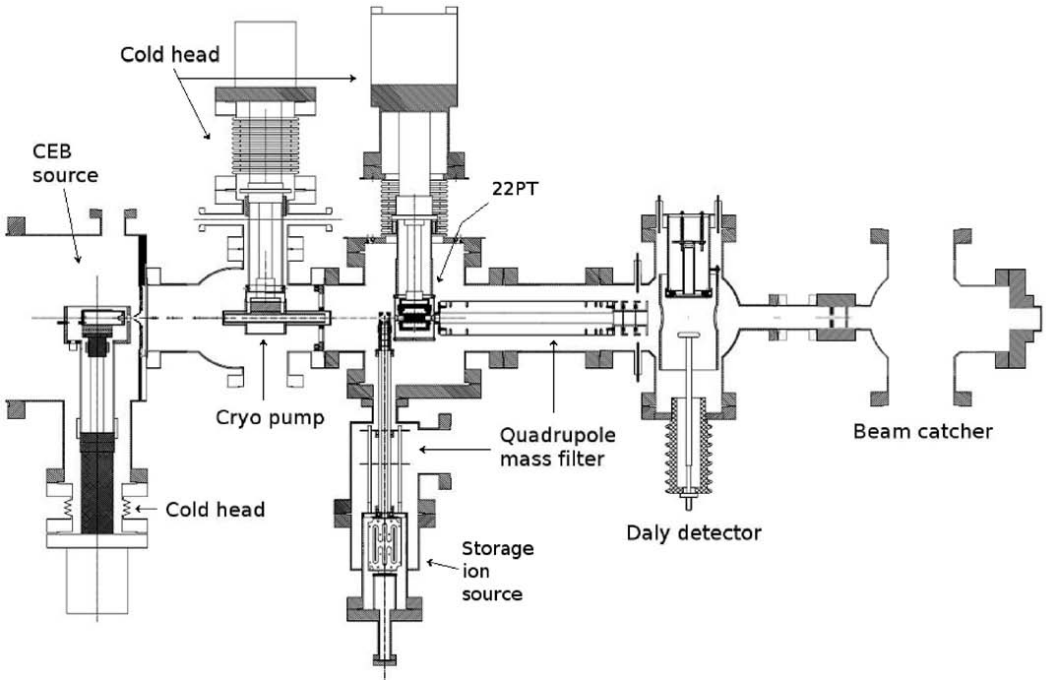

Fig. 2.2: Technical overview of the combination of CEB (left side) and a variable temperature 22PT (center).

In Fig. 2.2 a more detailed drawing of the CEB-22PT apparatus can be seen. A limitation to low temperature ion traps experiments can be condensation of the neutral species on the walls. One way to overcome this situation is the addition of the Cold Effusive Beam to the previous 22PT setup. This is due to the capability of creating a slow beam of neutrals and, of special interest, of condensable gases, allowing a more broadened range towards lower temperatures studies. A deeper description of the CEB is presented in Sec. 2.4.

2.2 Vacuum system

If one intends to study gas phase reactions it is of fundamental importance to have a good ultra high vacuum (UHV) system. Impurities or high pressure may lead to discharges or malfunctions in the equipment and most important, secondary reactions with background are to be avoided or at least minimized. Otherwise, reactions with air constituents like water, molecular nitrogen or oxygen normally make it impossible to correctly isolate and determine the characteristics of the reaction to be studied in the first place. Therefore leaks or gas desorption from walls must be avoided.

The vacuum chambers are based on standard UHV stainless steel chambers with ConFlat flanges and separated by differential walls. Please refer to Appendix B for a schematic drawing of the CEB-22PT vacuum system (Fig. B.1) and to nominal values of vacuum pumps used during our experiments (Tab. B.1). There are 6 main pumping lines. The CEB and the beam catcher chambers can be isolated from the central part of the machine through manual valves. Each of the vacuum lines is composed normally of three stages: a first stage of turbomolecular pumps (Pfeiffer TPU 2200 for the CEB chamber and magnetically suspended turbo pumps Leybold T340M for the remaining ones), and backed by: turbo-molecular pump Pfeiffer TPU 240 or drag pumps Pfeiffer TPD011, and finally as a last stage, a rotary pump Pfeiffer DUO016B, a Dry scroll SH-110 or a diaphragm pumps Pfeiffer MVP015. During the selection of the pumps, care was taken in order achieve sufficient compression for hydrogen and to avoid possible oil contamination. Several sensors (Balzers TPR-010 Pirani Gauge) were used in order control pressures in the pumping system.

Calibrated ion gauges (Huntington TK 150 and more recently SRS Nude-UHV Gauge with operating pressures ranging from 10^{-4} to 10^{-13} mbar) were used to monitor the pressures in the chambers. The settings of the ion gauges had, in our specific case, a sensitivity of 19 $mbar^{-1}$ and an emission current of 0.1 mA. The calibration was done with an absolute pressure spinning rotor gauge (MKS SRG2). Due to the working principles of the last one, where the decay of frequency of a magnetically suspended spinning sphere is measured due to friction with its surroundings, special care has to be taken in order to decouple unwanted vibrations, mainly originated in the vacuum pumping system.

At our laboratory, it was reached an accuracy of 5 %. The MKS SRG2 is advised to be used only for pressures above 10^{-7} mbar.

As observed in Fig. 2.3, the calibration procedure consists in plotting the absolute pressure values of the spinning rotor gauge (P_{XX}) vs. the one from the ion gauge *PIG* for a given gas at room temperature in a specific chamber, and fitting the data with the linear function $P = C\,PIG$ where C is the calibration factor. The linearity of both instruments provides a straight forward calibration and pressure values are obtained through extrapolation to the lower pressure regime suitable for our experimental purposes.

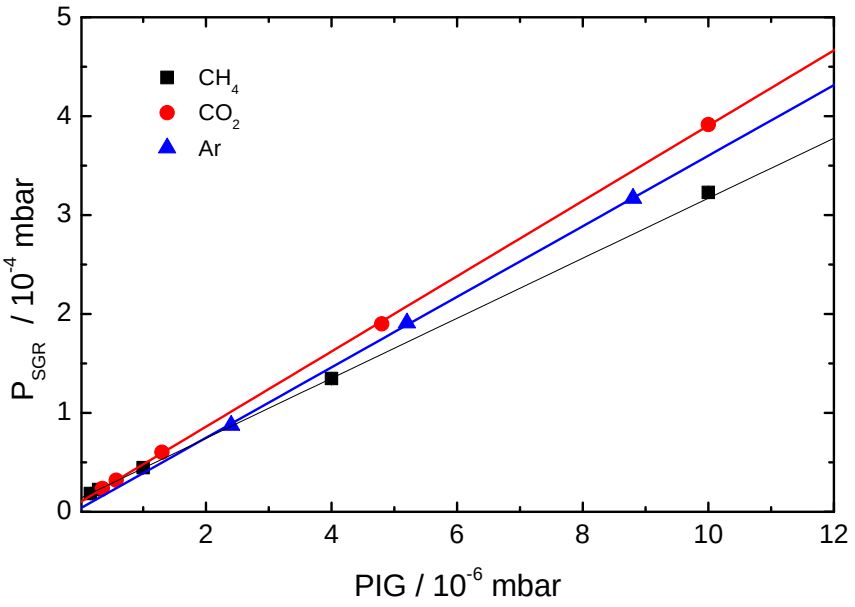

Fig. 2.3: Calibration of the 22PT ion gauge (SRS Nude-UHV) with the absolute pressure rotor gauge (MKS SRG2) for Ar, CH_4 and CO_2 gases corresponding to a calibration factor (C) of 36, 31 and 38, respectively. These relatively high factors are related to the fact that, in the case of the 22PT chamber, the MKS was connect directly to the interior of the trap using a flexible stainless steal tube, while the ion gauge is located outside, measuring the pressure on the chamber.

2.3 The 22-pole ion trap apparatus

2.3.1 Principles of rf technology

In a linear $2n$-pole, the potential Φ is given by:

$$\Phi(r,\phi) = \Phi_0 \hat{r}^n \cos(n\phi) \tag{2.1}$$

where $\Phi_0 = U_0 - V_0 \cos\Omega t$ is the applied dc and rf potential, $2n$ is the number of poles, and $\hat{r} = r/r_0$ is the reduced radius, where r_0 is the inner radius of

the multipole. In standard applications one operates a multipole “rf-only”, with $U_0 = 0$. By satisfying the condition that the angular frequency Ω is high enough, the resulting force can be described by the so called effective potential (V^*), and in the case of a multipole:

$$V^* = n^2/4(qV_0)^2/(m\Omega^2 r_0^2)\hat{r}^{2n-2}, \tag{2.2}$$

where m is the mass, and q is the charge of the particle. The r dependence of the effective potential for two electrode arrangements are compared in fig. 2.4.

It can be observed that the effective potential of the 22-pole, which is proportional to r^{20} is steeper than in the quadrupole. It results in a wider near field-free region while comparing to the harmonic effective potential of the rf quadrupole, minimizing the undesired rf heating effect.

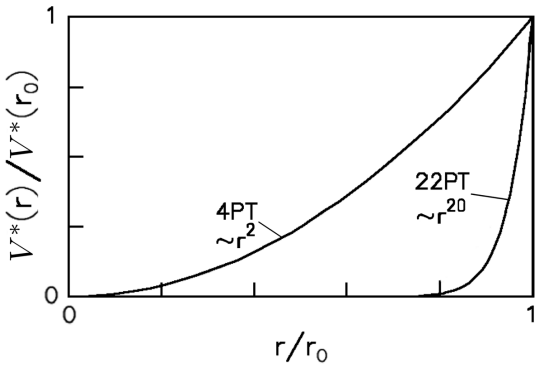

Fig. 2.4: Radial dependence of the normalized effective potentials of a 4 and 22 linear pole trap, with a large number of electrodes tending to a box potential [ger08a].

Due the fact that ions are restrained in the radial direction by V^*, ions become trapped if DC potentials are applied at the entrance and exit of the multipole, restraining their movements along the axis. By introducing quantified amounts of neutral gases in to the trap, reactions can be studied by following in time the primary and product ions concentrations.

2.3.2 The ion source

Primary ions are produced in the rf storage ion source (SIS) shown in Fig. 2.5, by means of electron bombardment of a precursor gas. The principles have already been well described [ger92].

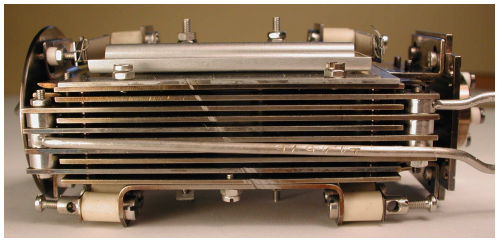

Fig. 2.5: Ion source.

The ion source is based on a symmetric geometry design, with two filaments (rhenium - 0.3 mm) for control purposes, with a high ion production efficiency geometry. The double-H-shaped storage volume is formed by a set of 8 molybdenum plates alternately connected to the two phases of an 4.98 MHz rf generator, while being confined in the outer bounds (end plates) by an applied DC voltage and an exit lens (B_0). The electron beam emitted by the filament goes through a slit in each plate and

crosses through the ionization region, interacting with the precursor gas. Pressure inside the SIS is relatively low, around 10^{-6} mbar. Furthermore, there is still the possibility for it to work in a continuous or pulsed mode by respectively setting a fixed or a pulsed DC voltage to the exit electrode.

This kind of ion source has several advantages such as high collection efficiency and controlled accumulation of ions. Furthermore, the SIS has distinct separation between the ionization and the exit regions. This allows thermalization by inelastic collisions (typically to the SIS temperature, 350 to 450 K) and chemi-ionization due to secondary reactions. This last property allows the production of ions which cannot be obtained directly by electron impact such as CH_5^+. Pressure and composition of the precursor gas along with rf and trapping potentials applied to the SIS allows a wide range of choices for the produced ions. The precursor gas pressure and mixture influences the kind of ions produced, while setting potentials, allows to a certain extent, to search for a narrower energy distribution, to control the degree of ionization or even have influence over the energy population distribution of the produced ions.

2.3.3 Operation of the quadrupoles

The description and use of quadrupoles, specially in the mass spectroscopy field, have been thoroughly and widely described in a large number of publications [daw76, mar89, ger92]. Therefore only a few remarks are made here.

In the CEB-22PT, two quadrupole mass filters are used. The first one (QPI), right after the storage ion source, filters out the primary ions. It is driven by a self-built 1.37 MHz rf power supply, with four rods 245 mm long and half-circle shape (d_{eff} = 10 mm), forming an inner circle of a radius r_0 = 4.35mm. A potential of the form $+[U_0 - V_0\, cos(\Omega t)]$ is applied to two opposite rods while the remaining two are connected to the negative of the same potential (U_0 is the DC-voltage, V_0 the amplitude of the rf voltage, $\Omega = 2\pi f$ is the angular frequency and t is the time).

Fig. 2.6: Quadrupole mass spectrometer used for the selection of the ions before detection (QPII).

The exact solution for the equation of motion of an ion moving in a quadrupole is found based on the well-know Mathieu differential equation [daw76]. By defining the stability parameters a_2 and q_2 as in Eq. 2.3 for a given particle charge q:

$$a_2 = \frac{8qU_0}{m\Omega^2 r_0^2}, \quad q_2 = \frac{4qV_0}{m\Omega^2 r_0^2} \tag{2.3}$$

it is possible to construct a stability diagram (Fig. 2.7), where several working conditions (unstable, mass selective and low-mass band-pass modes) are easily recognized.

In an operating condition, where the stability parameters a_2 and q_2 lead to a point of operation within the triangle area, the ions trajectories subjected to the quadrupole field are stable. Thus, the ions will pass through the quadrupole. Otherwise, standing outside the stability diagram, their oscillations become wider and broader. Ions will be lost due to collisions with the rods.

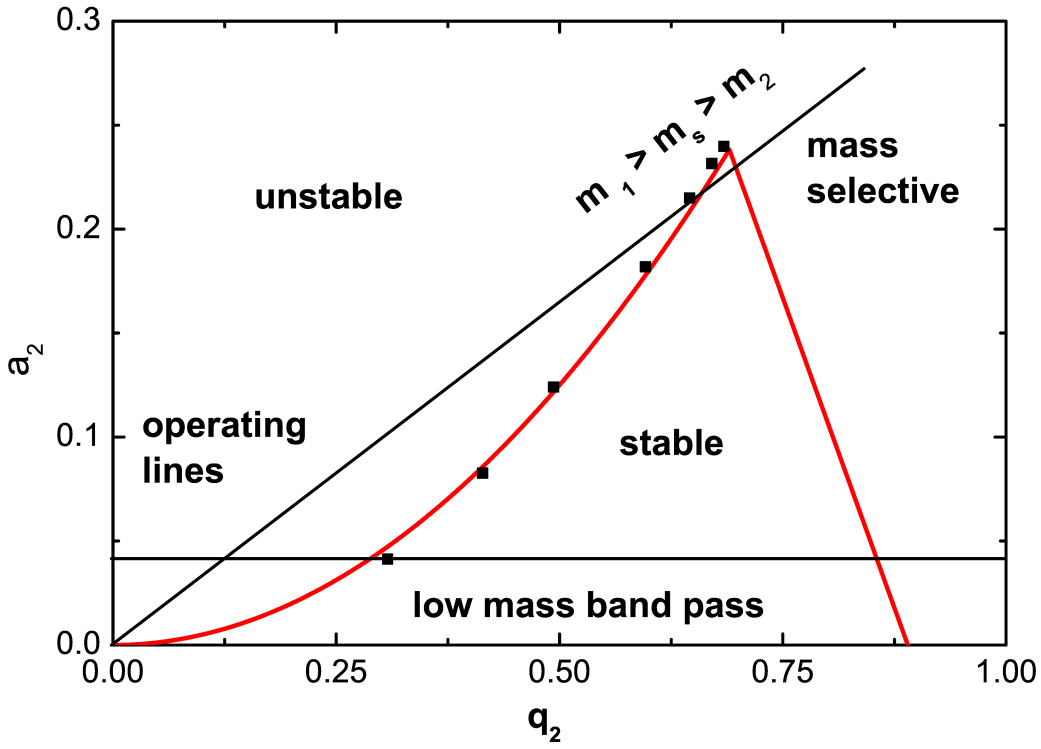

Fig. 2.7: Stability diagram (—) and experimental data for Ar^+ (■) taken for the first quadrupole (4 half-moon shape rods with effective diameter of 10 mm, r_0 = 4.35 mm, 245 mm long, at f = 1.37 MHz).

There are two modes of operation. On the one hand, mass selective mode, where $(a_2, q_2) \approx (0.237, 0.706)$, situated on the tip of the stability diagram leads to a high mass resolution. This mode of operation is well suited for mass analysis. On the other end, low-mass band pass mode, by setting $q_2 < 0.3$, gives rise to

an ion beam with a narrow energy distribution, because it operates in the region where the kinetic energy is an adiabatic constant of the motion. All the ions which are under a well defined mass number:

$$m < \frac{qV_0^2}{U_0\Omega^2 r_0^2}. \tag{2.4}$$

are able to move through the quadrupole.

As an example of the quadrupole working conditions, experimental points which correspond to a 80 % loss of the ion current in the first quadrupole output, can be seen in Fig. 2.7. Measurements were done by fixing one value for V_0 and therefore correspondent q_2, and by varying U_0 which is related to a_2, until a loss of 80 % would be observed in the output ion current of the quadrupole. Experimental results show a good agreement with the theory.

The second quadrupole (QPII) seen on Fig. 2.6 is located at the exit of the 22PT and works mainly in the mass-selective mode, thus used for a selection of specific ions before their detection. It is driven by a commercial 1.637 MHz rf power supply (BALZERS rf generator QMH510 and control unit QHS511), with 260 mm rods long, a full circle shape with a diameter of d = 18 mm and inner circle of radius r_0 = 7.84 mm.

2.3.4 The 22-pole trap

Trapping of ions in inhomogeneous rf fields is well established and thoroughly documented in the literature [ger92, ger94].

22 stainless steel rods of 1 mm diameter are parallel and mounted over a circle of 1 cm diameter (Fig. 2.8). These rods are alternatively connected to a rf two phases power supply restraining the movements of the ions in the radial direction. Electrostatic fields, given by a set of entrance and output lenses, confine the ions in the axial direction.

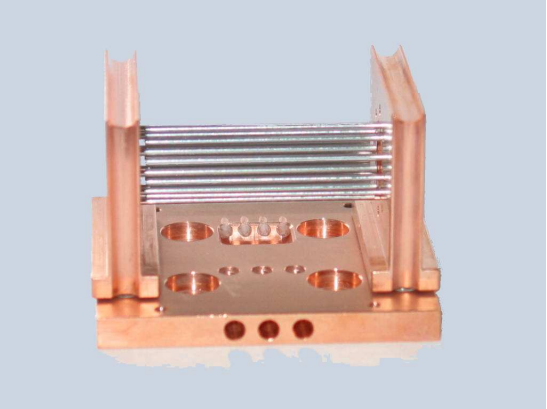

Fig. 2.8: Photograph of the 22PT without the cover. 22 stainless steel rods in a 1 cm circle radius disposition are shown. The surrounding walls are made in copper.

As an example, if one uses CO_2^+ ions, and according to the standard formulation [ger92], by applying an rf voltage with frequency f = 15.86 MHz and rf amplitude V_0 = 50 V, an effective potential (Eq. 2.2) of V^* = 0.668 eV is created with a correspondent stability parameter of $\eta(r = r_0) = 0.097$.

Stored ions are able to move within a region in radial direction. Considering a transverse energy of 10 meV, the turning radius becomes 0.8 r_0, meaning the ions are allowed to circulate over an 4 mm radius cylindrical area. The wide field nearly free region created by the arrangement of the 22-pole rods provides short interaction with the rf-wall. Ions move without any acceleration by the electrical field during a relatively long time, comparing with the time needed to collide against a neutral molecule.

Satisfying an adiabaticity condition [ger92], storing of singly charged ions with masses ranging from 17 to 45 at 300 K is possible without any significant losses in time scales of seconds. The praxis shows, that in similar trapping device two ions with masses different by factor of ≈ 60 can be trapped simultaneously [luc01].

The 22PT is surrounded by copper walls and mounted on a cold head of close-cycled helium refrigerator (Leybold RGD 210 with compressor RW2/3), so that its temperature can be varied between 10 and 300 K. From an experimental point of view, cautions have to be taken for the lower temperatures to avoid condensation of the neutral gases on the walls of the 22PT.

In order to study low temperature reactions, not only a cold environment of the 22PT is sufficient but an effective connection between trapped ions and cold walls is necessary. The rate of cooling has to be much faster than the rate of reactive collisions after ion injection. The translational and internal degrees of freedom of the ions are coupled to the cold environment by inelastic collisions, normally with helium. In some cases, reactant gases may also be used for cooling.

The buffer gas can be introduced into the trap in a continuous mode or in a synchronized pulsed mode. In the case of continuous mode, the buffer gas number density is limited by non-destructive ion extraction and their mass analysis. The pulsed mode is possible due to a piezo valve developed in our laboratories, with standard operation number density of 10^{13} cm^{-3}. This number density, a few orders of magnitude higher than those of the primary ions, allows a collision rate to be in the order of 10^4 collisions per second. Effective cooling of the ions is achieved in a few ms.

2.3.5 The Daly detector

As already described in Sec. 2.3.3, a quadrupole is located at the exit of the 22PT. By a standard procedure, ions are filtered and guided to the detection area, where a Daly-type detector [dal60] is used (Fig. 2.2 on the far right). Ions are focused and projected onto a perpendicular stainless steel converter (door knob) which is set to -30 kV. Due to the ions collision on to the surface of the door knob, secondary electrons are expelled and accelerated in opposite direction, against a grounded scintillator located on a 40 CF Quartz window. Thus, after colliding with the scintillator, electrons originate photons. After they pass

through a glass window, the photons are detected in the exterior at atmospheric pressure, being this one important aspect in this kind of detector. A photomultiplier, a Phillips Scientific 300 MHz discriminator and a 100 MHz counter conclude the detection unit.

In order to determine the detection efficiency, the Pulse High Distributions (PHD) was measured for CH_5 and HCO_2 (see Fig. 2.9 below). The final discrimination potential was then set to be 155 mV, allowing less then one count per second for the background. It is also possible to confirm that, with this settings, the detection efficiency for both ions is similar (approximately 90%).

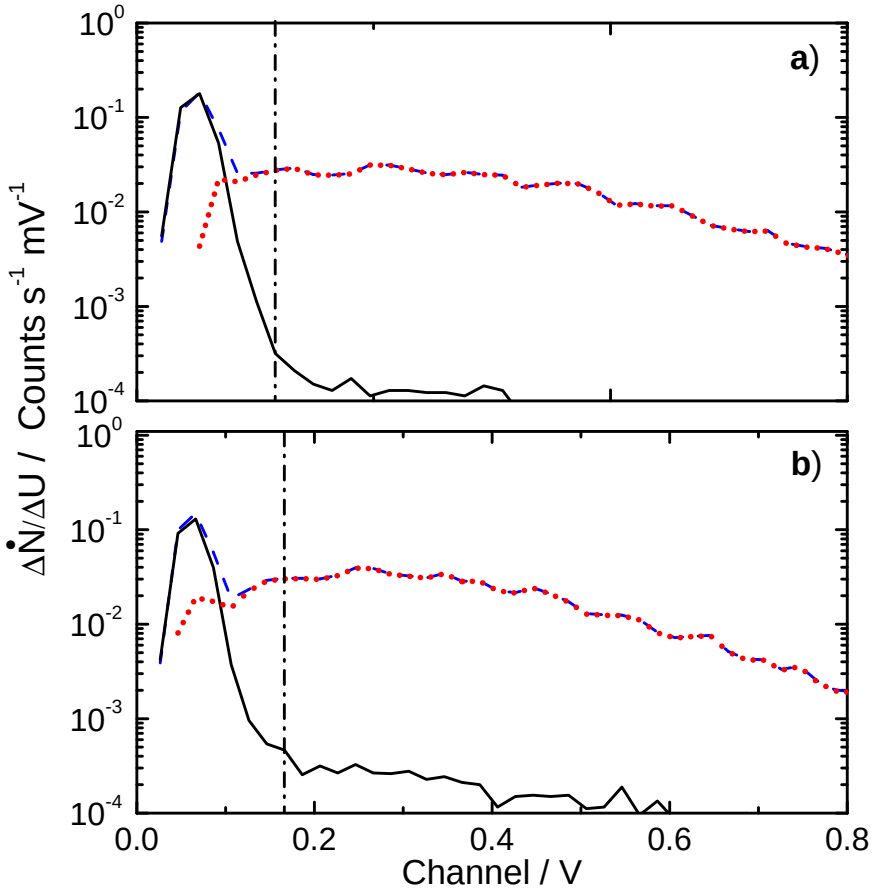

Fig. 2.9: Pulse high distributions for background and a) HCO_2^+ and b) CH_5^+. Background (—), ions plus background (– – –) and ions signal (· · ·). Voltage applied to the photomultiplier 2.2 kV, and channel width is 20 mV. For a 90% of the ion signal have a correspondent background signal of a) 0.9% at 146 mV for HCO_2^+ and b) 2% at 166 mV for CH_5^+ (– · –). After setting the threshold at 155 mV, it was obtained for the background less then one count per second.

2.3.6 Automation and data acquisition

Besides ion counting, ion gauge pressures from the several chambers (Huntington or SRS nude or glass tubulated gauges), gas inlet pressures (Swagelok PTU-F-AC3-32AH) or temperatures (K type thermocouples or Lakeshore DT-470 Silicon Diodes) among others, parameters had to be measured and registered. Furthermore, for measurements, control over experimental settings, such as frequency and lenses potentials, and mechanical shutters, all had to be done in parallel. While ion gauge signals were collected in control panels (Arun Microelectronics models PGC2 and NGC2), the remain of the other sensors were collected in a Keithley Model 7001. Communication with the controlling computer was done initially by RS232 connection, and more recently, through Ethernet connection. In order to automatize all this data acquisition, monitoring scripts were created based on the National Instruments Labview program.

2.3.7 Working conditions and advantages of the 22-pole ion trap technology

The 22-pole ion trap technology is characterized by: modular construction, therefore, very flexible in its applications; ion trapping temporal control over 10 s; large gas density range (10^8 to 10^{16} cm^{-3}); various methods for the target gas to be introduced into the trap (e.g. leaked from high pressure source, pulsed, or through molecular beams). The 22PT technique has a broad thermal window available (approximately between 1 and 40 meV, with expected broadening of the range in the next generations), and multiple detection choices available. The combination of a temperature-variable rf 22-pole ion trap with single ion counting detection has led to the extension of the range over which reaction rate coefficients can be examined. By choosing a suitable combination of target gas number density and trapping time, the rates of rather fast as well as very slow reactions can be measured [ger95]. Contrary to the FA and SIFT experiments, the rf ion trap allows radiative as well as ternary association rate coefficients to be measured under identical experimental conditions, simply allowing the target gas density to vary. Several experiments have showed that a variety of studies can be made, if the 22-pole trap technology is combined with other modules or tools.

2.3.8 Measuring procedure

In order to diminish statistical error, a measurement sequence is repeated, depending on several parameters, at frequencies between 0.1 and 100 Hz. It starts with ion extraction from the storage ion source, followed by their mass selection in a first quadrupole, deflection by 90° in a quadrupole bender static field and injection into the 22PT. By closing the input and output gate electrodes

the ions are trapped (approximately 1000 ions per filling) and undergo collisions with buffer and reactive gas particles. The target gas can be introduced into the 22PT or in the form of a CEB. The trapped ions are then subject to variations in its number composition or proprieties due to several causes: relaxation; reactions with gases which are present in the trap (e.g. target gas or simply background like H_2O); or even losses due to inappropriate trapping field in the trap or reactions leading to undetected masses. To follow the temporal changes of the ion cloud, after a well determined and consecutive trapping time, all ions are extracted through the exit lens electrode, mass analyzed in quadrupole mass filter and detected/counted by a Daly detector.

Constant temperature rate and densities determination

In the case of a simple ion-neutral binary reaction: $A^+ + B \Rightarrow C^+ + D$, and considering charge conservation, it leads to a time (t) dependent functions of the ion quantities $[A^+]$ and $[C^+]$:

$$\begin{aligned} [A^+] &= [A^+]_0 \; e^{-k[B]t} \\ [C^+] &= [A^+]_0 \, (1 - e^{-k[B]t}) \end{aligned} \tag{2.5}$$

where $[A^+]_0$ is its initial number density, k is the reaction rate coefficient, $[B]$ is the number density of the neutral gas. After collecting the data, rate coefficients or number densities are determined when ion curves are fitted with the adequate coupled rate equations system. In such a simple reaction, it is expected the exponential decay of the primary ions with the correspondent increase of product ions, while the overall ion sum remaining constant. Inert gases or even the target gas may be used as buffer gas. This leads to a simplification of the number of coupled equations to be used in order to define a system. Secondary reactions or background reactions tend to increase the degree of complexity of a system, as can be observed in Fig. 4.6. In such cases, a program is used for fitting the overall reaction system.

Absolute pressures of gases in the 22PT are known based on the use of calibrated ion gauges, already mentioned in Sec. 2.2. In this particular case, since the ion gauges are not directly connected to the 22PT, and due to the possibility of varying its temperature, the number density n is known by making use of the relation [ger92]:

$$n = 4.2 \times 10^{17} \, C \, \frac{PIG_{22PT}}{\sqrt{T_{22PT}}} \; \mathrm{cm}^{-3} \tag{2.6}$$

where C is the calibration factor, PIG_{22PT} is the pressure indicated by the ion gauge (mbar) and T_{22PT} is the temperature of the 22PT walls in K. The determination of the absolute number in this procedure has been estimated to have an accuracy in the range of 10% to 15%.

Detection efficiency

It was detected the existence of a non-temperature dependence discrimination factor (α_d) between different masses. This problem was thought to be connected with the quadrupole mass filter unit, located at the exit of the 22PT (although presently, the hypothesis that the origin of this miss behavior is related to the exit electrode of the 22PT, seems to be more probable).

Several attempts were made to overcome this misbehavior such as removing the quadrupole rods and cleaning them, or setting different potentials for the focusing lenses located in the exit of the quadrupole. Unfortunately it was not possible to totally overcome this undesired effect. After assuring that there was no uncommon loss of ions or generation of higher masses (at least, until masses lower than 150 u) during reaction time, the procedure followed was based on defining the relative discrimination for the different masses based on ion number conservation.

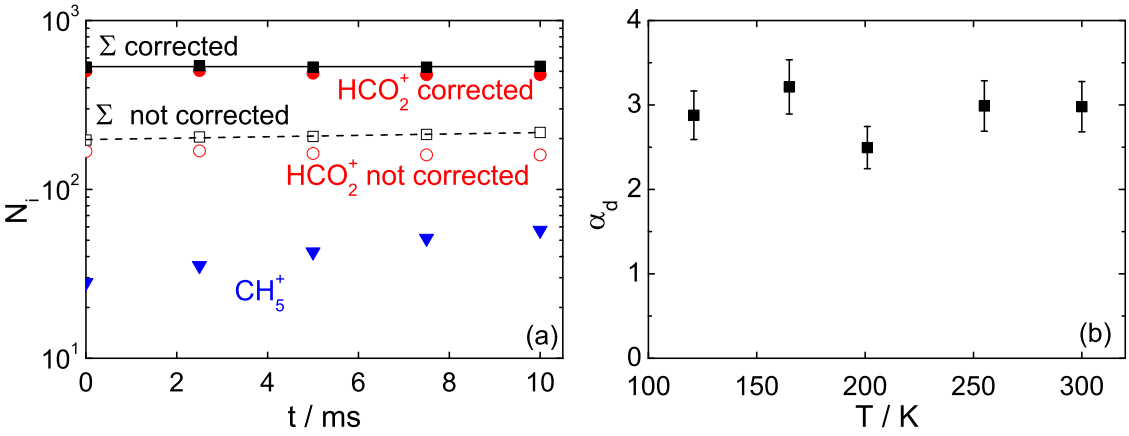

Fig. 2.10: a) Determination of the discrimination factor for the $HCO_2^+ + CH_4$ reaction (T_{22PT} = 255 K). The HCO_2^+ are multiplied with a constant factor α_d and the sum of all ions becomes constant. b) The discrimination factor for the same reaction is considered to be constant for a temperature range of 120 to 300 K, with an average value of $\alpha_d = 2.9 \pm 0.3$.

In the example given for the $HCO_2^+ + CH_4$ reaction (Fig. 2.10 (a)), the mass correction is assured by multiplying HCO_2^+ ions with $\alpha_d = 3$, so that the sum of all ions (HCO_2^+ and CH_5^+) gives a constant value during the reaction time. Several measurements for a temperature range of 120 to 300 K were done for this system and the final result gave a value of $\alpha_d = 2.9 \pm 0.3$, which can be observed in Fig. 2.10 (b). Similar masses, with a small difference between mass number, such as H_2O^+ and H_3O^+ or CH_5^+ are considered to have no discrimination between each other.

The same procedure was done for the Ar^+ and N_2^+ ions. In this case the correction had the value $\alpha_d = 2.5 \pm 0.3$. From this point on all results will be presented in their corrected form.

2.3.9 The $He^+ + N_2$ reaction.

The $He^+ + N_2$ was used as a test reaction, and later on, the N_2 number density in the cold effusive beam (Sec. 2.4.2) will be determined based on this same reaction. With several studies already published [bol70, row85, woo07], the branching of this reaction is well known [ada76]:

$$\begin{array}{rcll} He^+ + N_2 & \rightarrow & N^+ + N + He & (60\%) \\ & \rightarrow & N_2^+ + He & (40\%), \end{array} \tag{2.7}$$

but the purpose of this work was mainly to define a fast and reliable way to determine the N_2 density. The overall decay of the primary ions was, in this case, sufficient.

For obtaining the rate coefficients, the neutral reactant was leaked directly into the trap with a temperature range T_{22PT} between 80 and 300 K. A typical measurement is shown in Fig. 2.11 for a trap temperature of $T_{22PT} = 175$ K, where the exponential decay of the primary ions is observed. The resulting rate coefficients are shown in Fig. 2.12 as a function of T_{22PT}.

An ion-non-polar neutral interaction is dominated by the charge-induced dipole r^{-4} potential leading to the Langevin limit k_L [ger92d]:

$$k_L = 23.4\sqrt{\frac{\alpha_{N_2}}{\mu_{He+N_2}}} \tag{2.8}$$

where the units of k_L are 10^{-10} cm^3 s^{-1}, $\alpha_{N_2} = 1.7403$ Å is the N_2 neutral polarizability which is just slightly temperature dependent [lin05], and $\mu_{He+N_2} = 3.5$ amu is the reactant reduced mass. In the present case $k_L = 1.7 \times 10^{-9}$ cm^3 s^{-1}, is the value which is actually reached within the error bars. Our values are also, in agreement with previous measurements, obtained by other groups and techniques [row85, ada76, bie76].

Inspection of Fig. 2.12 reveals a slight negative slope in the temperature rate dependence:

$$k(T) = -2.0 \times 10^{-12}\,\mathrm{K}^{-1}\,\mathrm{cm}^3\,\mathrm{s}^{-1} \times T/\mathrm{K} + 2.0 \times 10^{-9}\,\mathrm{cm}^3\,\mathrm{s}^{-1}. \tag{2.9}$$

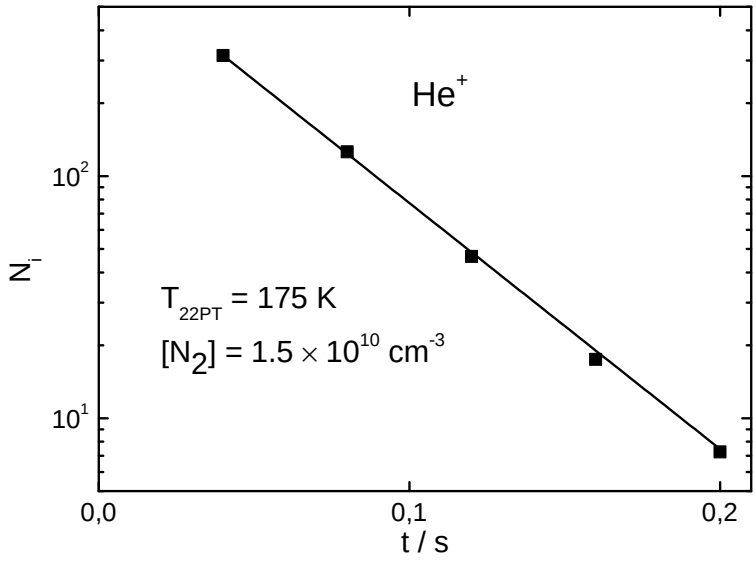

Fig. 2.11: $He^+ + N_2$ time dependence of primary ions at 175 K. Products are not detected. This reaction will be used for N_2 density calibration purposes. The solid line represents the fit of the exponential decay leading to the rate coefficient $k = 1.5 \times 10^{-9}$ cm^3 s^{-1}.

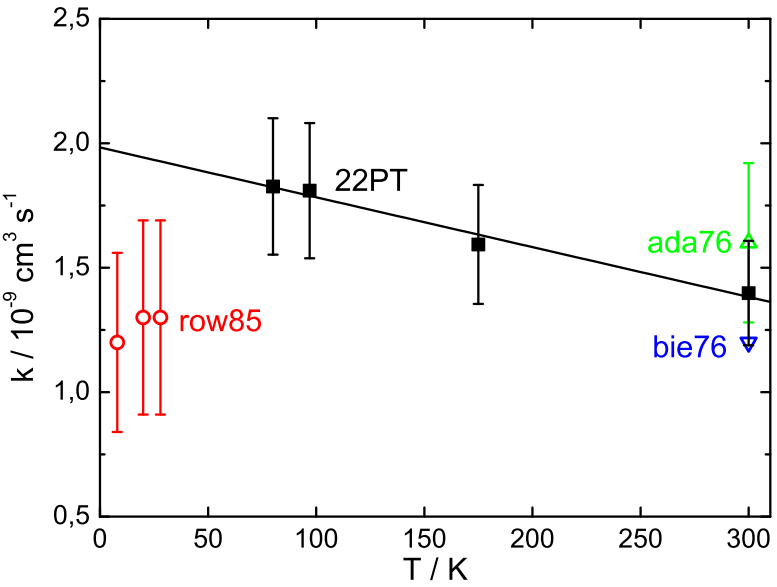

Fig. 2.12: A measured $He^+ + N_2$ temperature rate dependence between 80 and 300 K. For comparison, previous published values are presented, which are based on CRESU [row85], SIFT [ada76] and FA [bie76] techniques.

The nitrogen number density in the trap can now be determined, simply by

letting it react with He^+ and evaluating the rate measurements with the proper rate coefficient, based on equation 2.9. By extrapolation, values which temperatures reside below the freezing point can also be estimated.

2.4 The Cold Effusive Beam

2.4.1 Theoretical basis

Recent results were obtained in our group, namely the introduction and characterization of an H atom beam in conjugation with a 22PT [bor08]. Based on such efforts, and on the pursue for constructing a Pulsed Effusive Beam Source [ger08a], a cold effusive beam source (CEB) was added to the existing setup (Fig. 2.2). The study of reactions at low energies (below 1 meV), specially with condensable gases, gave rise to this new approach.

The basis of an effusive beam consists in allowing a gas to effuse through a small aperture, from a closed to a evacuated chamber, while assuring a molecular flow regime. This condition is normally described in terms of the Knudsen number k_n, which has to satisfy the condition $k_n \geq 1$, where $k_n = \lambda/D$ (λ being the mean free path of the particles and D the diameter of the aperture). Meaning that, gas particles move through the hole and within the beam without undergoing collision. Such a condition is easily achieved by maintaining a low pressure of the gas in the first chamber. The differential beam intensity $I(\theta)$, in function of an angle θ relative to the forward direction of the beam, and into a solid angle element $d\omega$ is given by the cosine distribution:

$$I(\theta) = n_0 A_0 \nu f(\nu) cos(\theta) d\omega d\nu, \tag{2.10}$$

being n_0 the source gas density, A_0 the cross sectional area of the aperture. The Maxwell-Boltzmann velocity distribution function $f(\nu)$ is given by:

$$f(\nu)d\nu = \pi^{-3/2}\nu^2\zeta^{-3}e^{-(\nu/\zeta)^2}d\nu, \tag{2.11}$$

where $\zeta = (2k_B T_0/m)^{1/2}$ is the corresponding most probable velocity of the particles of mass m, at the source temperature T_0, with k_B being the Boltzmann constant. The beam peak intensity $I(\theta = 0)$ takes the form:

$$I(0) = \phi_0/\pi \text{ particles s}^{-1} \text{ sr}, \tag{2.12}$$

where $\phi_0 = 1/4 n_0 A_0 \langle\nu\rangle$ particles s^{-1} sr is the total flow rate through the orifice and $\langle\nu\rangle = (8k_B T_0/\pi m)^{1/2}$ is the average velocity of the particles with a temperature T_0. By replacing the simple opening with a tube and relaxing the molecular flow condition, the intensity in the forward direction is considerably increased.

Taking into consideration the possibility of intermolecular collisions while inside the tube ($\lambda \ll L/2$), $I(0)$ takes the form:

$$I(0) = 0.065 \left(\frac{\langle \nu \rangle \, d}{\sigma} \right)^{1/2} \phi_t^{1/2} \, \text{part.} \, \text{s}^{-1} \, \text{sr}, \tag{2.13}$$

where $\sigma = (\sqrt{2}\lambda n)^{-1}$ and ϕ_t is the total flow rate [pau88, sin89].

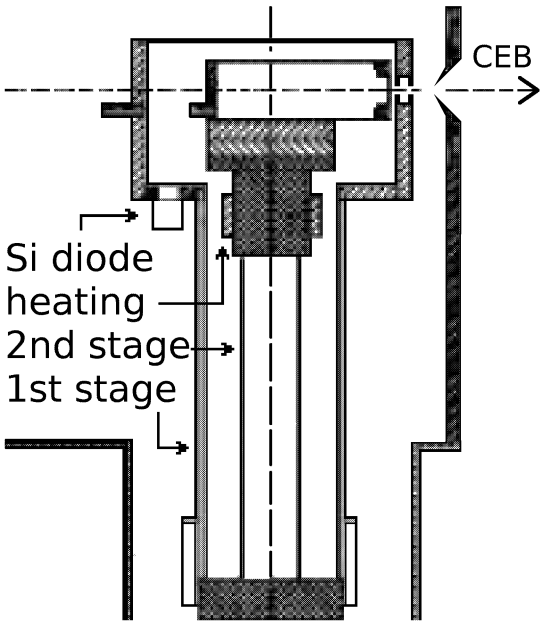

Fig. 2.13: The cold effusive beam source. The temperature of the effusive beam is coupled to the source due to wall collisions or desorption. The CEB source is connected to a cold head closed-cycle helium refrigerator, and temperature stabilization is based on a heating coil. A Si diode is used for temperature control.

In our specific case, the CEB source can be described as a copper cold tube coupled with a cold head closed-cycle helium refrigerator (Leibold RGD 210 with compressor RW2/3), and a skimmer, a vapour/condensed phase equilibrium will be reached finally. Based on Lide et al. [lid03], a partial pressure on the order of 10^{-5} mbar at 30 K for N_2 is expected. Large differential pumping capacity is provided using several turbomolecular pumps and cryo-pumping, decreasing the existent background signal.

2.4.2 Beam characterization: TOF and number density

Time of Flight measurements

The CEB source was coupled to a Time of Flight detection (TOF) system. A mechanical chopper with two radial opposite slits (2 mm width) was mounted

perpendicular to the molecular beam axis. The distance between the center of the disc and the beam axis was 74 mm and with a rotating frequency ranging between 30 Hz and 1 kHz and time resolution of 280 and 9 μs respectively). Mounted at a fixed distance of 37 cm, the Extranuclear Ionizer (Fig. 2.14) ionizes the neutral particles on the beam due to electron bombardment, and enables their subsequent detection by the Daly detector.

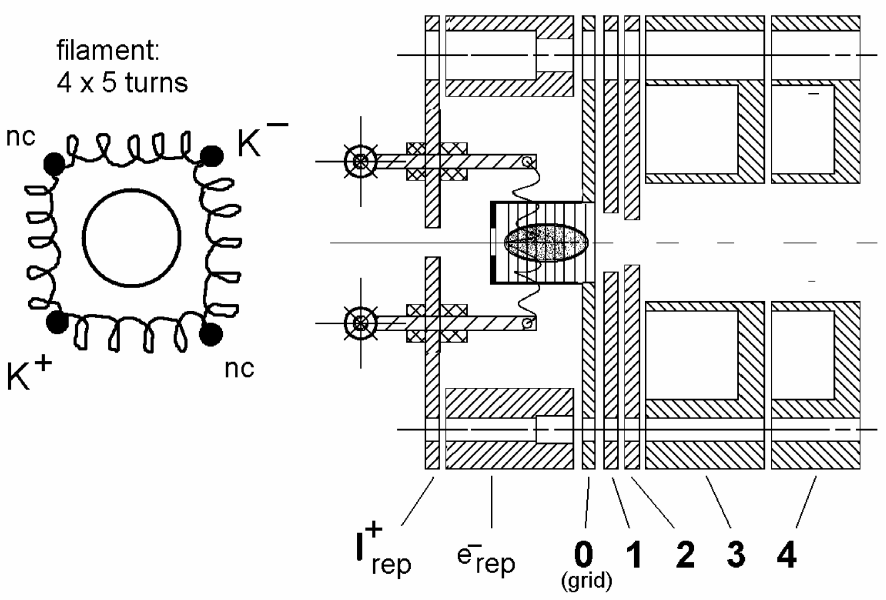

Fig. 2.14: Schematic of the Extranuclear Ionizer used during time of flight measurements. The several electrodes can be seen on the right side, while a sketch of the filament is seen on the left.

Finally the outcome signal is collected and analysed by a Multichannel Scaler (MCS-PCI PerkinElmer Instruments). The CEB, together with the detection system can be seen in Fig. 2.15.

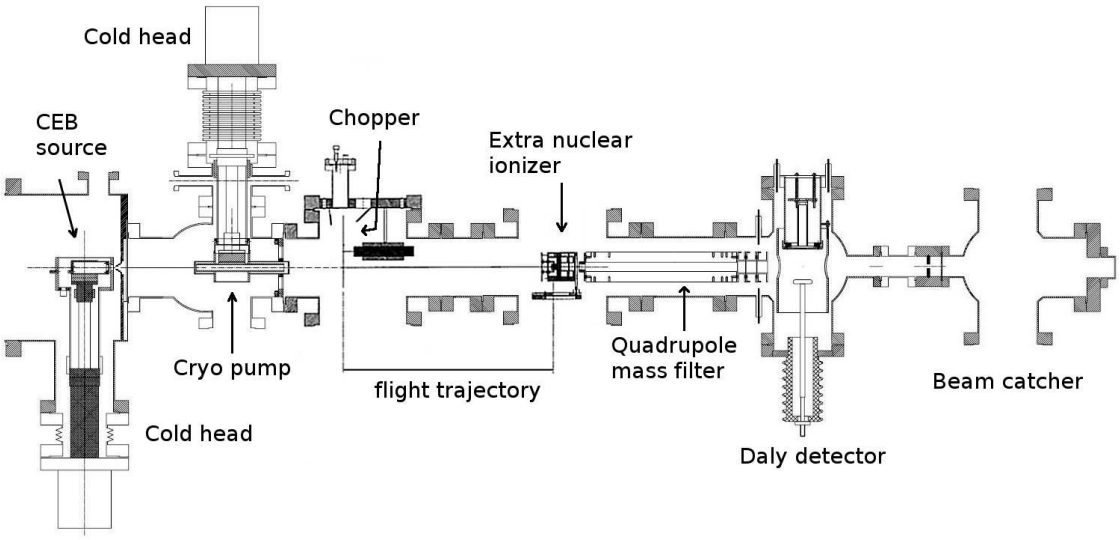

Fig. 2.15: Setup for determining the velocity distribution of the CEB via TOF. A beam is formed in the CEB source and goes through a Cryo pump before being intercepted by the chopper. After a flight trajectory of 37 cm, the beam is ionized by the Extranuclear ionizer and detected.

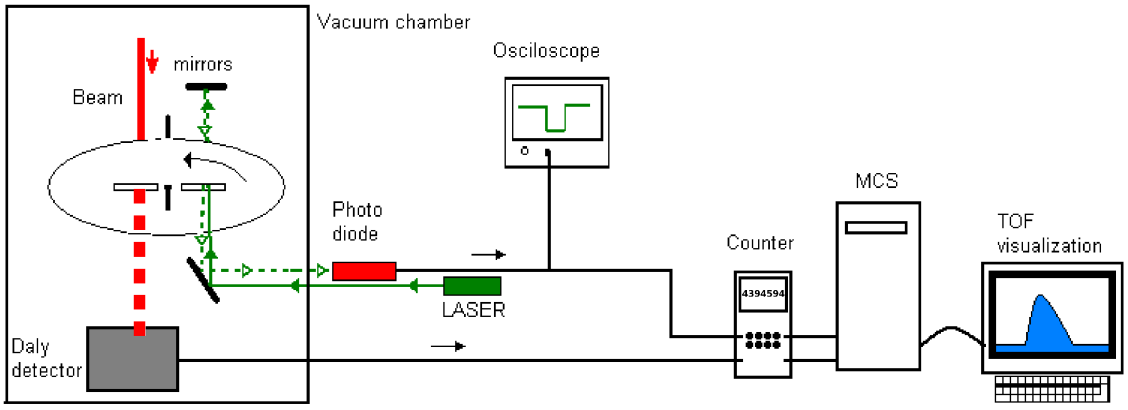

Fig. 2.16: Schematic drawing for the TOF triggering and detection. A green laser goes through the slit of the chopper, on the opposite side of the beam, and is reflected back to be detected by a photodiode. The output signal of the photodiode is used parallel in the 100 MHz counter, and used a trigger in the Multichannel Scaler.

The triggering of the data acquisition with the chopper is accomplished based on light barrier setup, schematically represented in Fig. 2.16. It consists in directing a green laser through the second slit of the chopper, on the opposite side of were the beam is located, and reflecting it back to be detected by a photodiode. The output signal of the photodiode is used parallel in the 100 MHz counter, and as trigger in the Multichannel Scaler.

For a characterization of the CEB, velocity distributions have been recorded. For fitting the data, a Maxwell-Boltzmann based function was used:

$$\begin{aligned} y &= C_0 \\ &+ C_1 \left(\frac{L}{t - t_{det}} \right)^4 e^{-\left(\frac{L}{t-t_{det}}\right)^2 \frac{m}{2K_B T_{fit}}} \\ &+ C_1 \left(\frac{L}{t - t_{det} + 1/(2f)} \right)^4 e^{-\left(\frac{L}{t-t_{det}+1/(2f)}\right)^2 \frac{m}{2K_B T_{fit}}} \end{aligned} \tag{2.14}$$

where y is the intensity, C_0 and C_1 are constants, L = 37 cm is the path travelled by the beam between the chopper and the detection, t is time, t_{det} is the detection time (explained below), m is the atomic mass, k_B the Boltzmann constant, T_{fit} is the fitted temperature and f is the rotating frequency of the chopper. The last term enables us to account for overlapped TOF distributions due to too high frequency of the chopper.

The detection time (t_{det}), defined as the time between the beam ionization and its detection in the Multichannel Scaler, was measured simply by leaking a small continuous flow into the ionizer chamber, while momentaneously pulsing the ionizer grid potential from P_0 = 0 to -5 V, leading to an absence of ion production as can be observed in Fig. A.1 for several molecules.

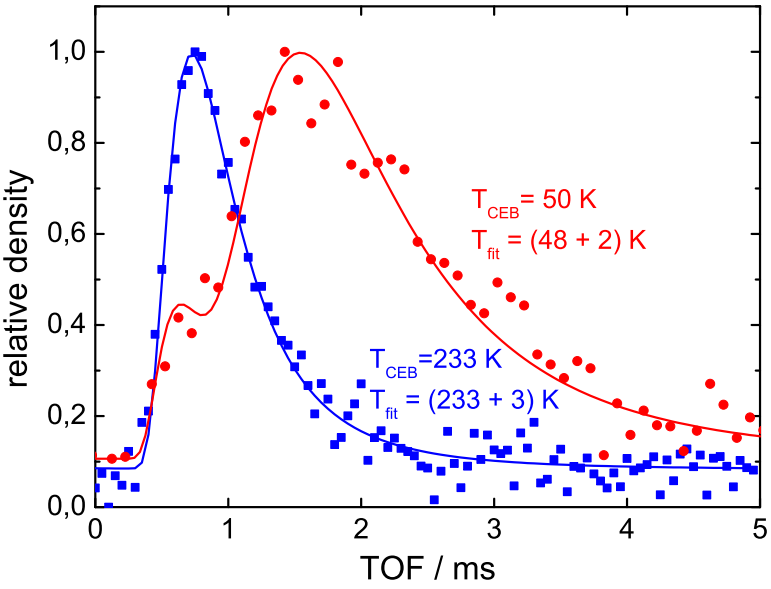

Fig. 2.17: TOF distributions for N_2 molecules for T_{CEB} = 233 K - (■) and 50 K - (●) with correspondent Maxwell-Boltzmann distributions (full line) giving (233 ± 3) K and (48 ± 2) K. It is also possible to observe in the left side a small 300 K contribution in the 50 K beam.

In the N_2 experiment (Fig. 2.17), the results are in good agreement with the predicted distribution for a CEB source temperature of T_{CEB} = 50 and 233

K. A fourth term was later added to Eq. 2.15 in order to fit properly a second distribution caused by non thermalized background contributions. Following the same procedure, measurements were also made with D_2. Once again, results show that the beam temperature is in equilibrium with the CEB chamber (Fig. A.2).

N_2 number density in the CEB

To determine the number density in the beam, one has to use other method besides the one already referred to in Sec. 2.3.8. When target gas is leaked into the trap, molecules are equally distributed throughout all available space. The molecular beam is localized along the 22PT axis, meaning, the effective volume for the reaction and respective number of neutral molecules available to react is indeed different. In this special case, after determining the N_2 beam translational energy as seen just above (Sec. 2.4.2), the chemical reaction - $He^+ + N_2$ - was used for number density calibration purposes.

Fig. 2.18 shows a set of data used for calibrating the N_2 number density. In this case, the CEB and the 22PT temperature were kept constants for a period of 5 hours at a temperature of $T_{CEB} = T_{22PT} = 40$ K. The measurement was done in a continuous mode. The decay of He^+ ions was followed during a defined time interval $\Delta t = t_2 - t_1$. A shutter located immediately before the 22PT would automatically and synchronously for every second measurement cut the path of the beam. In this way it was possible to follow the influence of the beam presence on the He^+ decay. According to the temperature rate dependence presented in Eq. 2.9, 40 K temperature corresponds to a reaction rate $k = 1.9 \times 10^{-9}\,\mathrm{cm^3\,s^{-1}}$. Finally one obtains the data in terms of N_2 number densities by applying the formula:

$$[N_2] = \frac{\ln([He^+(t_1)]/[He^+(t_2)])}{k\,\Delta t}. \tag{2.15}$$

Measuring only with the background pressure (shutter closed), an average value for the N_2 number density of $[N_2]_{bg} = 1.5 \times 10^9\,\mathrm{cm^{-3}}$ was obtained, while with the background and beam (shutter open) $[N_2]_{bgb} = 1.0 \times 10^9\,\mathrm{cm^{-3}}$. Subtraction of these two values gives out the beam number density $[N_2]_b = 5 \times 10^8\,\mathrm{cm^{-3}}$, and considering the relative error between the two measurements and making a conservative evaluation, we estimated a 30% average error.

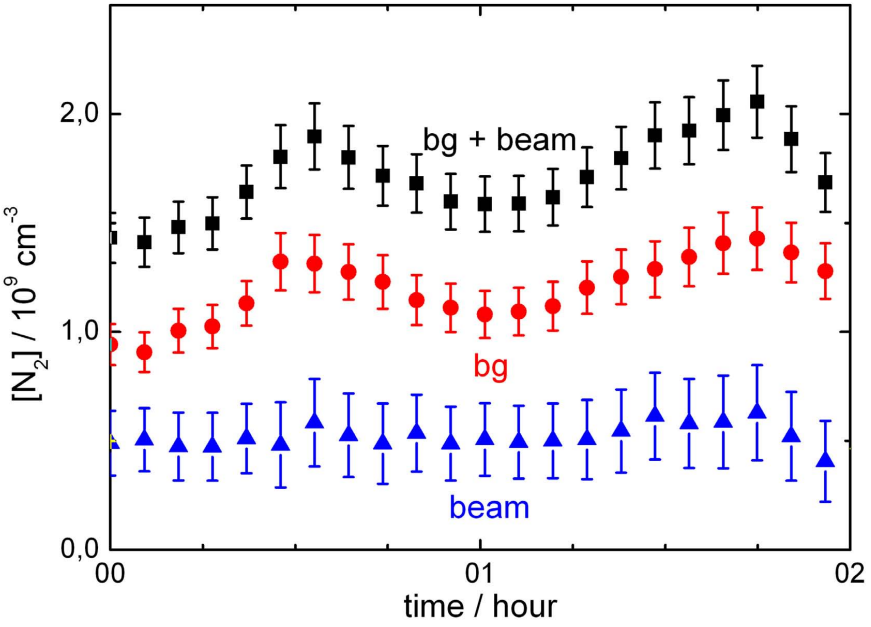

Fig. 2.18: [N_2] beam measurement. T_{CEB} = T_{22PT} = 40 K and average number densities for background and beam plus background are 1.5 $\times$ 10^9 cm^{-3} and 1.0 $\times$ 10^9 cm^{-3} , respectively. By subtraction the beam's number density is therefore 5 $\times$ 10^8 cm^{-3}, with an estimated error of 30 %.

Chapter 3

THE PROTON AFFINITY OF METHANE

3.1 Introduction

The concept of bond energy, the energy changes associated with forming or breaking bonds between atoms, is well known among molecule synthetic chemists and material scientists. It has been be used for testing empirical and *ab initio* theories of electronic structures, and is also important for atmospheric and combustion modeling [ber94].

Considering a gas-phase reaction of a proton (H^+) and a neutral species (M) leading to the formation of the protonated species (MH^+):

$$M + H^+ \rightarrow MH^+, \tag{3.1}$$

the term proton affinity (*PA*) is related to the correspondent enthalpy change for the gas phase reaction, normally at 298 K [hun98]:

$$PA(M) = \Delta_f H°_{298}(M) + \Delta_f H°_{298}(H^+) - \Delta_f H°_{298}(MH^+). \tag{3.2}$$

The corresponding entropy change ($\Delta S°_{298}$) can be defined in terms of absolute entropies:

$$\Delta S°_{298} = S°_{298}(MH^+) - S°_{298}(M) - S°_{298}(H^+). \tag{3.3}$$

If the temperature dependence of the equilibrium constant $K(T)$ is known in a proton transfer reaction:

$$XH^+ + Y \leftrightarrow YH^+ + X, \tag{3.4}$$

one can determine the difference of the proton affinities of the species involved. In the case of a system such as the one represented in Eq. 3.4, the standard enthalpy change ($\Delta H°_{298}$) is a direct quantitative measure of the difference between the proton affinities of the two neutral species:

$$\Delta H°_{298} = \Delta PA = PA(X) - PA(Y). \tag{3.5}$$

Determining the preferred direction of these reactions opens a door for an ordered proton affinity table.

The determination of standard entropy change $\Delta S°_{298}$ has also practical applications. The relative values of the proton affinity of molecules can be based upon a single temperature measurement of the equilibrium constant. But the $\Delta S°_{298}$ value is needed in order to validate the assumption that the standard free energy change ($\Delta G°_{298}$) is approximately $\Delta H°_{298}$. $\Delta S°_{298}$ can also give us an insight into the geometries of the protonated species XH^+ and YH^+ [hem73].

Several experimental techniques have been used for determining the heat of formation of ionic species in the gas phase. The heat of formation of an ion in the gas phase can, in principle, be obtained through a straightforward treatment of the thermo-chemistry of the ionization process [ber94]. This approach fails for species like the protonated methane (CH_5^+), where no neutral molecule exists.

Studies of the chemical equilibrium kinetics, such as those involving the reaction of a hydrogen molecule with an ion M^+, can provide very accurate thermochemical information on the ion MH^+ that is formed [haw89]. More specifically, kinetic measurements of the reaction of CH_5^+ with hydrogen atoms, provide a route for the determination of the hydrogen bond energy for this non classical hydrocarbon ion [ger05a, luc05]. Given the exact knowledge of the thermochemical data for the other reactants, the heat of formation for CH_4^+, H_2 and H, the heat of formation for CH_5^+ can be derived, and an absolute value for the proton affinity of CH_4 can be evaluated [hun98].

3.2 Previous experiments

Since the first mass spectrometric observation of the interaction of CH_4^+ and H_2 by Munson et al. [mun63]:

$$CH_4^+ + H_2 \underset{k_{-1}}{\overset{k_1}{\rightleftarrows}} CH_5^+ + H, \tag{3.6}$$

reaction 3.6 in reverse direction has been the subject of several experimental [kim75, ada77, fed85, asv04a, luc05, ger09] and computational studies [wan05].

Using the selected ion flowing drift tube (SIFT) technique, Federer et al. [fed85] investigated reaction 3.6 from thermal energy (300 K) to 0.12 eV center of mass kinetic energy. A van't Hoff plot from measured rate coefficients for the forward and backward reaction yielded a reaction enthalpy of $\Delta_r H° = -5.0\,\mathrm{kJ\,mol^{-1}}$ and a reaction entropy ($\Delta_r S°_{297}$) of $31.4\,\mathrm{J\,mol^{-1}\,K^{-1}}$ at 297 K. Based on the proton affinities given by Walder and Franklin [wal80], the heat of formation of CH_5^+ was evaluated in $\Delta_f H°_{298}(CH_5^+) = (912 \pm 13)\,\mathrm{kJ\,mol^{-1}}$.

The entropy of reaction was interpreted from the already known $\Delta S°_{297}(H_2) - \Delta S°_{297}(H) = 15.9\,\mathrm{J\,mol^{-1}\,K^{-1}}$ and it was concluded that the entropy of CH_5^+ is smaller than for CH_4^+ by more than $13\,\mathrm{J\,mol^{-1}\,K^{-1}}$ [fed85]. The authors inferred

that the reaction is exoergic and endoentropic, i.e., the free energy $\Delta G° = \Delta H° - T\Delta S°$ must become negative above a certain value of T. In a recent computational study, the potential energy surfaces for reaction 3.6 have been calculated using several high level *ab initio* methods [wan05]. The reaction is predicted to be slightly exothermic, with $\Delta_r H°_0 = (-12.7 \pm 5.2)\,\mathrm{kJ\,mol^{-1}}$, for ground states.

Reaction 3.6 has been recently studied from the left to the right, using the variable temperature 22-pole ion trap from room temperature down to 15 K [asv04a]. Temperature dependent reaction rates using different isotopic configurations were measured to reveal the dynamics for the reaction. In that paper, the authors were raising the questions, whether a bimolecular reaction can be treated with simple thermodynamic quantities as presented by Fereder et al. [fed85] and whether it is allowed to say that reaction 3.6 is endoentropic. The answer was found negative in both cases.

Applying the definition of enthalpy change to reaction 3.6 we obtain:

$$\Delta_r H°_{298} = \Delta_f H°_{298}(CH_5^+) + \Delta_f H°_{298}(H) - \Delta_f H°_{298}(CH_4^+) - \Delta_f H°_{298}(H_2). \quad (3.7)$$

But recently, the determination of the rate coefficients (k_{-1}) at temperatures from 10 up to 100 K show that the reverse reaction is close to thermoneutral ($\Delta_r H°_{298} = -3.5 \pm 0.1\,\mathrm{kJ\,mol^{-1}}$) [ger05a, luc05]. Since $\Delta_f H°_{298}(H_2) = 0$, and based on recommended thermodynamic data [lid03]:

$$\Delta_f H°_{298}(H) = 218\,\mathrm{kJ\,mol^{-1}}$$
$$\Delta_f H°_{298}(CH_4^+) = 1143\,\mathrm{kJ\,mol^{-1}}$$

a $\Delta_f H°_{298}(CH_5^+) = (922 \pm 2)\,\mathrm{kJ\,mol^{-1}}$ can be evaluated.

If one considers the reaction:

$$CH_4 + H^+ \rightarrow CH_5^+, \quad (3.8)$$

and by making use of the standard value for the enthalpy of formation for methane $\Delta_f H°_{298}(CH_4) = -74.6\,\mathrm{kJ\,mol^{-1}}$ [lid03], it leads to an absolute proton affinity of $PA(CH_4) = (534 \pm 2)\,\mathrm{kJ\,mol^{-1}}$.

Several compilations of proton affinities of molecules have been published [wal80, szu93]. In the most recent compilation, according to Hunter et al. [hun98], the absolute value for proton affinity for methane $PA(CH_4)$ is based on the relative proton affinity of CH_4 to the absolute value of the proton affinity of carbon dioxide $PA(CO_2)$ (543.5 and 540.5 $\mathrm{kJ\,mol^{-1}}$ respectively). The stated accuracy of the proton affinity scale for molecules, that have not been measured by key measurements like ionization or appearance energy is $8\,\mathrm{kJ\,mol^{-1}}$. Based on these values for $PA(CH_4)$ and $PA(CO_2)$, the reaction enthalpy for the proton transfer reaction:

$$HCO_2^+ + CH_4 \underset{k_r}{\overset{k_f}{\rightleftarrows}} CH_5^+ + CO_2, \quad (3.9)$$

becomes: $\Delta_r H° = PA(CO_2) - PA(CH_4) = -3.0\,\mathrm{kJ\,mol^{-1}}$. The relative reaction enthalpy published values for the same reaction have been determined in the range of $\Delta_r H° = -11.72$ [meo77] to $-3.35\,\mathrm{kJ\,mol^{-1}}$ [szu93], whereas the change in entropy $\Delta_r S°$ for the same reaction has fallen in the range of $-10.04\,\mathrm{J\,mol^{-1}\,K^{-1}}$[meo77] to $+6.0\,\mathrm{J\,mol^{-1}\,K^{-1}}$ [szu93].

Therefore, several are several experiments and theories pointing out to different outcomes, concerning enthalpies and related proton affinities. With the purpose of clarifying this question, we have decided to study the proton affinity of CH_4 relative to CO_2 using a variable temperature 22-pole ion trap apparatus. The parameters will be derived either from the equilibrium constant which will be determined by measuring independently the forward and reverse reaction, or by monitoring the thermodynamic equilibrium in the trap. The following section is dedicated to the description of the two methods used, while in the subsequent one, the final results and discussion is presented.

3.3 Experimental

Two methods have been used for determining the equilibrium rate temperature dependence ($K_{eq}(T)$), which directly leads to the reaction enthalpy and entropy. This section follows a description of these two methods, how they were implemented, and their results.

The equilibrium rate is defined as:

$$K_{eq} = \frac{k_f}{k_r}, \tag{3.10}$$

where k_f and k_r are the rate coefficients in forward and reverse direction in equation 3.9 respectively. Independent rate coefficient measurements for the forward and reverse reactions were taken for a given set of fixed temperatures, following the procedure already mentioned in Sec. 2.3.8. This allow us to determine $K_{\mathrm{eq}}(T)$. And in a more direct approach, the equilibrium constant K_{eq} for Eq. 3.9 can be determined from the measured ratio of the product ions and the number densities of the neutral reactants, by using the equation:

$$K_{\mathrm{eq}} = \frac{\left[CH_5^+\right]\left[CO_2\right]}{\left[HCO_2^+\right]\left[CH_4\right]}, \tag{3.11}$$

but the thermodynamic equilibrium of the system must be assured. This second method, besides needing only one measurement, has the major advantage of having a smaller uncertainty in the final results, since there is no adding of the errors from the two independent rate measurements [ber94].

In order to infer the relative proton affinity, one has first to determine the dependence of the equilibrium constant on the temperature ($K_{\mathrm{eq}}(T)$), and the

enthalpy $\Delta_r H°$ and entropy $\Delta_r S°$ changes can be derived from the slope and intercept of a van't Hoff plot, according to the equation [hun98]:

$$\ln(K_{eq}) = -\frac{\Delta_r H°}{RT} + \frac{\Delta_r S°}{R}. \tag{3.12}$$

In case of a linear behaviour, one can assume that $\Delta_r H°_{298} = \Delta_r H°$ and $\Delta_r S°_{298} = \Delta_r S°$

3.3.1 The forward and the reverse reaction

As an example, Fig. 3.1 demonstrates the results obtained for determination of the absolute rate (k_f) for the forward reaction $HCO_2^+ + CH_4 \rightarrow CH_5^+ + CO_2$ (22PT trap temperature T_{22PT} = 255 and 120 K). The precursor gas used for the HCO_2^+ ions production in the storage ion source was an approximate 50/50 % mixture of CO_2 and CH_4. Initially, CO_2^+ or CH_4^+ ions are produced due to electron bombardment. They immediately react with the remaining CH_4 ($k = 5.5 \times 10^{-10}\,cm^3\,s^{-1}$) or CO_2 ($k = 1.2 \times 10^{-9}\,cm^3\,s^{-1}$) respectively, and in both cases producing HCO_2^+ ions [woo07], which are then filtered and guided into the 22PT. Using the effusive gas inlet, CH_4 is leaked into the trap leading to a stationary number density of $[CH_4] = 2.3 \times 10^{10}\,cm^{-3}$ and $3.3 \times 10^{10}\,cm^{-3}$, respectively, which after reaction with HCO_2^+, leads to the formation of CH_5^+ and CO_2. Helium is added continuously as buffer gas with a number density of $[He] = 5.8 \times 10^{12}\,cm^{-3}$ in the first case and $8.4 \times 10^{12}\,cm^{-3}$ in the second.

During preliminary measurements, the existence of traces of water in the background was observed. Although reacting with HCO_2^+ at a considerable high rate ($k = 2.3 \times 10^{-9}\,cm^3\,s^{-1}$ [woo07]), its influence in the overall reaction was below 5 % at 300 K due to its low density ($[H_2O] = 5 \times 10^7\,cm^{-3}$) comparing with CH_4 (three orders of magnitude larger). This effect obviously diminishes even further by extending the measurements in the direction of lower temperatures, reason why it was not taken in to account for the rate evaluation. After fitting, we obtained a rate coefficient of $k_{255} = 2.6 \times 10^{-10}\,cm^3\,s^{-1}$ and $k_{120} = 4.3 \times 10^{-10}\,cm^3\,s^{-1}$.

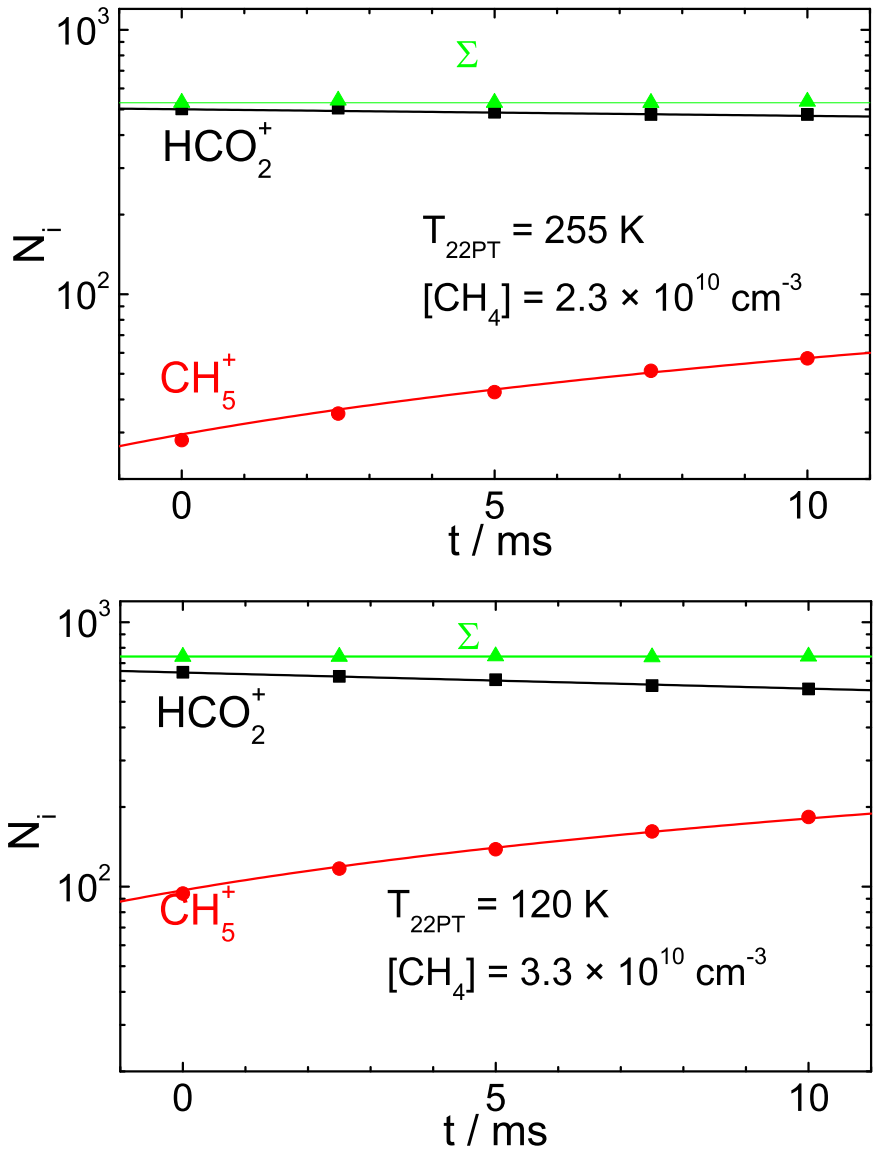

Fig. 3.1: Reactions of HCO_2^+ ions with CH_4 molecules, leaked into the trap. For cooling the ions to T_{22PT} = 120 and 255 K, helium gas has been added with a number density of $8.4 \times 10^{12}\,cm^{-3}$ and $5.8 \times 10^{12}\,cm^{-3}$, respectively. The number of primary and product ions per filling, N_i, is plotted as a function of the storage time t. At each iteration a new ensemble of HCO_2^+ ions is introduced into the trap and undergoes reaction with the neutrals, leading to the rate reactions k_{120} = $4.3 \times 10^{-10}\,cm^3\,s^{-1}$ and $k_{255} = 2.6 \times 10^{-10}\,cm^3\,s^{-1}$.

To avoid condensation on the walls of CH_4, the measurements were done in a temperature range between 300 and 100 K. The obtained results, an endothermic behavior, for the reverse temperature dependence of the reaction rate coefficient ($k(T) = (-1.0 \pm 0.1) \times 10^{-12}\,\mathrm{K}^{-1}\,\mathrm{cm}^3\,\mathrm{s}^{-1} \times T/\mathrm{K} + (5.3 \pm 0.4) \times 10^{-10}\,\mathrm{cm}^3\,\mathrm{s}^{-1}$) are showed below in Fig. 3.2.

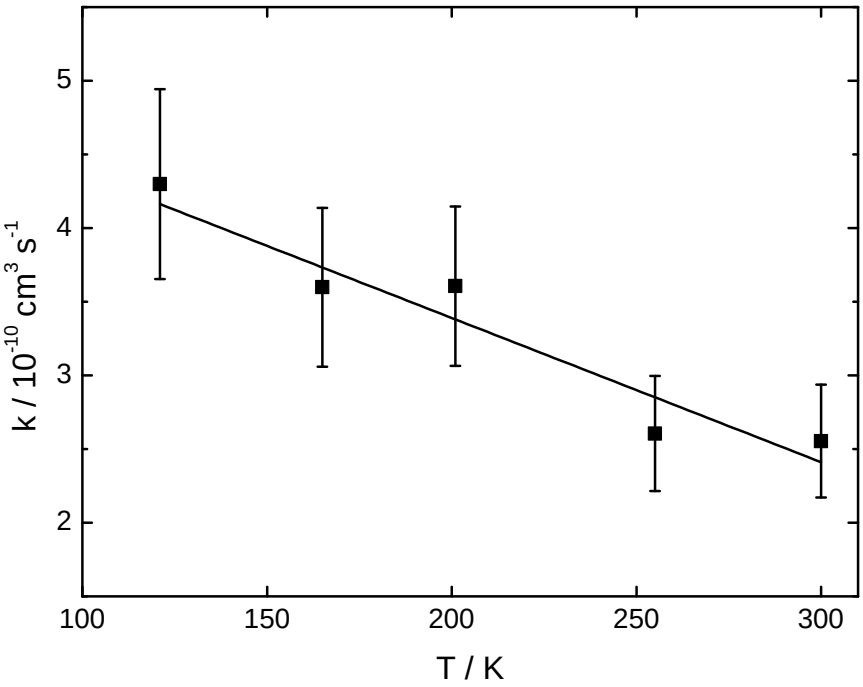

Fig. 3.2: Temperature rate dependence for the $HCO_2^+ + CH_4 \rightarrow CH_5^+ + CO_2$ reaction, measured between 120 and 300 K ($k(T) = (-1.0 \pm 0.1) \times 10^{-12}\,\mathrm{K}^{-1}\,\mathrm{cm}^3\,\mathrm{s}^{-1} \times T/\mathrm{K} + (5.3 \pm 0.4) \times 10^{-10}\,\mathrm{cm}^3\,\mathrm{s}^{-1}$), denoting a weak endothermic behavior.

The determination of the reverse reaction rate k_r in Eq. 3.9 was done in a similar procedure, as already described before, although in the present case, the CH_5^+ production was based on methane (CH_4). Also, in order to measure this reaction rate, slower than the forward reaction, the target gas number density was increased in approximately one order of magnitude. Like in the previous case, background contributions were negligible. In Fig. 3.3 two measurements done for a 22PT temperature T_{22PT} = 300 and 197 K with a respective target gas number density $[CO_2] = 1.5 \times 10^{11}\,\mathrm{cm}^{-3}$ and $2.8 \times 10^{11}\,\mathrm{cm}^{-3}$, are presented. They lead to the rate reactions $k_{300} = 2.9 \times 10^{-11}\,\mathrm{cm}^3\,\mathrm{s}^{-1}$ and $k_{197} = 8.0 \times 10^{-12}\,\mathrm{cm}^3\,\mathrm{s}^{-1}$ respectively.

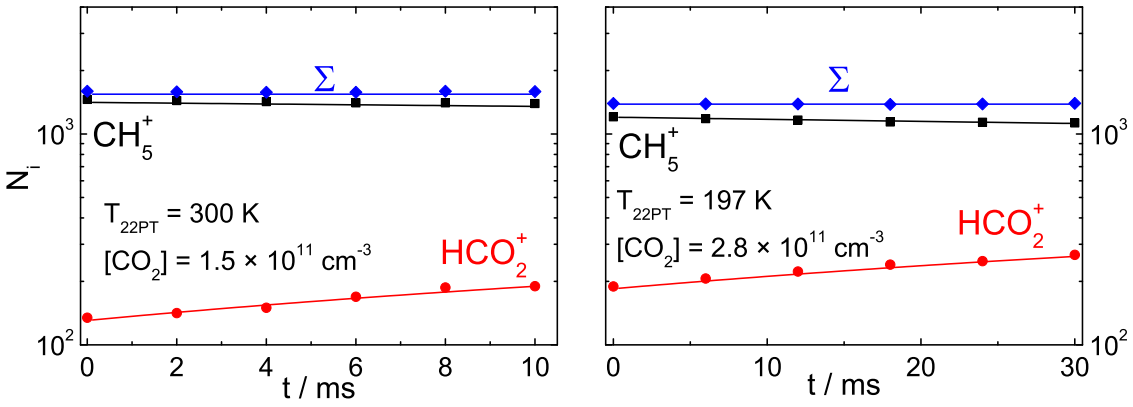

Fig. 3.3: Constant temperature rate measurement for the $CH_5^+ + CO_2 \rightarrow HCO_2^+ + CH_4$ reaction ($k_{300} = 2.9 \times 10^{-11}\,cm^3\,s^{-1}$; $k_{200} = 8.0 \times 10^{-12}\,cm^3\,s^{-1}$).

The measurements were done at a 22PT temperature T_{22PT} = 300, 253 and 197 K. Fig. 3.4 shows the respective temperature rate dependence for this exothermic reaction $k(T) = (2.0 \pm 0.2) \times 10^{-13}\,K^{-1}\,cm^3\,s^{-1} \times T/K - (3.2 \pm 0.5) \times 10^{-11}\,cm^3\,s^{-1}$.

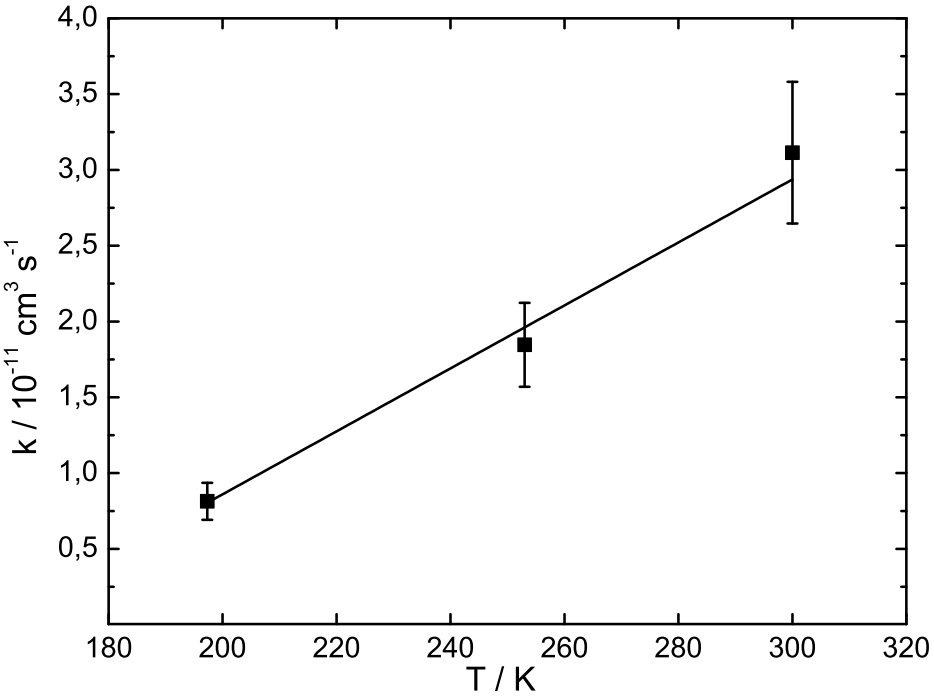

Fig. 3.4: Temperature rate dependence for the $CH_5^+ + CO_2 \rightarrow HCO_2^+ + CH_4$ reaction ($k(T) = (2.0 \pm 0.2) \times 10^{-13}\,K^{-1}\,cm^3\,s^{-1} \times T/K - (3.2 \pm 0.5) \times 10^{-11}\,cm^3\,s^{-1}$.).

3.3.2 The constant temperature equilibrium rate measurement

In this experiment, according to Eq. 3.11, we observe the ratio between the ions HCO_2^+ and CH_5^+ in the presence of a well defined mixture of CH_4 and CO_2 in the 22PT. This is done until an equilibrium is reached, and the ratio remains constant.

In order to determine the equilibrium constant (K_{eq}), the density of neutral reactants was determined based on the pressure readings done with the calibrated ionization gauges according to Eq.2.6. Due to the relatively long storage times and a typical number density of the helium buffer gas ([He] = $2\times10^{13}\,cm^{-3}$ indicating a collision frequency of $\approx 10^4\,s^{-1}$), this technique is well suited for reaching thermodynamic equilibrium in the 22PT ion trap. The 22PT lowest temperature was limited to 140 K, once more to avoid gas condensation on the surrounding walls. In the described experiment, the point of equilibrium is determined by reaching a constant time independent ratio between the reactant and product ion intensities. In our case this equilibrium is reached in a time between 0.4 to 0.6 seconds. As an example, Fig. 3.5 shows the time dependence of ion counts in the CH_5^+, HCO_2^+, CO_2, CH_4 and He mixture at 300 and 200 K.

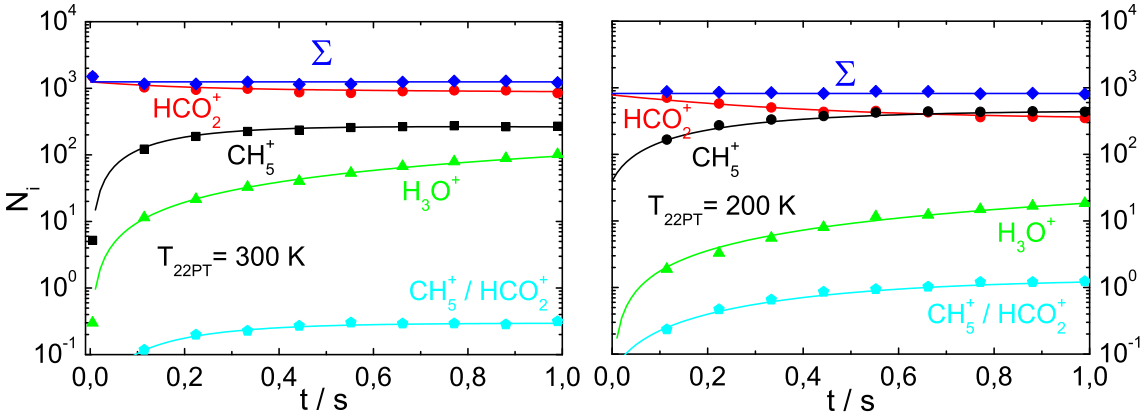

Fig. 3.5: Constant temperature equilibrium rate measurements (K_{eq}) for the HCO_2^+ + $CH_4 \rightleftarrows CH_5^+ + CO_2$ system. The thermodynamic equilibrium is reached for $t \approx 0.45\,s$ at 300 K, while at 200 K this happens at 0.65 s. Ratio of the target gases $[CH_4]/[CO_2]$ = 34.8 and ions ratio when equilibrium is reached $[CH_5^+/HCO_2^+]_{eq}$ = 0.29 for T_{22PT} = 300 K and 1.12 for 200 K leading to a respective K_{eq} = 10 and 39, with an estimated accuracy of 25%.

The number density of CH_4 was $[CH_4] = 4.4\times10^9\,cm^{-3}$, and the number density of CO_2 was chosen to be $[CO_2] = 1.5\times10^{11}\,cm^{-3}$, leading to a CH_5^+ and HCO_2^+ ion counting within the same order of magnitude when reaching equilibrium condition. In this experiment, about 1000 HCO_2^+ ions are injected per pulse into the trap filled with CO_2, CH_4 and He. The HCO_2^+ ions are transformed via reaction 3.9 into CH_5^+, which in return react with CO_2 to form once again HCO_2^+ until an equilibrium is reached.

In addition, H_3O^+ ions are also formed, via proton transfer of the stored ions to background water molecules. The solid lines represent the numerical solution of a set of coupled rate equations describing the formation and destruction of the corresponding ions. Initial conditions are the number of the injected ions as well as the densities of the neutral reactant gases including H_2O background.

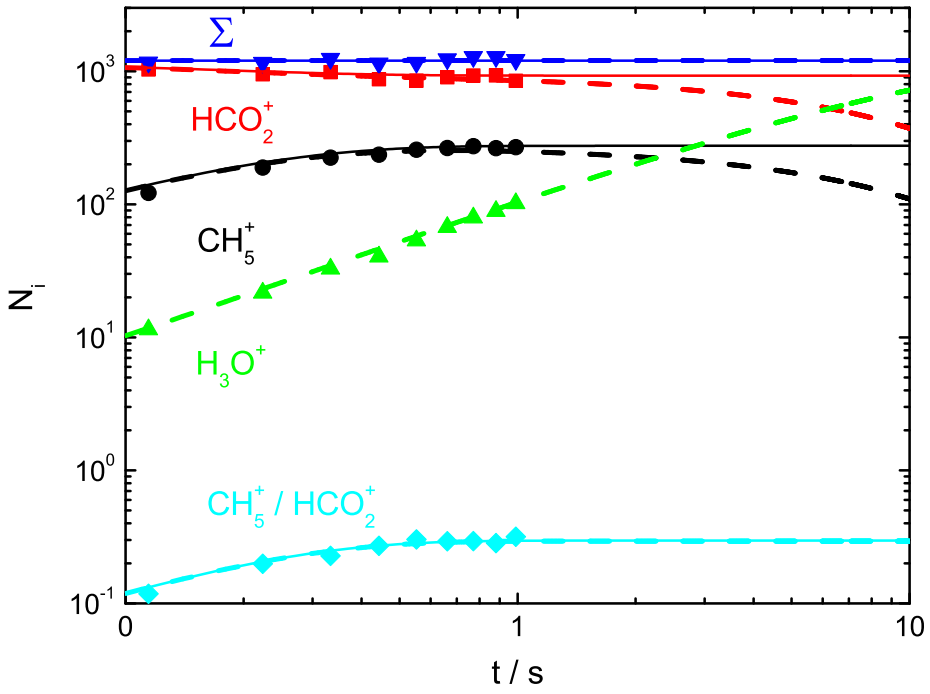

Fig. 3.6: Measurement at room temperature and simulation over the existence (dashed lines) or not (continuous lines) of H_2O background and its influence on the CH_5^+/HCO_2^+ ratio (observed to be less then 1 %). Main reaction rate values for the simulation were taken from our previous studies. The *k* value for reaction between H_2O and HCO_2^+ was $2.3\times10^{-9}\,cm^3\,s^{-1}$ and for CH_5^+ $3.7\times10^{-9}\,cm^3\,s^{-1}$ [woo07].

One main question was the influence of H_2O background in the determination of the ratio between HCO_2^+ and CH_5^+ ions. The reactions:

$$\begin{aligned} HCO_2^+ &+ H_2O \rightarrow H_3O^+ + CO_2 \\ CH_5^+ &+ H_2O \rightarrow H_3O^+ + CH_4 \end{aligned} \tag{3.13}$$

with reaction rates of 2.3 and $3.7 \times 10^{-9}\,cm^3\,s^{-1}$ [woo07], respectively, the considerable amount of H_2O density ($[H_2O] \approx 1 \times 10^7\,cm^{-3}$) at room temperature, and specially the longer time needed for the thermodynamic equilibrium to be reached, made us question the reliability of our measurements. As can be observed in Fig. 3.6, simulation shows that, although there is an expected decrease in the CH_5^+ and HCO_2^+ ions counting due to formation of H_3O^+, their

ratio (CH_5^+/HCO_2^+), even if extended to 10 s storage time, remains essentially the same, being the difference below 1%.

Due to this decay observed in both $HCO2^+$ and CH_5^+ ions, and considering that their ratio is not altered, and the ions are thermalized to the walls temperature, it would be more proper to refer that the system reached a relative thermodynamic equilibrium condition. For simplification, thermodynamic equilibrium may be referred, but having in mind these particular constrain.

3.4 Results and discussion

Fig. 3.7 shows the determined equilibrium constant (K_{eq}) for reaction 3.9 at selected temperatures in the range of 120 to 300 K, using helium as a buffer gas. According to the linearity in the $\ln(K)$ vs. $1000/T$ plot, the change in the total heat capacity accompanying reaction 3.9 is sufficiently small to ensure constancy of $\Delta_r H°$ and thus also $\Delta_r S°$ in the temperature range 120 to 300 K. A least square fit of the data yields values for the standard enthalpy change $\Delta_r H° = -6.5 \pm 0.5\,\mathrm{kJ\,mol^{-1}}$ and the standard entropy change $\Delta_r S° = -1.7 \pm 1\,\mathrm{J\,mol^{-1}\,K^{-1}}$ in the range 120 to 300 K.

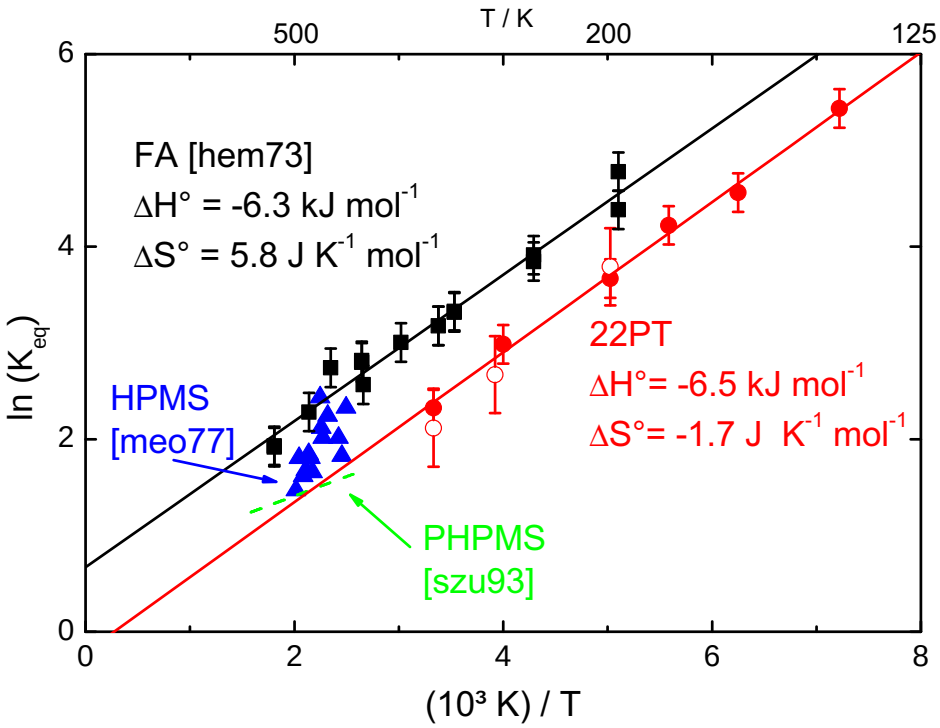

Fig. 3.7: Comparison of van't Hoff plots of experimental results for the proton transfer between CO_2 and CH_4: obtained in this study (K_{eq} measurements – ●; absolute rate measurements – ○), experimental data from a flowing after glow kinetic study (■) [hem73], high pressure mass spectrometry study [meo77] (▲) and [szu93] (- - -).

It was also verified that, in the case of existence of any unknown systematic error, e.g. temperature or number density determination, the outcome will only have influence on the offset ($\Delta_r S°_{298}$) but not on the slope ($\Delta_r H°_{298}$) of the resulting line. An experiment was carried without helium buffer gas. The data measured with helium has 10% steeper slope, corresponding to a lower $\Delta_r H°_{298}$. It is our conviction that this effect is derived from the thermal excitation of the reactants due to rf heating. The use of helium as a buffer gas allowed us to reach really stationary thermal equilibrium and we chose the values from the experiments with He buffer gas for further discussions.

3.4.1 Comparison with other experimental techniques

Most measurements of proton exchange equilibrium constants have been carried out using one of three types of ion instruments, which operate in very different pressure regimes: an ion cyclotron resonance spectrometer (ICR), a high pressure mass spectrometer (HPMS), or a flowing afterglow apparatus (FA). In Fig. 3.7 we compare the present results with published experimental studies

[hem73, meo07, szu93]. The most important questions are, whether thermodynamic equilibrium is in fact attained, the accuracy of the temperature measurement [hun98], and the exact determination of the number densities of the reactants [gal01].

In Tab. 3.1 a summary of experimental determined K_{eq} is given, including the extracted heat of reaction, i.e. the difference of the proton affinities (ΔPA) for CH_4 and CO_2 , along with the entropy changes ($\Delta_r S°$) for reaction 3.9. The presented value for $\Delta PA = (-6.5 \pm 0.2)\,\mathrm{kJ\,mol^{-1}}$ is in excellent agreement with the values from flowing afterglow (FA) $\Delta PA = (-6.3 \pm 0.4)\,\mathrm{kJ\,mol^{-1}}$ [hem73, boh80] in the temperature range from 196 K to 553 K and selected ion flow tube (SIFT) experiments $\Delta PA = -6.3 \pm 1.7\,\mathrm{kJ\,mol^{-1}}$ [ada89] in the temperature range from 300 to 500 K within the stated error. On the other hand, values from the pulsed high pressure mass spectrometry (PHPMS) study is $\Delta PA = -3.35\,\mathrm{kJ\,mol^{-1}}$, measured in the temperature range of 420 to 620 K [szu93].

The value for the entropy changes, $\Delta_r S° = -2\,\mathrm{J\,mol^{-1}\,K^{-1}}$ is slightly negative. In reaction 3.9, the absolute entropy at 298 K is well known for the neutral species $S°_{298}(CH_4) = 186.25\,\mathrm{J\,mol^{-1}\,K^{-1}}$ and $S°_{298}(CO_2) = 213.79\,\mathrm{J\,mol^{-1}\,K^{-1}}$. For the ionic reactants, the absolute entropy is more difficult to establish. Commonly, statistical thermodynamics is used along with high quality *ab initio* calculations to calculate $S°_{298}$. East et al. calculated $S°_{298} = 240.3\,\mathrm{J\,mol^{-1}\,K^{-1}}$ for HCO_2^+ [eas97a] in reasonable agreement with the experimental value of $S°_{298}(HCO_2^+) = 236\,\mathrm{J\,mol^{-1}\,K^{-1}}$ [ada89]. Hemsworth et al. calculated the value $S°_{298}(CH_5^+) = 210.9\,\mathrm{J\,mol^{-1}\,K^{-1}}$ [hem73, dyc70] where the equilibrium geometry corresponds to one of two possible structures with C_s symmetry between which there is practically free rotation but where vibrational and electronic contributions to the entropy are neglected. Based on these values we would expect a value of $\Delta_r S° = 2.00\,\mathrm{J\,mol^{-1}\,K^{-1}}$ in agreement with our experimentally determined value.

Tab. 3.1: ΔPA and $\Delta_r S°$ for several experimental values. In addition, calculations based on the absolute proton affinity of CO_2 and of CH_4 are presented [hun98].

	ΔPA $kJ\,mol^{-1}$	$\Delta_r S°$ $J\,mol^{-1}\,K^{-1}$	technique
this work	-6.5	-2	22PT
[hem73]	-6.3	5.8	FA
[meo77]	-11.7	-10	HPMS
[szu93]	-3.35	5	PHPMS
[hun98]	-3.00	6.00	

3.4.2 The absolute proton affinity

According to the value for proton affinity of methane previously calculated, and equation 3.5, we have $PA(CO_2) = PA(CH_4) - \Delta PA$ leading to the value $PA(CO_2) = (542 \pm 2)\,kJ\,mol^{-1}$. Tab. 3.2 presents a compilation of results derived from several studies.

Tab. 3.2: Compilation of results obtained for CH_4 and CO_2 proton affinities (kJ mol^{-1}).

PA (CH_4)	references	PA (CO_2)	references
534 ± 2	present work	540 ± 2	present work
546 ± 8	[boh80]	530	[hem73]
543 ± 4	[ada89]	536 ± 3	[tra91]
537.2	[pop87] *ab initio*	541 ± 2	[szu93]
536.4	[hes90] *ab initio*	541	[kom92] *ab initio*
542.2	[kom92] *ab initio*	540.5	[lin05]
543.5	[lin05]		

It can be observed that there is a general good agreement, within error bars, between the several experiments. In the case of CH_4, it is interesting to observe, although slightly below the NIST accepted standard value [lin05], it is similar to the results obtained by two of the *ab initio* calculations [pop87, hes90]. Our value for the proton affinity of CO_2 is coincident with the NIST accepted value.

3.5 Conclusion

In summary, using the protonation of methane as an example, we demonstrated that a temperature variable 22-pole ion trap can be used to study ion/molecule systems under defined thermal equilibrium conditions.

The equilibrium constants have been obtained by two independent schemes: (a) from a measurement of the rate coefficients in the forward and reverse direction k_f/k_r or (b) from a measurement of the relative concentration of ions and neutrals once relative stationary equilibrium is achieved. In relation to the second method, cautions were taken with proper cooling of the products and specially with background reactions. Attenuation rate for both primary ions and products were time independent and equilibrium constants were directly measured in the 22PT. Although equilibrium constants were measured, a real TDE was not possible to be reached in our experiment. Consequence of the observed attenuation of the HCO_2^+ and CH_5^+ ions due to the presence of watter. But rather a relative thermodynamic equilibrium, since their ratios were not altered and their were in thermal equilibrium.

The agreement between the two types of measurements was within the experimental error. This second technique provides a direct and straight forward

mean to obtain equilibrium constants at various temperatures from 120 to 300 K. From a van't Hoff plot we derived a reaction enthalpy of $-6.5 \pm 0.5\,\mathrm{kJ\,mol^{-1}}$. The entropy change ($\Delta_r S°$) was found to be $(-2.0 \pm 1.0)\,\mathrm{J\,mol^{-1}\,K^{-1}}$. Based on the absolute proton affinity for methane of $PA(CH_4) = (534 \pm 2)\,\mathrm{kJ\,mol^{-1}}$, we obtained a value for $PA(CO_2) = (540 \pm 2)\,\mathrm{kJ\,mol^{-1}}$ in good agreement with previous studies.

Based on this reliable method, further measurements could be made in order to determine the proton affinity ladder from CO_2 down to CO.

Chapter 4

THE (Ar-N_2)$^+$ SYSTEM

4.1 Introduction

The studies of gas-phase charge-transfer reactions and an insight into their reaction mechanisms may be of use in modeling the ion chemistry of planetary atmospheres [gov84]. Its relevance is also known as a temperature diagnostics in argon plasmas [lin04], or to infer the temperature of cold environments based on the method of laser induced charge transfer [ger08b, sch99]. Furthermore, understanding of the relative efficiency of different forms of energy in promoting this kind of elementary reactions, is a central issue in reaction dynamics. A good case study is the (Ar-N_2)$^+$ system:

$$N_2^+(\nu', J') + Ar \underset{k_f}{\overset{k_f}{\rightleftarrows}} Ar^+(^2P_j) + N_2(\nu, J) \tag{4.1}$$

where the symbol ^2P_j denotes the fine-structure levels of the ion in the electric field due to the weak intermolecular potential, ν represents the vibrational state, and J the rotational state. This system has been studied both theoretically [ng92, gis92, can01, can03] and experimentally [smi81, reb89, ng92, vig93, wic94, smi94].

This particular system is a model system for a non-Born-Oppenheimer reaction mechanisms, which display a temperature dependency not easily explained via simple energy-dependent capture cross sections. Due to interaction of several Potential Energy Surfaces (PES), reactants can give rise to products in more than one electronic state [mik06], where the several competing channels already known [smi81] are:

$$\begin{aligned}
Ar^+(^2P_{3/2}) + N_2 &\rightarrow N_2^+(\nu = 0) + Ar + 179\,\text{meV} && (4.2)\\
&\rightarrow N_2^+(\nu = 1) + Ar - 90\,\text{meV}, && (4.3)\\
Ar^+(^2P_{1/2}) + N_2 &\rightarrow N_2^+(\nu = 0) + Ar + 357\,\text{meV} && (4.4)\\
&\rightarrow N_2^+(\nu = 1) + Ar + 88\,\text{meV}, && (4.5)
\end{aligned}$$

with N_2, N_2^+, and Ar being in their ground electronic states. The particular case of the role of vibrational excitation has been the subject of a large number of investigations. In the long run, one goal of these studies is related to the possibility of controlling the outcome of chemical reactions [zar98], for example by a selective preparation of reactant states. According to recent research, the experimentally determined vibration-state selected cross sections for the forward reaction and the state-selected and state-to-state cross sections for the back reaction in Eq. 4.1 are in general good agreement with theoretical predictions [ng92, can01, can03]. Although there is still the need for more low temperatures measurements.

The role of N_2^+ and N_2 rotational energy is also not totally determined. The $N_2^+(\nu > 0, J)$ presents an interesting reaction dynamics for its rotational dependence via Laser Induced Reaction (LIR). Schlemmer et al. pointed out that the rotational relaxation of ortho-$N_2^+(X^2\Sigma_g, \nu\text{“} = 0, J'' = 6.5)$ in collisions with Ar is much less effective than what expected on the basis of simple dynamical and statistical assumptions [sch99]. In this context, the study of $N_2^+(\nu = 0, J)$ is therefore of importance.

The reverse electron transfer reaction has an interesting low temperature behaviour, and not totally clarified. Results obtained by merged beam experiment [wic94] are in contradiction with several other experiments that point out the existence of a minimum in the rate coefficient at approximately 0.02 eV [smi81] and the increase towards lower temperatures [smi94].

From the technical point of view this work also presents interesting features. One can point out the combination of a low temperature trap with an effusive beam of neutrals, while measuring the $Ar^+ + N_2$ reaction. A second interesting aspect is the production and filtering of N_2^+ in the ground vibrational state, used during the forward $N_2^+ + Ar$ reaction. This and some of the previous questions will be addressed in the following sections.

4.2 Electron transfer from Ar to N_2^+

4.2.1 Previous experimental and theoretical studies

The first experiments

The forward charge-transfer reaction presented in Eq. 4.1 is an example of how vibrational energy can determine an chemical reaction. First observed in an ion flow tube experiment [smi81], measurements were done at room temperature and ion-source electron energy of 100 eV. Under such conditions, it was showed that two differently reacting species were present: a rapidly reacting one ($4 \times 10^{-10}\,cm^3\,s^{-1}$), and another one which reacted extremely slowly ($2 \times 10^{-13}\,cm^3\,s^{-1}$). Measurements were also carried out with an electron energy approximately 1 eV above the threshold energy for production of N_2^+ (15.581 eV

[joh06]). This value was below the one necessary for production of metastable electronic states (in the 21 to 22 eV range). The presence of two different reaction channels was confirmed. At 80 K the rate coefficient for the excited state remained the same but the slower reaction dropped even further to a value below $10^{-13}\,cm^3\,s^{-1}$. This difference was, according to the authors, due to the vibrational excited state or states of N_2^+. Lindiger et al. performed a similar experiment in a DRIFT tube and obtained similar results [lin81]. In the following years, more results for this reaction were published [kat82, gov84, scu91].

The reaction $N_2^+(\nu = 0) + Ar \rightarrow Ar^+(^2P_{3/2}) + N_2(\nu = 0)$ is slightly endoergic (0.179 eV). However, the cross-section of $N_2^+(\nu = 0)$ is between one and three orders of magnitude smaller than that of vibrationally excited N_2^+, even when the collision energy is set well above the threshold. Therefore, vibrational energy of N_2^+ is much more efficient in promoting the charge-transfer reaction than collision energy. The experimental results for the total partial state-to-state cross section for the $N_2^+(\nu') + Ar$ reaction indicated that in the low-energy range (between 1 and 4 eV) the cross-section decreases with the increase of collision energy [sha87, lia86, tos92].

Based on laser induced reaction, Schlemmer et al. presented studies on the rotational relaxation processes after N_2^+ laser excitation in a 22-pole ion trap [sch99]. It is pointed out that the method is not only appropriate for receiving spectroscopic information, but also to use it for detailed dynamical studies of the various reaction steps involved. Here they defended that by determining rotational temperatures and Doppler temperatures, through Ar^+ product ions spectroscopy, it is possible to show that the internal and translational degrees of freedom of the parent ions are well coupled to the trap temperature via collisions with the Ar buffer gas. Unfortunately measurements have not been extended to temperatures below 50 K, due to condensation of the argon gas on the surrounding walls. This present work points out several solutions which can be used for overcoming such a problem.

The theoretical studies

The first theoretical studies based on the vibronic semi-classic method [par88, par89] were not able to fully justify the measured behavior for the forward reaction, described above. The majority of these studies was based on collision energies higher than 1 eV.

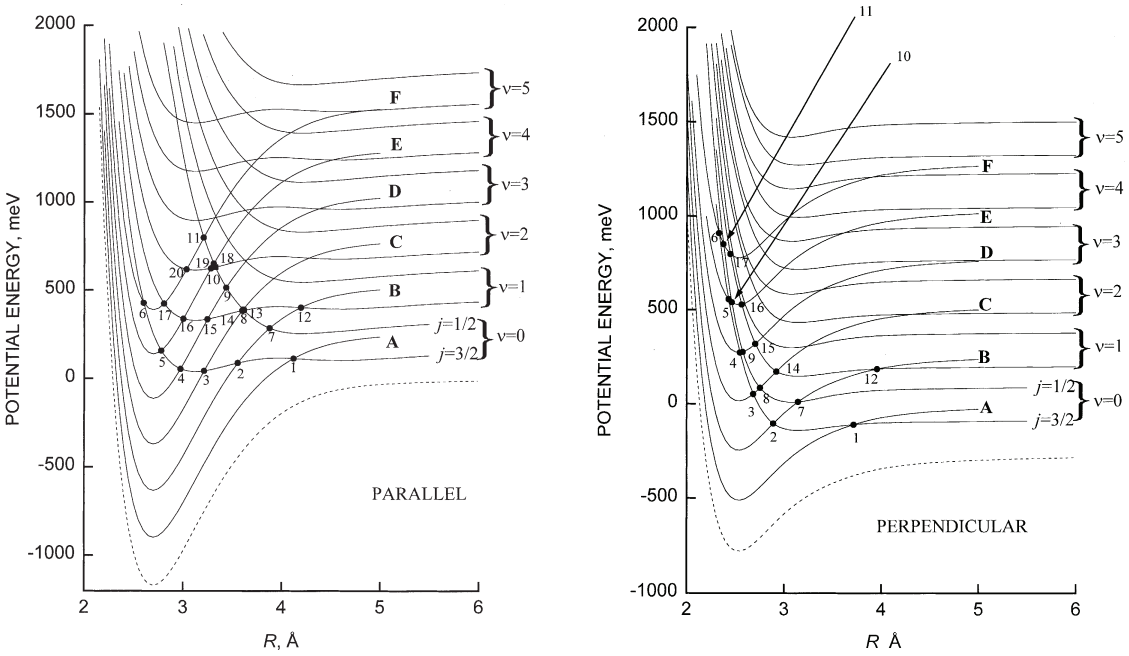

Fig. 4.1: Vibronic potential energy curves for the (Ar + N_2)$^+$ complex (parallel and perpendicular configurations seen on the left and right side respectively). The vibrational quantum number ν represents the vibronic states correlated with the $Ar^+(^2P_j)$ + $N_2(\nu)$ channels, while letters refer to the Ar + N_2^+ (ν'). Crossings are indicated with numbers. The dashed curve represents the Ar + $N_2^+(\nu' = 0)$ state with the respective asymptotic energy being assumed as the zero of the energy scale. For more detailed information please refer to [can03].

Candori et al. made an evaluation first from thermal to 2 eV [can01], and later from 0.01 to 5 eV [can03] of the interaction potential energy surfaces (PES) for the (Ar-N_2)$^+$ system. The potential took into account specific components of the interaction such as polarizability, charge, quadrupole moment, ionization potential, and electron affinity. The resulting adiabatic PES included also an interaction term for the charge exchange couplings and the spin-orbit term. State-to-state cross-sections determinations for the forward reaction in Eq. 4.1 at low energies were calculated. Unfortunately, the rate coefficients obtained by Smith and Lindinger in the early 80's [smi81, lin81] were the only available experimental data for comparison which were below 1 eV. Agreement between calculated and experimental results was obtained by assuming that the duration of the nonadiabatic transition matched the time required for the molecular rearrangement into the final vibrational state. A main consequence was that, the efficient formation of products into specific vibrational states is limited to well defined ranges of impact parameters as observed experimentally.

The role of nonadiabatic transitions behavior at localized crossings was also investigated. Calculations were shown to be in agreement with experimental results confirming the strong state-selective chemistry occurring in the (Ar-N_2)$^+$ system. Fig. 4.1 represents the vibronic states relevant for these calculations.

The $N_2^+(\nu' = 0)$+ Ar channel resides below all the others, exhibiting no crossings with other vibronic states. The reactivity and probability of its formation as a reaction product, is considered to be negligible, also in accordance with the experimental studies.

More work is therefore needed, concerning the behavior of this reaction for lower energies. In the following section it is shown that it is possible to create and filter $N_2(\nu = 0)$, while results are presented for the forward reaction's extended measurements (60 to 300 K).

4.2.2 N_2^+ + Ar measurements

Initially, a similar procedure as already described in Sec. 2.3.8 was followed for the N_2^+ + Ar temperature rate determination: N_2 electron bombardment for the N_2^+ ion production, filtering and trapping in the 22PT, and adding the target gas Ar ($1.3 \times 10^{12}\,cm^{-3}$). Helium was used was used as buffer gas ($4 \times 10^{12}\,cm^{-3}$).

The main problem in this experiment turned out to be the fact that, from the first moments of the trapping time, a considerable amount of Ar^+ product ions was already present (approximately 15% of the parents ions counts). After the first 100 ms, all excited N_2^+ would have been thermalized or would have reacted with Ar, producing Ar^+. This initial high background of Ar^+ ions would have made it more difficult to measure accurately an already expected small rate coefficient.

It is known that internal and translational degrees of freedom couple with the trap temperature due to buffer gas collisions [sch99]. But quenching effects are not so efficient for vibrational levels. This was demonstrated by Kato et al. by measuring a very small rate of $(9.8 \pm 0.7) \times 10^{-16}\,cm^3\,s^{-1}$ for the vibrational cooling of $N_2^+(\nu > 0)$ with He [kat95]. Therefore, more preponderant for the explanation of this effect of high Ar^+ counts already before 100 ms, is the fact that, with a relatively high charge transfer rate for the excited vibrational states ($k_f(\nu > 0) = 4 \times 10^{-10}\,cm^3\,s^{-1}$ [smi81, lin81]) and with a considerably high Ar number density used during the experiment ($1.3 \times 10^{12}\,cm^{-3}$), all $N_2^+(\nu > 0)$ will need less than 100 ms to go through reaction, leaving only the non-excited N_2^+ and the produced Ar^+ ions.

The next step, after this first 100 ms, was to extract the already formed Ar^+ ions in order to be able to measure the expected small reaction rate. This was accomplished by momentaneously reducing the 22PT amplitude (V_0) during a short period of time ($\approx$ 20 ms). As example, Fig. 4.2 presents one measurement taken for a 22PT temperature of 300 K ([He] = $6 \times 10^{12}\,cm^{-3}$ and [Ar] = $1.3 \times 10^{12}\,cm^{-3}$), corresponding to a forward rate coefficient of $k_f = 1.7 \times 10^{-14}\,cm^3\,s^{-1}$. In the first 100 ms approximately 2300 of N_2^+ primary ions and 160 of Ar^+ have been detected. Immediately after lowering the 22PT amplitude, the number of N_2^+ ions decreases only by 2% while the presence of Ar^+ inside the 22PT was removed. This effect is due to the fact that the effective

potential (Eq. 2.2) is inversely proportional to the ions mass, resulting in a better confinement for the N_2^+ ions trajectories when compared with the ones from Ar^+.

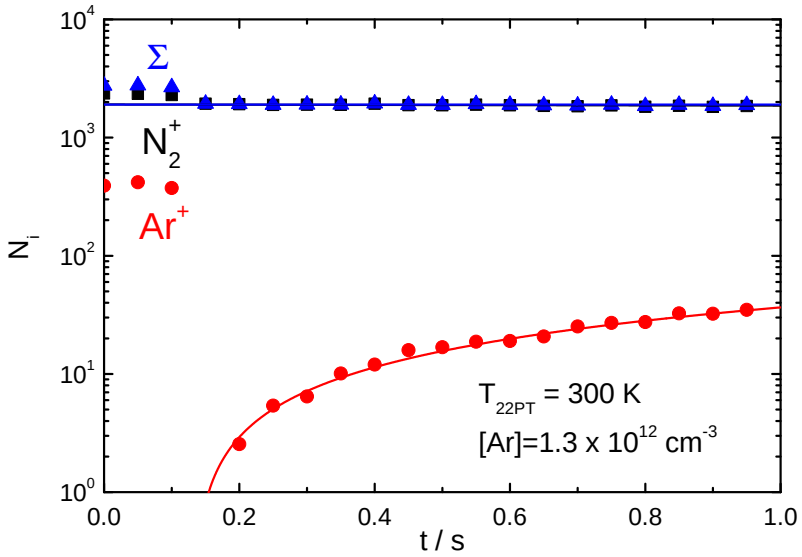

Fig. 4.2: Reaction of the $N_2^+(\nu = 0)$ ions with Ar. Due to the existence of non-thermalized N_2 primary ions, it can be observed already in the first 100 ms a constant number of produced Ar^+ ions. After reducing the 22PT amplitude and letting the Ar^+ ions escape, the remaining N_2^+ ions are considered to be thermalized and in their ground vibrational state. The solid lines correspond to a solution of the system differential equation, giving out a forward reaction rate at 300 K of $k_f = 1.7 \times 10^{-14}\,\mathrm{cm^3\,s^{-1}}$.

Already well established, the charge transfer with the N_2^+ ground vibrational state ($\nu = 0$) is endothermic by 0.179 eV but for the first excited state ($\nu = 1$) is exothermic by 0.090 eV [scu91]. Thus, within a simple model, one would expect an upper limit (k_{theo} for the room-temperature (T) observed value of $k_{f,\nu=0}$ [lin81] to be:

$$k_{theo}(T) \leq k_L e^{-\Delta E/(k_B T)}, \tag{4.6}$$

with ΔE being the endothermicity of the reaction and k_L, the Langevin limiting value [gio58] for the reaction. With $k_L \approx 7 \times 10^{-10}\,\mathrm{cm^3\,s^{-1}}$, we get $k_{theo}(300\,\mathrm{K}) \leq 6.9 \times 10^{-13}\,\mathrm{cm^3\,s^{-1}}$, which is one order higher than the measured value of $1.6 \times 10^{-14}\,\mathrm{cm^3\,s^{-1}}$. Therefore, the rate coefficient presented in Fig. 4.2 after the first initial 100 ms represents $k_f(\nu = 0)$ for the reaction:

$$N_2^+(\nu = 0) + Ar \xrightarrow{k_f} Ar^+(^2P_{3/2}) + N_2(\nu = 0) \tag{4.7}$$

In Fig. 4.3 is presented the obtained reaction rate temperature dependence results for the forward reaction taken between 300 and 60 K. Former published values obtained by other groups at 300 K are also represented.

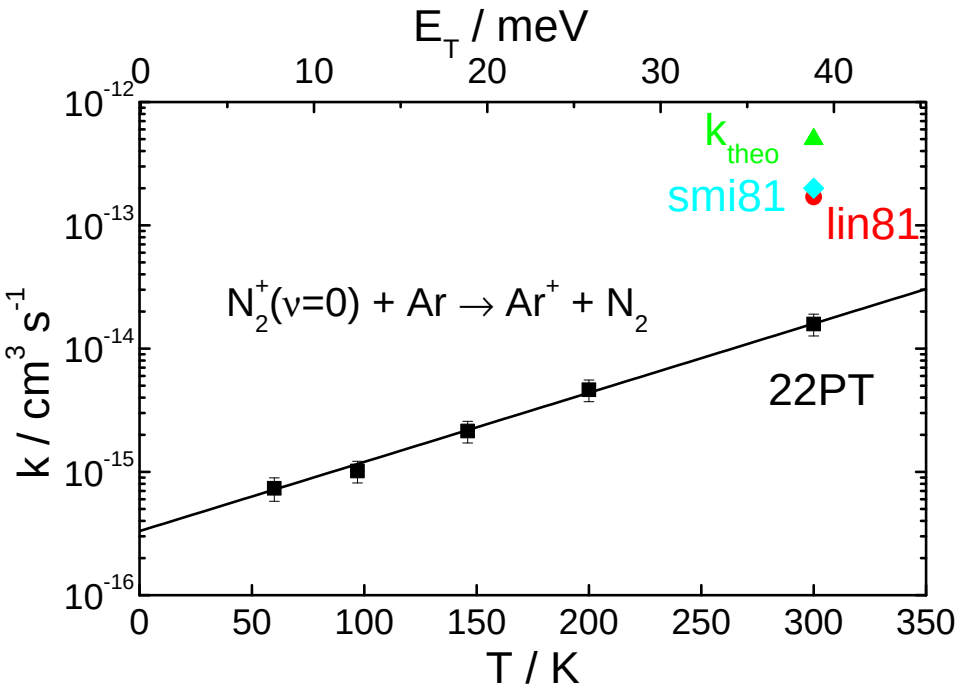

Fig. 4.3: $N_2^+(\nu = 0) + Ar \rightarrow Ar^+ + N_2$ reaction rate temperature dependence measurement (22PT), the temperature variable SIFT [smi81], DRIFT apparatus [lin81], and expected value (K_{theo}) based on the Langevin rate, all for for 300 K. The mono-exponential decay (solid line) points out to the presence of only one product ion - $N_2^+(\nu = 0)$.

A striking difference can be observed between our reported 300 K reported and those obtained in earlier experiments [smi81, lin81], with one order of magnitude of difference between them. This difference might indicate that these first experiments suffered a contamination of $N_2(\nu > 0)$.As pointed out before, the fact that we reset our experiment, letting all excited N_2^+ states to react and then extracting all produced Ar^+ ions, makes this experiment, more reliable.

4.3 The Ar^+ + N_2 reaction

4.3.1 Previous experiments

Viggiano et al. [vig93] measured rate constants for the reaction of $Ar^+(^2P_{3/2})$ with N_2 as a function of N_2 vibrational temperature (300 to 4700 K) for a rotational and translational temperature of 300 K, showing that its influence in carrying this reaction is significantly more effective in comparison with the translational or rational energies. More recently, velocity map imaging of ion-molecule reactive scattering technique indicates, that for relative collision energies of 0.6 and 2.5 eV for the same reaction, the dominant product channel corresponds

to $N_2^+(\nu' = 1)$ and around 0.8 eV the largest fraction is found to populate $\nu' = 2$ [mik06].

Once again, such studies are in their majority done in a relatively high kinetic energy range, leading to a limited amount of data available for lower energies. This fact limits a better understanding of this system reaction dynamics.

Based on a already published figure [ger08a], Fig. 4.4 is a compilation of several experiments for determining the rate reaction over a wide energy range. The langevin limit for the rate coefficient for this reaction, according to Eq. 2.8 is $k_L = 7.6 \times 10^{-10}$ cm^3 s^{-1}. One can observed that above 100 meV, the several experiments are in good agreement, namely: the Merged beam data and Guided Ion Beam (GIB) technique [wic94], the temperature variable DRIFT tube [vig93] and the flow tube [smi81].

Below 100 mV, discrepancies arise. While the merged beam maintains a value of approximately 2×10^{-11} cm^3 s^{-1} for the rate reaction, the DRIFT and flow tube experiments indicate a minimum at approximately $k_{min} = 8 \times 10^{-12}$ cm^3 s^{-1} at 0.01 eV. The CRESU experiment [reb89] followed by the free flow experiment [smi94] lead to a value close to 1×10^{-10} cm^3 s^{-1} at 0.4 meV, although still far away from the predicted Langevin rate coefficient. Observing more carefully the data from the merged beam experiment, although the reaction is exothermic by 179 meV, it proceeds very slowly at collision energies below 100 meV. One can observed that the increase of the reaction rate seems to start when approaching the 100 meV. The fact that this value is coincident with the energy needed to form N_2^+ in the first vibrational state, $\nu = 1$ [ger08a], seems to be consistent.

When looking to the remaining experiments below 100 mV, the question of the existence of a minimum arises. This minimum would be connected to the existence of the different possible reaction paths previously presented. At 300 K (corresponding to a translational energy $E_T \approx 40$ meV), the simultaneous presence of Ar^+ in both spin states in a reaction means that several channels are energetically allowed (Eq. 4.2, 4.4, and 4.5) and channel 4.3 can also proceed at a significant rate. Nevertheless, the presence of the excited $Ar^+(^2P_{1/2})$ in the free flow experiment is refuted by the authors based on already existing experimental evidences. They argued that reaction of N_2 with $Ar^+(^2P_{3/2})$ proceeds at a rate three times faster then with $Ar^+(^2P_{1/2})$ together with the linearity over more than two decades in Ar^+ decay, indicating the presence of only a single reacting species. By excluding $Ar^+(^2P_{1/2})$ from the system, we are confronted with the two remaining possibilities based on $Ar^+(^2P_{3/2})$: the exoergic reaction leading to the formation of $N_2^+(\nu = 0)$ and the endoergic formation of $N_2^+(\nu = 1)$.

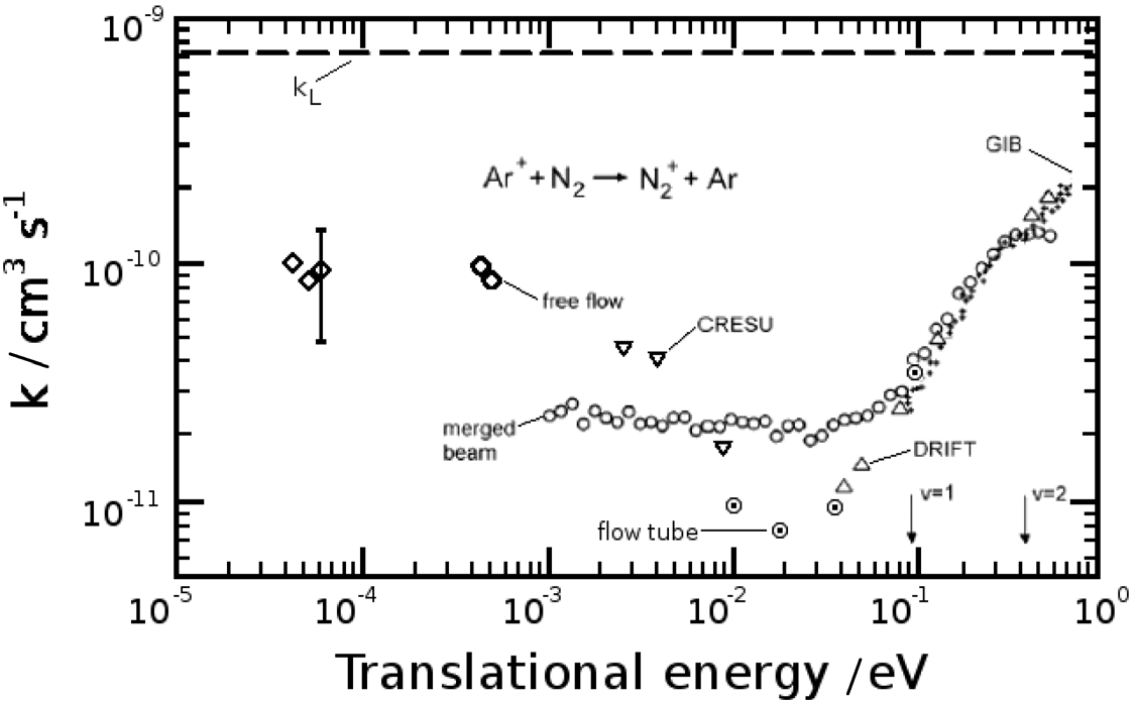

Fig. 4.4: Energy dependence of the effective rate coefficients for the exothermic charge transfer reaction $Ar^+ + N_2 \rightarrow N_2^+ + Ar$. Merged beam data (○) and Guided Ion Beam (GIB) technique (+) [wic94], temperature variable DRIFT tube (△) [vig93], free jet (◊) [smi94], CRESU experiment (▽) [reb89], flow tube (⊙) [smi81] and the line is the Langevin limiting rate coefficient. Above 100 meV the several experiments (GIB, DRIFT and merged beam) agree in the increase of the rate reaction with the increase of energy, which is coincident with the energy needed to form N_2^+ in the first vibrational state, $\nu = 1$. Below this value, the flow tube point to a minimum of the rate reaction rate to be approximately $k_{min} = 8 \times 10^{-12}\,cm^3\,s^{-1}$ at 0.01 eV.

Finally, at lower temperatures, the increase of the rate coefficient may be taken as an indication that the longer lifetime of the collision complex allows for non–adiabatic transitions, as already pointed out in published articles over similar systems such as $NH_3^+ + H_2 \rightarrow NH_4^+ + H$ [ger93]. Knowing of how much is this increase is still an open question. This reaction rate, towards lower temperatures, was measured with different techniques: flow tube, CRESU and free flow and they seem to point out to its stabilization around $10^{-10}\,cm^3\,s^{-1}$ at 0.5 meV.

The N_2 rotational states

This increase of the rate coefficient for the $Ar^+ + N_2$ reaction towards lower temperatures may be connected to the presence of specific N_2 rotational states. Similar assumptions have been recently pointed out, but for for the $CH^+ + H \rightarrow C^+ + H_2$ reaction [meh09].

The rotational energy levels of a linear rotor, such as the N_2 molecule can be

determined by:

$$E_J = BJ(J+1) - D_J J^2 (J+1)^2, \tag{4.8}$$

where the rotational constant ($B = 1.99824\,\mathrm{cm}^{-1}$) and the centrifugal distortion constant ($D_J = 5.8 \times 10^{-6}\,\mathrm{cm}^{-1}$) were taken from the NIST data base [lin05]. For comparison, the values for the N_2^+ ion are 1.92238 and 5.9E-06 respectively [bac94].

N_2 may occupy rotational states with even J if its nuclear spins are paired (*para*), and odd J states only if its nuclear spins are parallel (*ortho*). In general, the the ratio for the numbers of ways of achieving states of odd and even J, for a homonuclear diatomic molecule with nuclei spin I, can be found by [atk02, pg. 511]:

$$\frac{\text{Number of ways for odd } J}{\text{Number of ways for even } J} = \begin{cases} (I+1)/I & \text{for half-integral spin nuclei} \\ I/(I+1) & \text{for integral spin nuclei} \end{cases} \tag{4.9}$$

For N_2, with $I = 1$, the ratio is 1:2. In this case, the partition functions are:

$$Q_{even} = \frac{2}{3} \sum_{J_{even}} (2J+1) e^{\frac{hcE_{J_{even}}}{kT}} \tag{4.10}$$

and

$$Q_{odd} = \frac{1}{3} \sum_{J_{odd}} (2J+1) e^{\frac{hcE_{J_{odd}}}{kT}} \tag{4.11}$$

Tab. 4.1 shows the rotational energies (E_J) from $J = 0$ up to 8 and population of the several rotational states for different temperatures taking into account the nuclei spin contribution, while in Fig. 4.5 the rotational states population in a 1 - 10000 K range temperature is plotted.

Tab. 4.1: Results for the N_2 rotational population distribution for different temperatures when taking into account the nuclei spin $I = 1$.

J	E / meV	P / %				
		1 K	5 K	50 K	200 K	300 K
0	0.00	66.66666	57.52951	7.55513	2.61575	2.19502
1	0.50	33.33333	33.08755	10.19286	4.28800	3.74355
2	1.49	0.00001	9.13191	26.75357	11.99801	10.36186
3	2.97	0.00000	0.24577	13.38327	8.66570	7.93674
4	4.95	0.00000	0.00525	21.53136	17.65980	16.30972
5	7.43	0.00000	0.00001	7.47161	10.51326	10.49615
6	10.40	0.00000	0.00000	8.77981	18.59366	19.08093
7	13.87	0.00000	0.00000	2.28560	9.86638	11.15689
8	17.83	0.00000	0.00000	2.04680	15.79944	18.71914

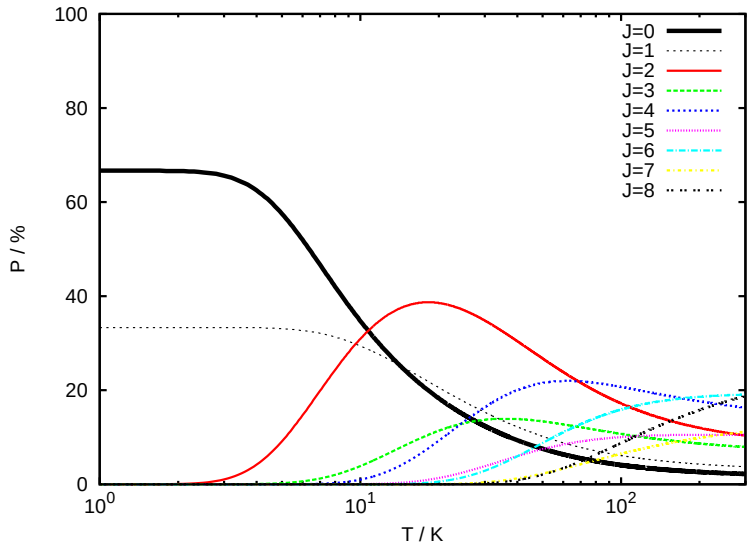

Fig. 4.5: Results obtained for the N_2 rotational states population for J = 0 up to 8. Even states of J are forbidden for ortho-nitrogen.

The relatively small difference between the several rotational states is explained by the rather small value of B, inversely proportional to the molecule moment of inertia. One can observe that only below 10 K, we have as main populated states J = 0,1 and 2. At this temperature J = 0 corresponds to approximately 60 %. Furthermore, only below 2 K we have J = 1 as the main populated state.

In an effort to clarify this several aspects, we have aimed our attention to the study of the reverse reactions (Eq. 4.1) of the $(Ar - N_2)^+$ system based on different and complementary methods in a temperature range between 300 and 30 K. Measurements and results will be presented in the following section.

4.3.2 Ar^+ + N_2 measurements

Four methods were used in order to study the backward reaction (Eq. 4.1): 1 - Fixed temperature reaction rate measurement with standard effusive neutral gas; 2 - During the down-cooling or warming up cycle; 3 -Through condensation of N_2 on the walls; 4 - Cold effusive beam. In the following, a description of methods used for both reactions and respective results is presented.

Fixed temperature rate measurements

In order to compare the several results based on other techniques, rate measurements done at constant temperature were performed by following the procedure already presented in Sec. 2.3.8. These measurements were done for tem-

peratures between 300 and 100 K. Two of this measurements can be observed in Fig. 4.6. Ar (ionization energy of 15.7596 eV [lin04]) was used as precursor gas and pulsed helium (number density $\approx 1.5 \times 10^{13}$ cm^{-3}) as buffer gas. After trapping in the 22PT the Ar^+ ions go through reaction with N_2 (7×10^{10} cm^{-3}). Due to the existence of H_2O background gas, H_2O^+ and H_3O^+ ions are formed. Finally, mass 29 is also formed. N_2H^+ is formed due to reaction between N_2^+ and H_2O, but also $^{15}N - N^+$, derived from the presence of the isotope ^{15}N (natural abundance of 0.368(7)% [lin05]), not being possible to distinguish between these two species.

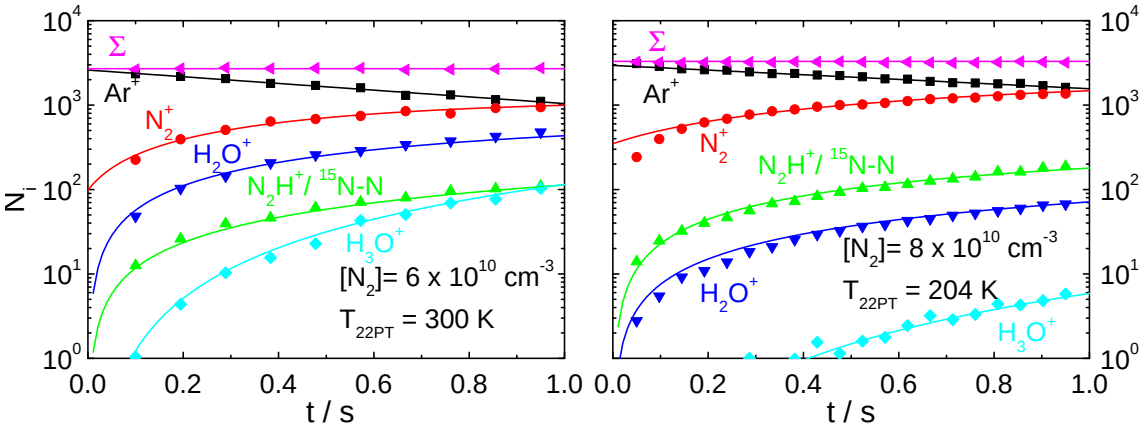

Fig. 4.6: $Ar^+ + N_2$ time dependence of primary and product ions for T_{22PT} = 204 K and 300 K. Approximately 3000 Ar^+ ions are injected into the trap initially (■) and quenched with pulsed helium buffer gas which is synchronized with the beginning of each measurement cycle (number density 1.5×10^{13} cm^{-3}), ensuring a low kinetic energy of the ions. H_2O^+(▼) and H_3O^+ (◆) are formed due to H_2O background (1.2×10^8 and 1.3×10^7 cm^{-3} for 300 and 204 K respectively). $N_2H^+/^{15}N - N$ (▲) derives from the reaction $N_2^+ + H_2O$ or from the reaction between $Ar^+ + (^{15}N - N)$. The lines represent fits of the experimental data. UMIST data base rate coefficients were used for the fitting of background reactions. The total number of ions remains constant throughout all the measurement time(◀). N_2^+ ions are formed with a rate of $k_{300} = 1.1 \times 10^{-11}$ cm^3 s^{-1} and $k_{204} = 8.3 \times 10^{-12}$ cm^3 s^{-1} (●).

In Fig. 4.7 the reaction system which was used as a base for the fitting procedure is shown. Reactions and correspondent used rate reactions are presented in Tab. 4.2.

Tab. 4.2: Reactions and reaction rate coefficients values used during the fitting procedure of the $Ar^+ + N_2$ reaction (units given in $cm^3\,s^{-1}$).

k_1	$Ar^+ + N_2$	$\rightarrow$	$N_2^+ + Ar$		
k_2	$Ar^+ + H_2O$	$\rightarrow$	$H_2O^+ + Ar$	1.8×10^{-09}	[mau78]
k_3	$Ar^+ + (^{15}N - N)$	$\rightarrow$	$(^{15}N - N)^+ + Ar$		
k_4	$H_2O^+ + H_2O$	$\rightarrow$	$H_3O^+ + HO$	3.0×10^{-09}	[woo07]
k_5	$N_2^+ + H_2O$	$\rightarrow$	$H_2O^+ + N_2$	2.3×10^{-09}	[woo07]
k_6	$N_2^+ + H_2O$	$\rightarrow$	$N_2H^+ + OH$	5.0×10^{-10}	[woo07]

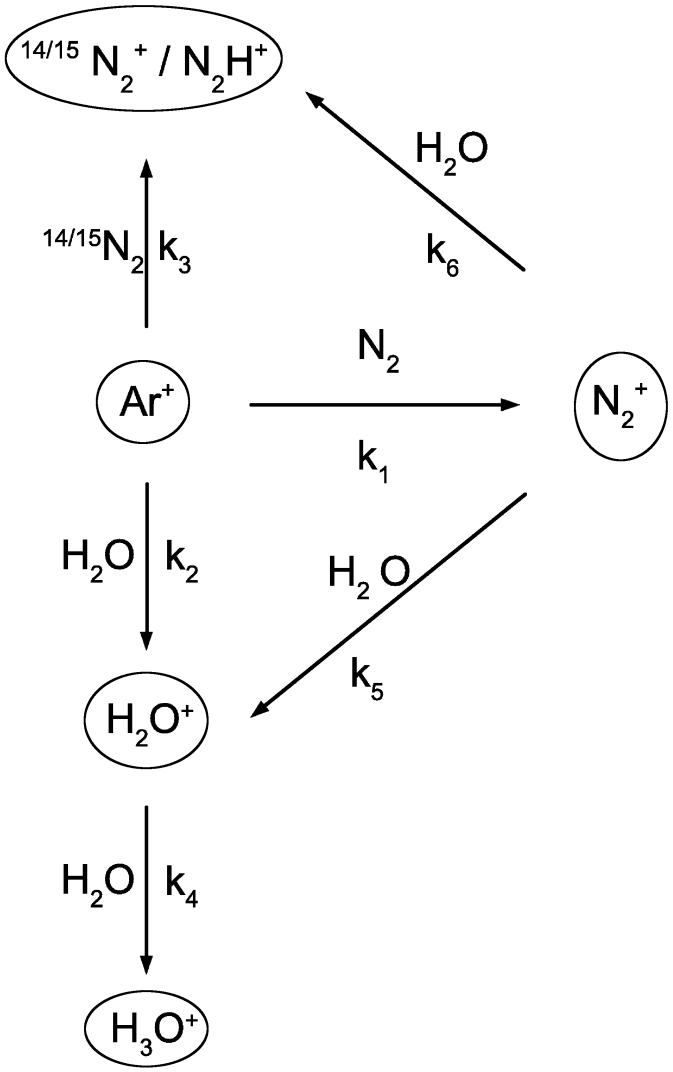

Fig. 4.7: $Ar^+ + N_2$ reaction scheme inside the 22PT including H_2O background and taking into account the $^{14/15}N$ natural isotope of nitrogen.

In Fig. 4.8 is presented the reaction rate temperature dependence for Ar^+ + N_2, reaching a minimum of $6.7 \times 10^{-12}\,cm^3\,s^{-1}$ at 200 K.

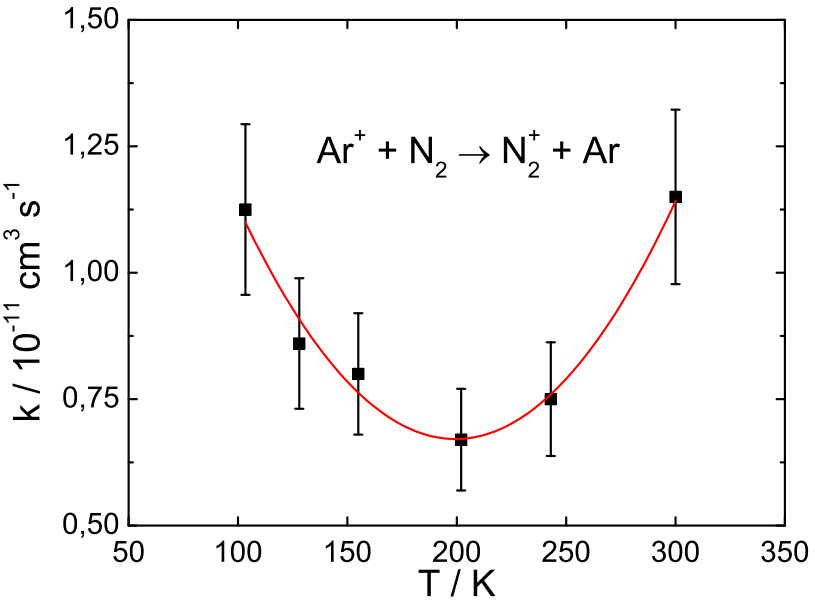

Fig. 4.8: Ar^+ + N_2 temperature dependence measurements between 100 and 300 K with a minimum at 200 K corresponding to a rate reaction of $6.7 \times 10^{-12}\,cm^3\,s^{-1}$.

Measurements during the down-cooling cycle

Based on Eq. 2.5, the reaction rate coefficient can be determined based on the measurement of the time constant decay (τ). In the present case:

$$\tau = \frac{t_2 - t_1}{\ln([Ar^+_{t_1}]/[Ar^+_{t_2}])} \tag{4.12}$$

As can be observed in Fig. 4.9, this procedure was based on repeated measurements, while the 22PT temperature was continuously decreasing from 300 to 78 K. The Ar^+ ions are introduced in the 22PT as already described and a constant flow of N_2 is introduced in to the trap leading to an initial value of $4.3 \times 10^{10}\,cm^{-3}$ number density along with pulsed helium ($\approx 1 \times 10^{13}\,cm^{-3}$).

A Savitzky-Golay smoothing method to the 22PT temperature decrease was applied, with an overall deviation of less then 2%. An evaluation of the N_2 number density was made by making use of Eq. 2.6.

By making an average for each each 5 K interval, the reaction rate coefficient was then calculated according to:

$$k = \frac{1}{\tau/s^{-1}[N_2]/cm^{-3}}. \tag{4.13}$$

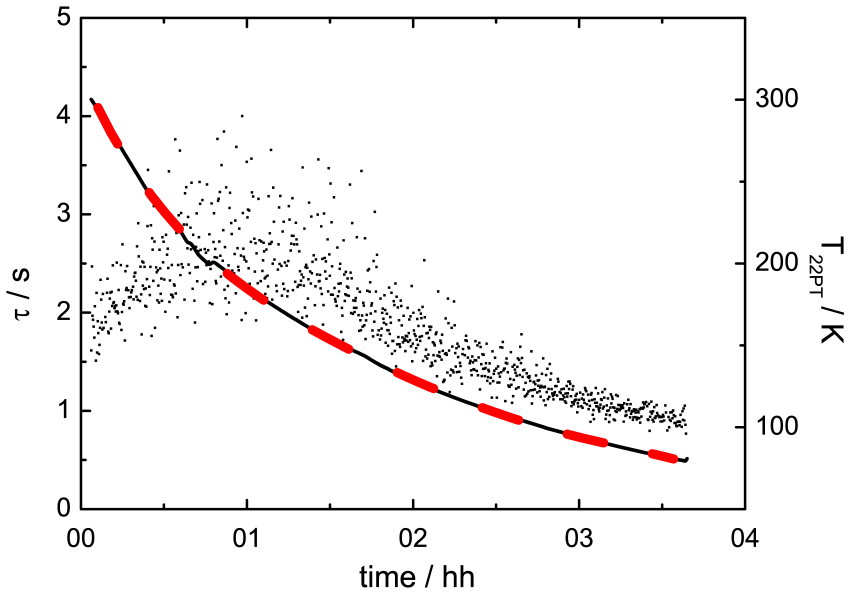

Fig. 4.9: $Ar^+ + N_2$ time constant decay (■ - left axis). It is also represented on the right axis the cooling down of the 22PT obtained through a silicon diode (Lakeshore DT-470) coupled to the walls of the trap, over which a Savitzky-Golay smoothing method was applied (— and - - - respectively).

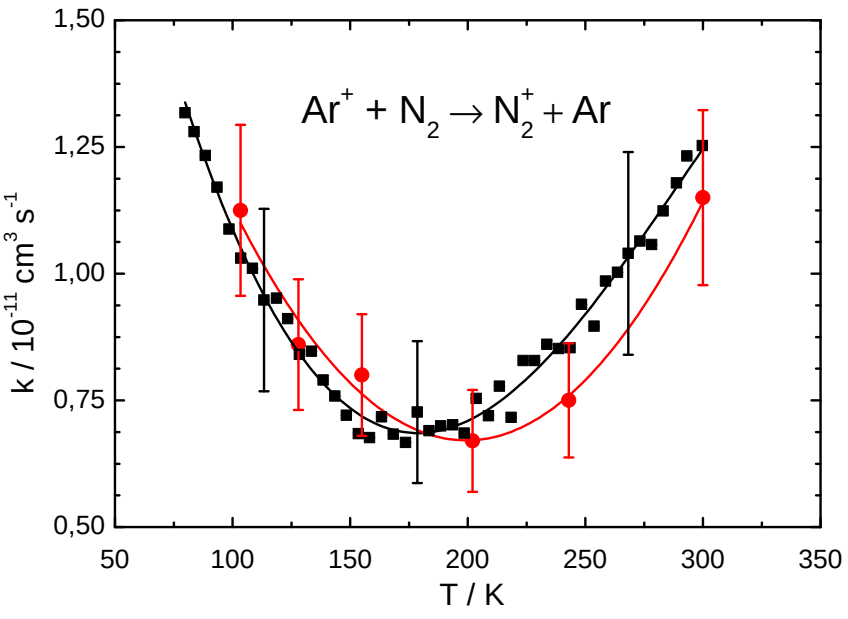

Fig. 4.10: Temperature dependence of the rate coefficient for the reaction $Ar^+ + N_2$ (■) . $[N_2] = 4.3 \times 10^{10}\,cm^{-3}$. $k_{min} = 6.8 \times 10^{-12}\,cm^3\,s^{-1}$ for $T_{22PT} = 180\,K$. For comparison, data obtained through standard procedure is shown. (●) already presented in section 4.3.2.

Although this procedure has the advantage of being faster, we point out the fact that this measurement we did not account for the presence of parallel and secondary reactions. This slightly increases the error for the determination of the rate coefficient for each point, specially for the higher temperatures, where the presence of water is more preponderant. Comparing with previous measurements presented above in Sec. 4.3.2, we estimate the total error to be approximately 25%. Nonetheless, as can be observed in Fig. 4.10, both measurements are good agreement. Although the minimum rate is similar to what was obtained before $k_{min} = 6.8 \times 10^{-12}\,\mathrm{cm^3\,s^{-1}}$, the temperature at which it happens is slightly shifted (180 K), but representing only 10% deviation, thus, considered acceptable. Undoubtedly the strong point of this technique is the possibility of measuring, in a very short time, rate coefficients over a wide range of temperatures with reliable results. In the present case, is now undeniable the existence of a minimum in this reaction as already mentioned, fact which will be discussed further on.

Measurements based on condensation of N_2

As it was stated before, one main set-back in these kind of trap experiments is the condensation of neutral species on the surrounding walls. Fortunately, this effect can also be used in our advantage. A 22PT is able to operate with very low number densities of target gas, and this number can be reached based only on the resulting vapor pressure at low temperatures, therefore extending the possible temperature range further down.

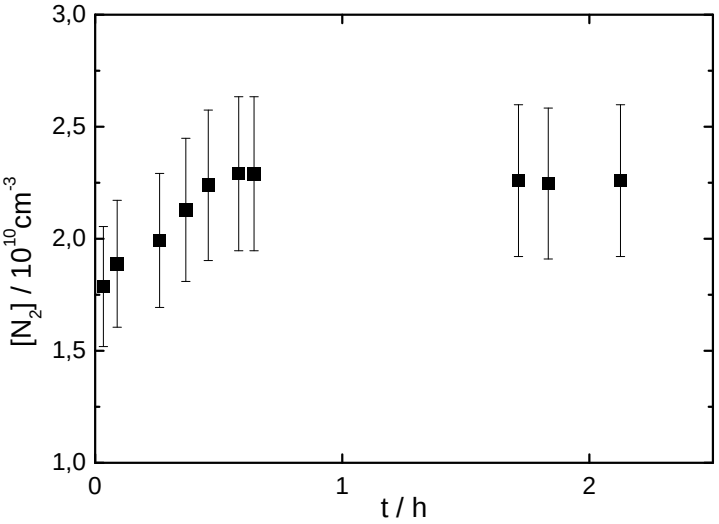

Fig. 4.11: The reaction $He^+ + N_2$ has been used to follow the time dependence of the nitrogen density in the trap at a temperature of 30 K. The gas flow has been hold constant at $6.8 \times 10^{-5}\,\mathrm{mbar\,l\,s^{-1}}$. It is shown that it takes less then 45 minutes to achieve stable conditions and that they are stable within the following hour.

Fig. 4.11 illustrates that one can operate a trap at 30 K and simultaneously maintain a nitrogen number density of $2.2 \times 10^{10}\,cm^{-3}$ by leaking a stationary gas flow of $6.8 \times 10^{-5}\,mbar\,l\,s^{-1}$ into the trap. In this test, the reaction $He^+ + N_2$, already mentioned in Sec. 2.3.9 has been used to follow, in situ, the time dependence of the nitrogen density. The measurement shows that it takes less than 1 hour to reach stationary conditions. At the beginning of the experiment, the pumping speed of the cold clean surfaces maintains a rather low stationary density. With increasing time, saturation reduces the sticking efficiency.

After N_2 number density was determined, standard procedure was used in order to study the $Ar^+ + N_2$ reaction. Two measurements based on this technique are shown in Fig. 4.12. The results for the rate coefficient, 1.3 and $3.0 \times 10^{-11}\,cm^3\,s^{-1}$ (±25%) at 66 and 30 K respectively, are in accordance within the error bars, with previous ones obtained by other groups, clearly indicating an increase in the rate reaction for this system towards lower temperatures.

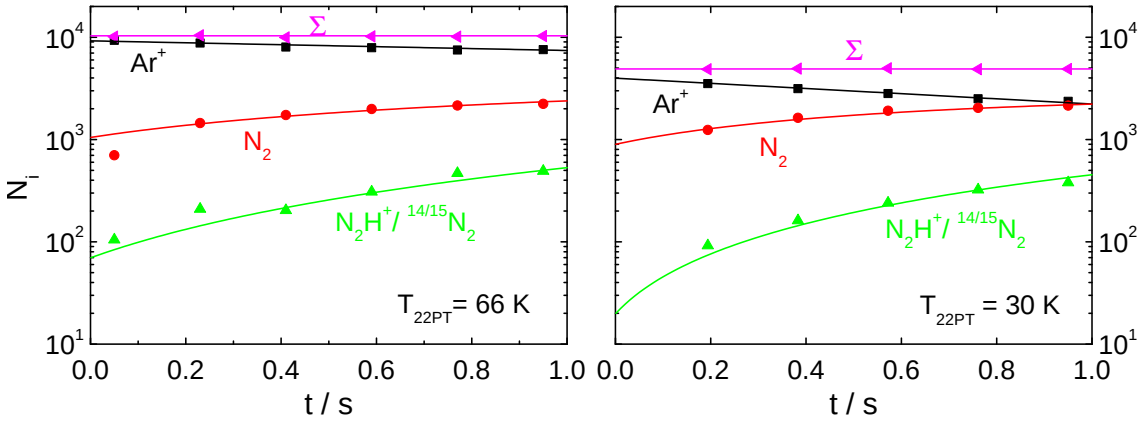

Fig. 4.12: Measurements done over a constant N_2 flux obtained through 66 K and 30 K cold surface saturation of the 22PT with respective N_2 number densities of 1.7 and $2.0 \times 10^{10}\,cm^{-3}$. This densities were obtained through chemical probing based on the $He^+ + N_2$ reaction. The rate reactions obtained were $k_{66} = 1.3 \times 10^{-11}\,cm^3\,s^{-1}$ and $k_{30} = 3 \times 10^{-11}\,cm^3\,s^{-1}$ (±25%).

A cold effusive beam of N_2

A final procedure, was based on the reaction of the trapped Ar^+ ions with a cold effusive beam of N_2, which was already introduced in Sec. 2.4. The measurement was done with 22PT temperature of $T_{22PT} = 40$ K. The same was applied to the accomodator temperature. The translational temperature of the N_2 beam (by means of Time of Flight) and its number density (based on the $He^+ + N_2$ reaction, Fig. 2.18) were characterized. The evaluation of the reaction rate for the beam (k_b) was then dependent on the measurement of the reaction with background (k_{bg}), and reaction with background and beam (k_{bgb}) Fig. 4.13. The control over the beam was made by means of a mechanical shutter, lo-

cated immediately before the 22PT. Due to the fact that this two N_2 contributions (the beam and the background) are at different temperatures and with different space distributions, their respective rates k_{bg} and k_{bgb} have to be considered as independent from each other.

Keeping in mind the $1.0 \times 10^9\,cm^{-3}$ number density for the background and $5.0 \times 10^8\,cm^{-3}$ for the beam, both previously determined (Sec. 2.4.2), and according to Eq. 4.14:

$$[Ar^+] = [Ar^+]_0\, e^{-(k_{bg}[N_2]_{bg}+k_b[N_2]_b)t}, \tag{4.14}$$

the resulting reaction rate coefficient for the beam after fitting was $4\times10^{-11}\,cm^3\,s^{-1}$. This result does not take into consideration the isotope contribution.

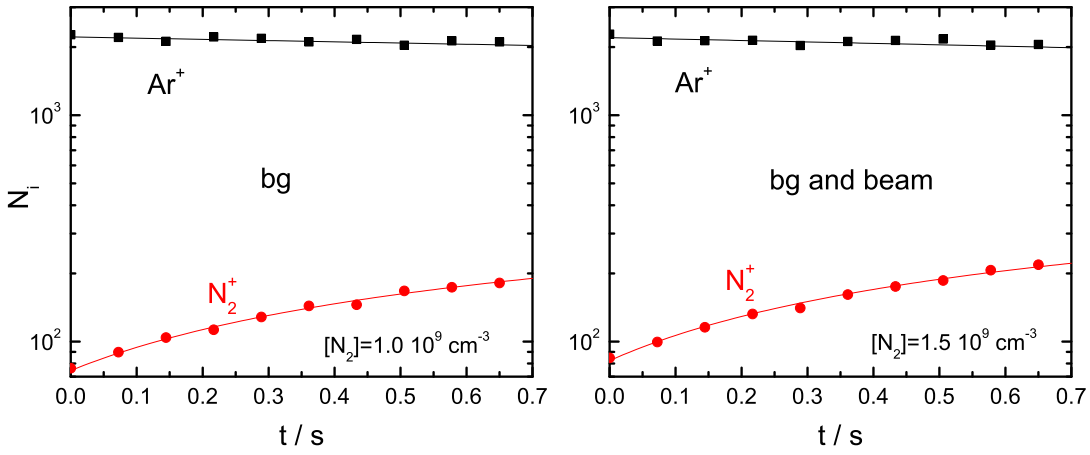

Fig. 4.13: Measurements based on 22PT background (bg) and by adding a N_2 cold effusive beam (bgb). The average number of ions, N_i, trapped and formed for each iteration, is plotted as a function of the storage time t. The solid lines are solutions of an adequate rate equation system leading to the rate coefficients $k_{bg} = 8.7 \times 10^{-11}\,cm^3\,s^{-1}$ and $k_{bgb} = 1.1 \times 10^{-10}\,cm^3\,s^{-1}$, respectively.

Compared results

Fig. 4.14 presents a compilation of the results obtained based on the several setups. The experiments based on the 22PT technique, when seen has a whole, show a strong consistency. In the $100-300\,K$ region, the measurements done based on standard procedure, not only are overlapped with the continuous time measurements with no significant deviation (approximately 10% as already mentioned), but also, both of them are in agreement with the flow tube data. This fact reinforces the notion of the existence of the minimum in this temperature range (located between 180 and 200 K). The values measured, based on the N_2 wall saturated 22PT procedure at 66 and 30 K, besides extending the temperature range of the previous procedures with minor deviation between them, are also in very good agreement with the CRESU experiment. Finally, the

measured point with the CEB-22PT setup, even if it is still a technique with a considerable room for improvement, with its slightly increased estimated error and higher final value, is still, within the error bars, reinforcing this tendency of the increased rate with the lower temperatures.

Also present in Fig. 4.14 is the $N_2(J = 0)$ rotational state population. Its maximum was adjusted to the expected rate coefficient in the Langevin limit, while its minimum was manually adjusted. The outcome points out to a preponderant role of the rotational states in the reaction rate coefficient for the lower temperature regime.

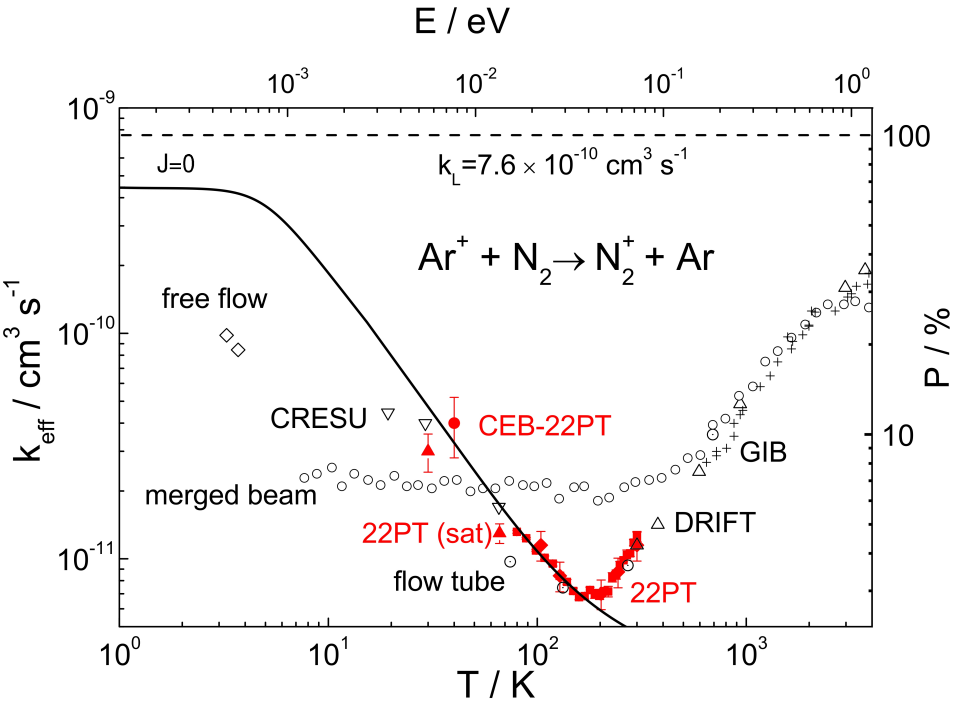

Fig. 4.14: Compared $Ar^+ + N_2$ rate reaction studies based on the 22PT (●, ■ and ◆) and CEB-22PT (▲) experiments and previous measurements: Merged beam data (○), Guided Ion Beam (GIB) technique (+) [ger08a], temperature variable DRIFT tube (△) [vig93], free jet (◊) [smi94], CRESU experiment (▽) [reb89] and the flow tube (⊙) [smi81]. It can be observed the decrease, minimum and increase, while moving from higher to lower temperatures. On the right axis is plotted the population in percentage for the rotational state J=1, where its maximum is adjusted to be coincident with the Langevin limit for this reaction $k_L = 7.6 \times 10^{-10}$ cm^3 s^{-1}, while its minimum was manually adjusted.

Reaction enthalpy and entropy determination

Following the same procedure as described in Sec. 3.3, a van't Hoff plot, a least squares fit to the plot of $-\ln K_{eq}$ vs 10^3/T (where $K_{eq} = k_f/k_r$), and the forward reaction and reverse reaction are already determined in Eq.4.1) would be able

to give us an insight on the reactions enthalpies and entropies.

It can be observed in Fig. 4.15 the expected nonlinear behaviour, due to the temperature dependency of the reaction rate coefficient of the reverse reaction. Two reaction enthalpies were obtained from the two distinct slopes: 0.5 kJ mol^{-1} in the lower temperature region and 3.6 kJ mol^{-1} in the higher region. The reaction ΔH and ΔS are highly temperature dependent, therefore, failing to comply with the method's criterion in this temperature range. In such a case case, it is not possible to extract any credible conclusion from this experiment.

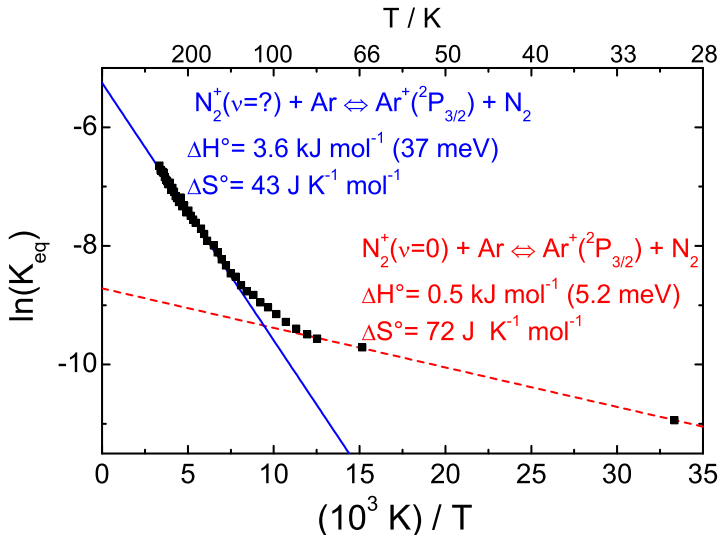

Fig. 4.15: The van 't Hoff plot for the N_2^++Ar $\rightleftarrows$ Ar^++N_2 system equilibrium constant ($K_{eq} = k_f/k_r$), obtained based on the independently forward and reverse temperature reaction rates measurements previously presented (Fig. 4.3, 4.15 and 4.10).

Lindinger et al. measured directly the equilibrium constant K_{eq} for the Ar^+ + N_2 $\rightleftarrows$ N_2^+ + Ar (approximately from 300 to 3000 K). From a linear van't Hoff plot they derived an enthalpy value of 0.15 eV. This value was then related to the energy difference of 0.183 eV between the lowest states of Ar^+ and of N_2^+ [lin81]. It was argued that in order to attribute a meaning to a Van't Hoff plot, taken from drift equilibrium data, "it is necessary that the relative kinetic energies between N_2^+ and Ar be very similar to those of Ar^+ and N_2". Furthermore, "owing to fortuitous mobility values of Ar^+ and N_2^+ in Ar this condition is met to some extent". Such a procedure, if possible to be considered valid in their higher temperature range, due to the better determined molecules energetic states, is not allowed in our case.

4.4 Conclusion

During this work, the forward (k_f) and backward reaction (k_r) of the $(Ar+N_2)^+$ system were studied in a 22PT apparatus by making use of several complementary techniques and approaches.

In the forward reaction, Eq. 4.1, the main question from the experimental point of view, was to avoid the already formed Ar^+ ions, due to the fast reaction of argon with the first rotational excited state of nitrogen $N_2^+(\nu = 1)$. This was overcome by making use of a momentary reduction of the 22PT amplitude (V_0). The initially formed Ar^+ ions were able to evade the 22PT, while the remaining nitrogen ions with rotational ground state $N_2^+(\nu = 0)$, were in their majority kept within the 22PT boundaries. From this point they reacted with argon gas, but with almost no Ar^+ background signal. At 300 K, our measured rate $1.6 \times 10^{-14}\,cm^3\,s^{-1}$ is one order of magnitude below compared with previous measurements [lin81, smi81]. But, it is our point of view, that this experiments with 30 years of existence, might have suffered from some problems. One of them could be related to the difficulty in achieving a nitrogen excited rotational states free environment, or some possible N_2 contamination.

The backward reaction from Eq. 4.1 presents itself as a more interesting system with its competing channels for the reaction rate to proceed. Several previous experiments agreed among each other for the higher temperatures (above 700 K) but differ for the lower temperature regime. The existence of a minimum for the absolute rate reaction and its steep increase below 100 K were still in need for a confirmation.

With a minor deviation from the fixed temperature rate measurements, the continuous time measurement gave a clear picture of the reaction temperature dependence in the 300 to 70 K temperature range. In such conditions we obtained a minimum for this reaction of $(6.8 \pm 20\%) \times 10^{-12}\,cm^3\,s^{-1}$ at $180\,K \pm 15\%$. This is a fast and reliable method for analysing similar systems, as long as the temperature measurements are not in the proximity of phase transitions.

In relation to the lower temperature range, below nitrogen condensation point, both measurement procedures, the one obtained based on the condensation of N_2 in the 22PT walls at 66 and 30 K, and the one based on the cold effusive N_2 beam at 40 K, clearly indicate an increase on the absolute rate reaction, fitting (within the error bars) between the free flow, CRESU and flow tube experiments.

In this reaction it was possible to observe the competition between the two exit channels $Ar + N_2^+(\nu = 0)$ and $Ar + N_2^+(\nu = 1)$, resulting in the measured minimum. Our studies also point out to the possible role of the $N_2(J = 0)$ rotational state in the reaction rate coefficient for lower temperatures. Based on some of the methods presented in this work, a new set of measurements at lower temperatures would be able to give a more definite answer.

Chapter 5

Conclusion

5.1 Summary

Besides the questions relative to the two systems presented here, this work was one more step forward to cement the position of the 22PT, as one of the most important tools in modern ion chemistry. Its flexibility, due to its modular construction, its consistency in the several obtained results, although based in different methods, its broad range of applications, not only in our laboratory but already throughout several locations in the world, reinforces the idea that, despite being relatively new, it will continue to give valuable support for many experimentalist and theoreticians in their quests for many years to come.

With the work based on the protonation of methane, presented in Chapter 3, the results demonstrate that the 22-pole trap technology can reach defined stationary thermal equilibrium conditions, and be used for determination of equilibrium constants. They were obtained through two different methods. The first one consisted in independently measuring the forward and backward reaction rate and determining the ratio between the two rates. The second, was based on directly measuring the relative ions and neutral gas concentrations, when a relative thermodynamic equilibrium was achieved. Both methods agree between each other within the experimental error. Measurements were made in the 120 to 300 K range. Based on a van't Hoff plot, the outcome for the reaction enthalpy was $-6.5 \pm 0.5\,\mathrm{kJ\,mol^{-1}}$, and for the entropy change ($\Delta_r S°$) was $(-2.0 \pm 1.0)\,\mathrm{J\,mol^{-1}\,K^{-1}}$. Finally we obtained the proton affinity values for methane of $PA(CH_4) = (534 \pm 2)\,\mathrm{kJ\,mol^{-1}}$, and for carbon dioxide $PA(CO_2) = (540 \pm 2)\,\mathrm{kJ\,mol^{-1}}$ in close agreement with previous studies.

In relation to the more challenging $(Ar\text{-}N_2)^+$ system, the forward (k_f) and backward reaction (k_r) were also determined.

The forward direction, after avoiding the undesired Ar^+ ions due to the presence of the first rotational excited state of nitrogen ($N_2^+(X, \nu = 1)$, was measured and was obtained at room temperature $k_f = 1.6 \times 10^{-14}\,\mathrm{cm^3\,s^{-1}}$, one order of magnitude bellow previous measurements. The arguments for such a difference

are related to the difficulty in achieving an environment free of nitrogen excited rotational states or possible N_2 contamination, in an experiment with 30 years of existence. The reverse direction was an excellent opportunity to try out the several possibilities offered by the 22PT and to measure one reaction under different methods. The several methods presented here were: measurement during the down-cooling or warming up cycle, and the three constant temperature measurements, from standard effusive neutral gas, through condensation of N_2 on the walls, and based on a cold effusive beam. All agreed with previous measurements. A minimum was obtained of $6.8 \times 10^{-12}\,cm^3\,s^{-1}$ ($\pm$20%) at 180 K ($\pm$15%).

The existence of this minimum is known to be derived from the existence of the two competing channels, $Ar^+(^2P_{3/2}) + N_2 \rightarrow N_2^+(\nu = 0) + Ar$ and $Ar^+(^2P_{3/2}) + N_2 \rightarrow N_2^+(\nu = 1) + Ar$. The steep increase for temperatures under 100 K which is also indicated in our results, is in accordance (within error bar) with free flow, CRESU and flow tube experiments. Finally, this steep increase, seems to be related with the $N_2(J = 0)$ rotational state population for the lower temperatures. Measurements below 5 K would give a more precise answer.

5.2 Outlook

Looking back, it is possible to state that there are several experiments which can be carried out based on our 22PT technology, and can be done in order to further increase our knowledge about this reactions. As already mentioned, based on a similar apparatus, the laser induced reaction: $N_2^+ + h\nu + Ar \rightarrow Ar^+ + N_2$ is of special interest [sch99], since it can be used for ion temperature determination, but measurements have not been extended to temperatures below 50 K, due to condensation of the argon gas on the surrounding walls. According to our experience, it was already observed that this effect can actually be used in our advantage. It was demonstrated that the door is open for a new set of measurements to be performed in cases where, the question of a target gas going through wall condensation at low temperatures, limiting the measurements temperature range, had to be previously considered. This feature re-enhances once more the potential of such rf pole traps in scientific research. The last, but maybe the most promising approach, is the coupling of a cold effusive beam with the 22PT. Already presenting very interesting results, it is now the quest to reach sub-kelvin temperatures by means of velocity selection [ger08b]. While in the previous cases, the temperature range is limited by the cold heads coupled to the 22PT, where we would be able to reach approximately 5 K, by beam velocity selection the temperatures and respective collision energies could be at least one order of magnitude less.

In relation to the systems presented here, it would be interesting, based on the CEB-22PT set-up, to determine the low temperature limiting rate value

for the $Ar^+ + N_2$ reaction, by having the nitrogen beam at such low temperatures and comparing its results with the free flow and CRESU experiments ($1 \times 10^{-10}\,cm^3\,s^{-1}$ at 4 K).

Appendices

Appendix A

H_2/D_2 TOF measurements

In Fig. A.1 can be observed the results obtained for H_2 and D_2 with a respective determination time of t_{det}= 14 and 20 μs. It follows, as expected, the square mass relation, considering the kinetic energy conservation: $\sqrt{m_2/m_1}\,t_1 = t_2$.

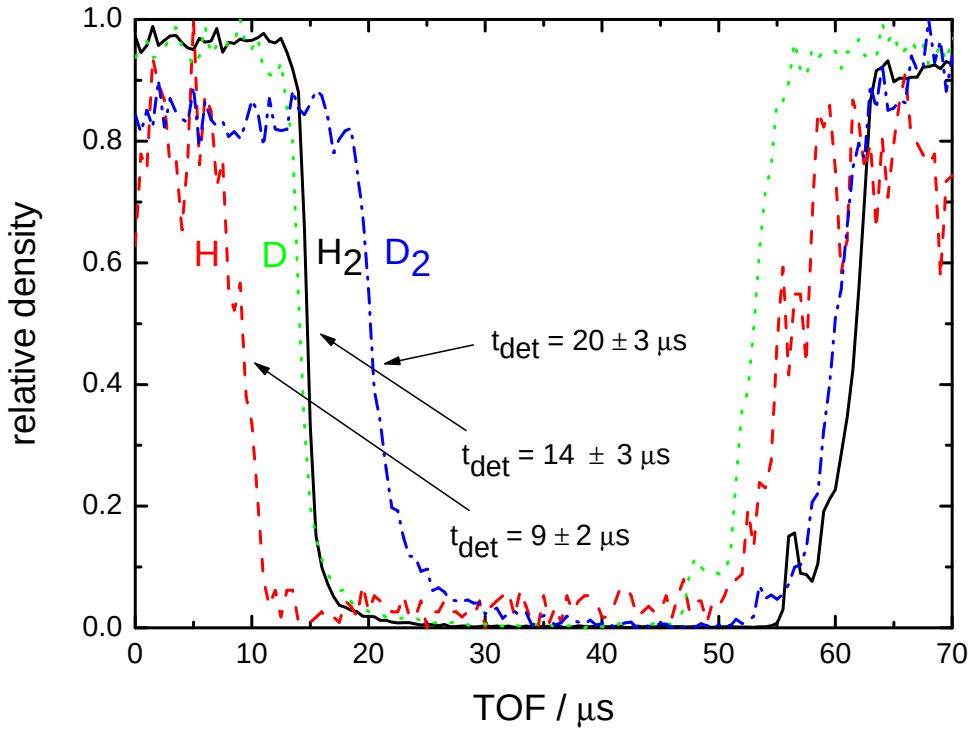

Fig. A.1: Determination of the detection time, which is the time between the ionization and the acquisition through the MCA for D_2 (— · —), H_2 (——), D (· · ·) and H (- - -).

In the case of D_2 TOF measurement observed in Fig.A.2, the CEB temperature has been set to T_{CEB} = 102 K and 11 K and with a throughput of $Q_{CEB_{D2}} = 2.5 \times 10^{-2}$ mbar l s^{-1}. The comparison of the data with the predicted Maxwell-Boltzmann distribution, reveals that the D_2 beam temperature is well coupled to the CEB chamber. Also in this case, is possible to observe a small non-thermalized contribution from the background corresponding to 244 K.

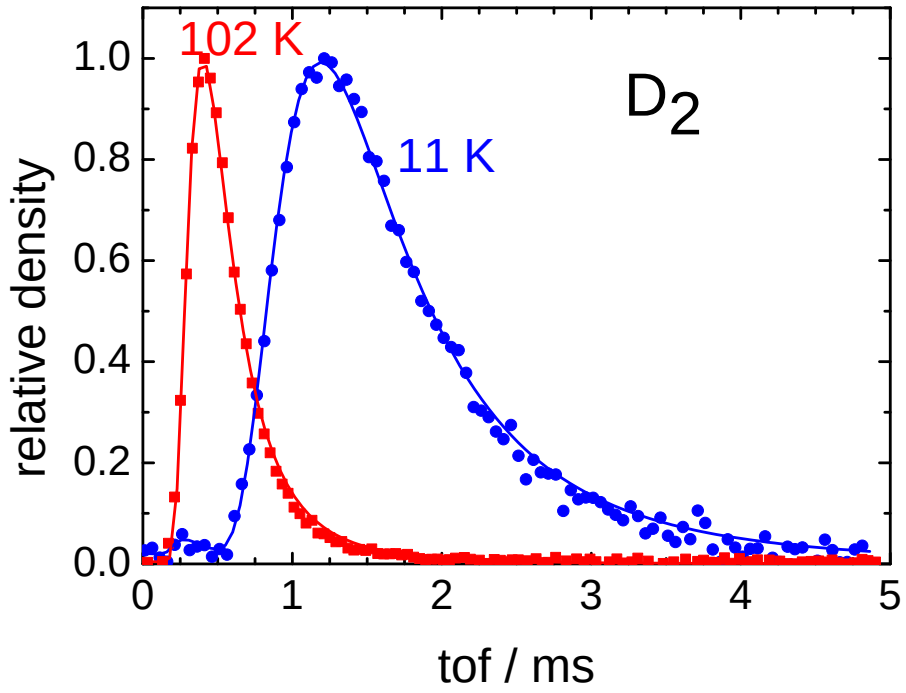

Fig. A.2: TOF distributions for D_2 atoms for T_{CEB} = 102 K - ■ and 11 K - ●. Correspondent Maxwell-Boltzmann distributions (full lines) gives (102.7 ± 0.1) K and (11.5 ± 0.1) K. It is possible to observe a small 211 K background contribution in the 11 K TOF, representing approximately 1% of the total distribution.

Appendix B

Vacuum system and nominal values of vacuum pumps

Tab. B.1: Nominal values for the vacuum pumps used in the CEB-22PT

Model	Manufactor	Pumping speed (N_2) / l s^{-1}
TPU 2200	Pffeifer	2200
TPU 240	Pffeifer	230
TV 340M	Leybold	340
TPD 011	Pffeifer	10
TMU 200MP	Pffeifer	180
TR DUO 016B	Pffeifer	5
MVP 015-4	Pffeifer	0.25
SH-110	Varian	1.5

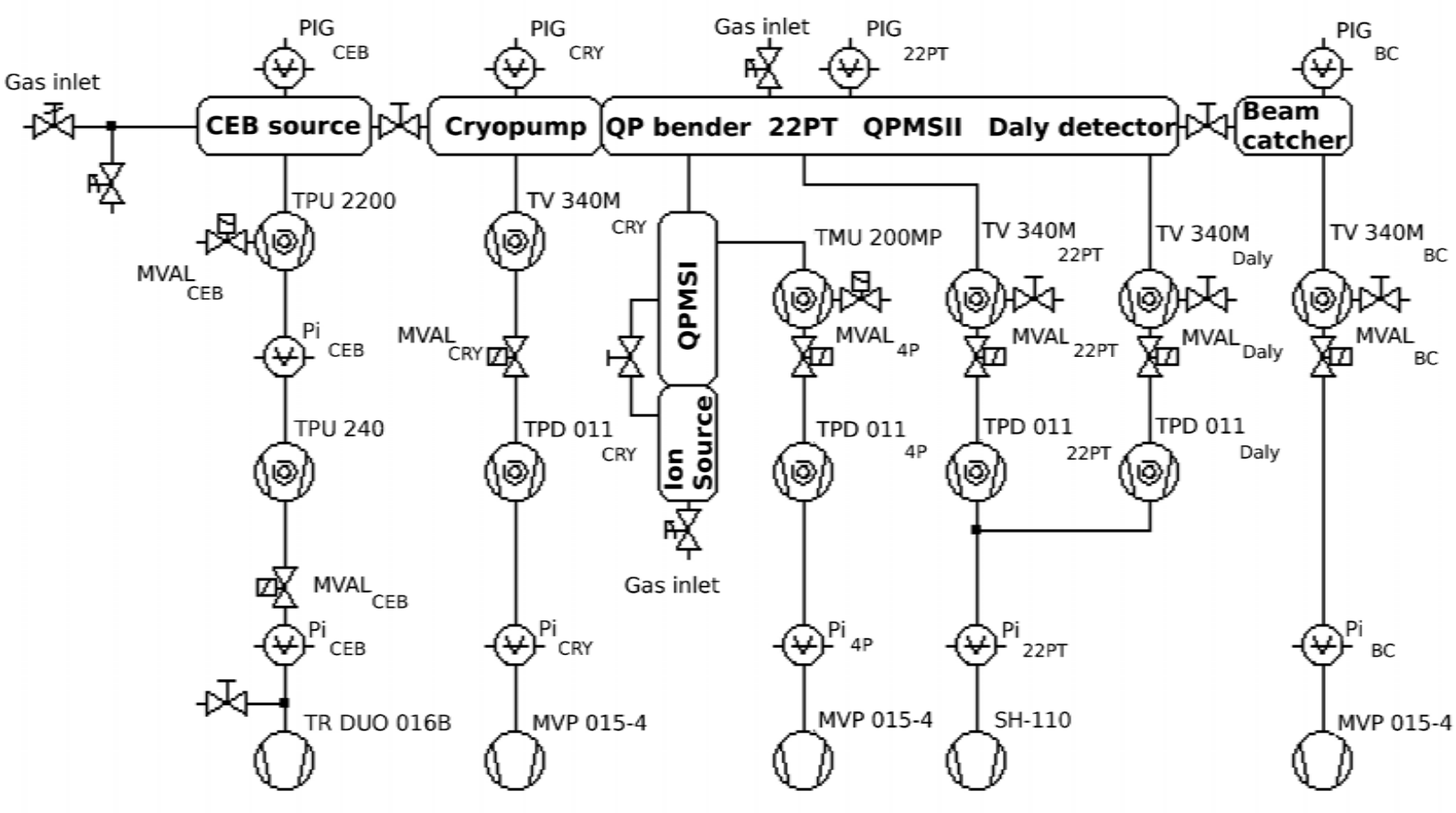

Fig. B.1: Vacuum system of the CEB-22PT apparatus. Nominal values of the pumping speeds are given in appendix

List of Figures

List of Tables

Bibliography

[ada76] N. Adams and D Smith. Selected Ion Flow Tube (SIFT) - Technique for studying ion-neutral reactions. *International Journal of Mass Spectrometry and Processes*, 21(3-4):349–359, 1976. [cited at p. 12, 32, 33]

[ada77] N. G. Adams and D. Smith. Reactions of hydrocarbon ions with hydrogen and methane at 300K. *Chemical Physics Letters*, 47(2):383–387, 1977. 18 ELSEVIER SCIENCE BV DE557. [cited at p. 42]

[ada89] N. G. Adams, D. Smith, M. Tichy, G. Javahery, N. D. Twiddy, and E. E. Ferguson. An absolute proton affinity scale in the approximately $130 - 140$ *Kcal* mol^{-1} range. *Journal of Chemical Physics*, 91(7):4037–4042, 1989. [cited at p. 53, 54]

[apl00] Karen Aplin. *Instrumentation for atmospheric ion measurements*. PhD thesis, The University of Reading, 2000. [cited at p. 11]

[asv04a] O. Asvany, I. Savic, S. Schlemmer, and D. Gerlich. Variable temperature ion trap studies of $CH_4 + +H_2$, *HD* and D_2: negative temperature dependence and significant isotope effect. *Chemical Physics*, 298(1-3):97–105, 2004. [cited at p. 15, 19, 42, 43]

[atk02] P. Atkins and J. Paula. *Atkins' Physical Chemistry*, pages 222–251,502. Oxford University Press, 7th edition, 2002. [cited at p. 17, 65]

[bac94] IH Bachir, H. Bolvin, C. Demuynck, JL Destombes, and A. Zellagui. High-resolution optogalvanic spectrum of N_2^+ using a Ti: sapphire laser: the (2,0) vibration band of the meinel system $A^2\Pi_u - X^2\Sigma_g^+$. *Journal of molecular spectroscopy(Print)*, 166(1):88–96, 1994. [cited at p. 65]

[bah69] R. Bahr. Untersuchung der eigenschaften eines hochfrequenz-ionenspeichers. Master's thesis, Physicalisches Institut der Universität Freiburg, 1969. [cited at p. 14]

[bar84] S. E. Barlow, G. H. Dunn, and M. Schauer. Radiative association of c*h*3+ and *h*2 at 13 k. *Phys. Rev. Lett.*, 52(11):902–905, Mar 1984. [cited at p. 12]

[bar86] S. E. Barlow, J. A. Luine, and G. H. Dunn. Measurement of ion/molecule reactions between 10 and 20 K. *International Journal of Mass Spectrometry and Ion Processes*, 74(1):97–128, 1986. [cited at p. 12]

[ber94] J. Berkowitz, G. B. Ellison, and D. Gutman. Three methods to measure RH bond energies. *Journal of Physical Chemistry*, 98(11):2744–2765, 1994. [cited at p. 18, 41, 42, 44]

[ber98] DJ Berkeland, JD Miller, JC Bergquist, WM Itano, and DJ Wineland. Minimization of ion micromotion in a Paul trap. *Journal of Applied Physics*, 83:5025, 1998. [cited at p. 14]

[bie76] Veronica M. Bierbaum, C. H. DePuy, R. H. Shapiro, and John H. Stewart. Flowing afterglow studies of the reactions of hydroxide, amide, and methoxide ions with ethylene oxide and propylene oxide. *Journal of the American Chemical Society*, 98(14):4229–4235, 1976. [cited at p. 32, 33]

[blu89] R. Blümel, C. Kappler, W. Quint, and H. Walther. Chaos and order of laser-cooled ions in a paul trap. *Phys. Rev. A*, 40(2):808–823, Jul 1989. [cited at p. 12]

[boh80] D. K. Bohme, G. I. Mackay, and H. I. Schiff. Determination of proton affinities from the kinetics of proton-transfer reactions .7. The proton affinities of O_2, H_2, *Kr*, *O*, N_2, *Xe*, CO_2, CH_4, N_2O, and *CO*. *Journal of Chemical Physics*, 73(10):4976–4986, 1980. 42 AMER INST PHYSICS KU256. [cited at p. 53, 54]

[boh83] H Bohringer, W Glebe, and F Arnold. Temperature dependence of the mobility and association rate coefficient of He^+ ions in He from 30-350K. *Journal of Physics B: Atomic and Molecular Physics*, 16(14):2619–2626, 1983. [cited at p. 15]

[bol70] R. C. Bolden, R. S. Hemsworth, M. J. Shaw, and N. D. Twiddy. Measurements of thermal-energy ion-neutral reaction rate coefficients for rare-gas ions. *Journal of Physics B: Atomic and Molecular Physics*, 3(1):45–60, 1970. [cited at p. 32]

[bor08] G. Borodi. *On the combination of a Low Energy Hydrogen Atom Beam with a Cold Multipole Ion Trap*. PhD thesis, Chemnitz University of Technology, 2008. [cited at p. 15, 34]

[bor09] G. Borodi, A. Luca, and D. Gerlich. Reactions of CO_2^+ with H, H_2 and deuterated analogues. *International Journal of Mass Spectrometry*, 280(1-3):218–225, 2009. Ion-molecule and ion-surface interactions: A special issue honoring Zdenek Herman on the occasion of his 75th birthday. [cited at p. 12, 15]

[can01] R. Candori, S. Cavalli, F. Pirani, A. Volpi, D. Cappelletti, P. Tosi, and D. Bassi. Structure and charge transfer dynamics of the $(ar–n_2)^{+1}$ molecular cluster. *The Journal of Chemical Physics*, 115(19):8888–8898, 2001. [cited at p. 56, 57, 59]

[can03] R. Candori, F. Pirani, D. Cappelletti, P. Tosi, and D. Bassi. State-to-state cross-sections for $N_2^+(X, \nu' = 1, 2) + Ar$ and $Ar^+(^2P_{j,mj}) + N_2(X, \nu = 0)$ at low

energies. *International Journal of Mass Spectrometry*, 223-224:499–506, 2003. [cited at p. 56, 57, 59]

[dal60] N. R. Daly. Scintillation type mass spectrometer ion detector. *Review of Scientific Instruments*, 31(3):264–267, 1960. [cited at p. 27]

[daw76] P. H. Dawson. *Quadrupol Mass Spectrometry and its applications*. Elsevier Scientific Publishing, Amsterdam, 1976. [cited at p. 24, 25]

[dun90] R.C. Dunbar. Polyatomic ion-molecule radiative association: theoretical framework and predictions: observations of no+ + c6h5cn as an example. *International Journal of Mass Spectrometry and Ion Processes*, 100(C):423–443, 1990. cited By (since 1996) 37. [cited at p. 12]

[dyc70] V. Dyczmons, V. Staemmler, and W. Kutzelnigg. Near hartree-fock energy and equilibrium geometry of CH_5^+. *Chemical Physics Letters*, 5(6):361–366, 1970. [cited at p. 53]

[eas97a] A. L. L. East, B. J. Smith, and L. Radom. Entropies and free energies of protonation and proton-transfer reactions. *Journal of the American Chemical Society*, 119(38):9014–9020, 1997. [cited at p. 53]

[fed85] W. Federer, H. Villinger, P. Tosi, E. Fergusson, and W. Lindinger. *In Molecular Astrophysics - State of the Art and Future Directions*, chapter Laboratory studies of ion reactions with atomic hydrogen, pages 649–655. Reidel Publishing Company, 1985. [cited at p. 42, 43]

[fell06] B. Fellmuth, Ch. Gaiser, and J. Fischer. Determination of the boltzmann constant – status and prospects. *Measurement Science and Technology*, 17(10):R145–R159, 2006. [cited at p. 13]

[flo07] D. Flower. *Molecular collisions in the interstellar medium*, chapter Interstellar molecules. Cambridge Univ Pr, 2007. [cited at p. 17]

[gal01] G. A. Galazutdinov, F. A. Musaev, and J. Krelowski. On the detection of the linear C_5 molecule in the interstellar medium. *Monthly Notices of the Royal Astronomical Society*, 325(4):1332–1334, 2001. 16 BLACKWELL SCIENCE LTD 469CF. [cited at p. 53]

[ger05a] D. Gerlich. Probing the structure of CH_5^+ ions and deuterated variants via collisions. *Physical Chemistry Chemical Physics*, 7:1583–1591, 2005. [cited at p. 42, 43]

[ger08a] D. Gerlich. The Study of Cold Collisions Using Ion Guides and Traps. In Ian W. M. Smith, editor, *Low temperatures and cold molecules*, pages 121–174. Imperial College Press, UK, 2008. [cited at p. 12, 13, 15, 19, 23, 34, 63, 74]

[ger08b] D. Gerlich. The Production and Study of Ultra-Cold Molecular Ions. In Ian W. M. Smith, editor, *Low temperatures and cold molecules*, pages 324–326. Imperial College Press, UK, 2008. [cited at p. 11, 15, 56, 78]

[ger09] D. Gerlich, G. Borodi, A. Luca, and M. Smith. Reactions between cold hydrocarbon ions and slow hydrogen atoms. *Journal of Physical Chemistry*, 2009. [cited at p. 42]

[ger09a] D. Gerlich and G. Borodi. Buffer gas cooling of polyatomic ions in rf multielectrode traps. *Faraday Discussions*, 142:57–72, 2009. [cited at p. 16]

[ger92] D. Gerlich. Inhomogeneous rf-fields - A versatile tool for the study of processes with slow ions. *Advances in Chemical Physics*, 82:1–176, 1992. 190 JOHN WILEY & SONS INC Part 1 HW311. [cited at p. 12, 15, 23, 24, 26, 27, 30]

[ger92c] Dieter Gerlich and Stevan Horning. Experimental investigation of radiative association processes as related to interstellar chemistry. *Chemical Reviews*, 92(7):1509–1539, 1992. [cited at p. 12, 19]

[ger92d] D. Gerlich. Ion trap studies of ternary and radiative association processes. In *Nuclear Physics Concepts in the Study of Atomic Cluster Physics*, volume 404, pages 194–200. Springer, 1992. [cited at p. 32]

[ger93] D. Gerlich. Experimental investigations of ion-molecule reactions relevant to interstellar chemistry. *Journal of the Chemical Society, Faraday Transactions*, 89(13):2199–2208, 1993. [cited at p. 15, 64]

[ger94] D. Gerlich. Recent progress in experimental studies of ion-molecule reactions relevant to interstellar chemistry. In *Physical Chemistry of molecules and grains in space - 50th International Meeting of Physical Chemistry*, Mont Ste-Odile, Strasbourg, 1994. [cited at p. 26]

[ger94a] D. Gerlich. Recent progress in experimental studies of ion-molecule reactions relevant to interstellar chemistry. In Nenner I., editor, *Molecules and Grains in Space*, pages 489–500. AIP Press, New York, 1994. [cited at p. 16]

[ger95] D. Gerlich. Ion-neutral collisions in a 22-pole trap at very low energies. *Physica Script.*, T59:256–263, 1995. [cited at p. 12, 19, 29]

[gio58] George Gioumousis and D. P. Stevenson. Reactions of gaseous molecule ions with gaseous molecules. v. theory. *The Journal of Chemical Physics*, 29(2):294–299, 1958. [cited at p. 61]

[gis92] E. A. Gislason. The Semiclassical Time-Dependent Approach to Charge-Transfer Processes. In C. Y. Ng and M. Baer, editors, *State-Selected and State-to-State Ion-Molecule Reaction Dynamics: Part 2. Theory*, page 321. Wiley, New York, 1992. [cited at p. 56]

[glo06a] S. C. O. Glover and T. Abel. Uncertainties in H_2 and HD chemistry and cooling and their role in early structure formation. *Monthly Notices of the Royal Astronomical Society*, 388(4):1627–1651, 2008. [cited at p. 11]

[glo06b] S. C. Glover, D. W. Savin, , and A. K. Jappsen. Cosmological Implications of the Uncertainty in H- Destruction Rate Coefficients. *The Astrophysical Journal*, 640(2):553–568, 2006. [cited at p. 11]

[gov84] Thomas R. Govers, Paul Marie Guyon, Thomas Baer, Keith Cole, Horst Fröhlich, and Michel Lavollée. State-selected ion-molecule reactions: $N_2^+(X, \nu'')$, $N_2^+(A, \nu')$ + Ar $\rightarrow$ N_2 + Ar^+. *Chemical Physics*, 87(3):373–387, 1984. [cited at p. 56, 58]

[haw89] M. Hawley and M. A. Smith. Chemical-reaction mechanisms at unusually low-temperatures - The gas-phase reaction of $C_2H_2^+ + H_2$. *Journal of the American Chemical Society*, 111(21):8293–8294, 1989. [cited at p. 42]

[hem73] Hemswort.Rs, H. W. Rundle, D. K. Bohme, H. I. Schiff, D. B. Dunkin, and Fehsenfe.Fc. Determination of proton affinity from kinetics of proton-transfer reactions .3. Measurement of equilibrium constant at various temperatures. *Journal of Chemical Physics*, 59(1):61–69, 1973. 18 AMER INST PHYSICS Q2644. [cited at p. 42, 52, 53, 54]

[hes90] B. Andes Hess and Rudolf Zahradnik. Theoretical study of reactivity of methane, methyl fluoride, and methyl chloride: interaction with their radical cations and proton donors. *Journal of the American Chemical Society*, 112(15):5731–5735, 1990. [cited at p. 54]

[hun98] E. P. L. Hunter and S. G. Lias. Evaluated gas phase basicities and proton affinities of molecules: An update. *Journal of Physical and Chemical Reference Data*, 27(3):413–656, 1998. 73 AMER CHEMICAL SOC ZW486. [cited at p. 18, 41, 42, 43, 45, 53, 87]

[joh06] Russell D. Johnson III. NIST Computational Chemistry Comparison and Benchmark Database. *NIST Standard Reference Database Number 101, Release 14*, Sept 2006. http://srdata.nist.gov/cccbdb. [cited at p. 58]

[kat82] Tatsuhisa Kato, Kenichiro Tanaka, and Inosuke Koyano. State selected ion–molecule reactions by a TESICO technique. V. $N_2^+(\nu)$ + Ar $\rightarrow$ N_2 + Ar^+. *The Journal of Chemical Physics*, 77(2):834–838, 1982. [cited at p. 58]

[kat95] Shuji Kato, Veronica M. Bierbaum, and Stephen R. Leone. Laser fluorescence and mass spectrometric measurements of vibrational relaxation of $N_2^+(\nu)$ with He, Ne, Ar, Kr, and Xe. *International Journal of Mass Spectrometry and Ion Processes*, 149-150:469–486, 1995. Honour Biography David Smith. [cited at p. 60]

[kim75] J. K. Kim, L. P. Theard, and W. T. Huntress. ICR studies of some hydrogen-atom abstraction reactions: $X^+ + H_2 \rightarrow XH^+ + H$. *Journal of Chemical Physics*, 62(1):45–52, 1975. 33AMER INST PHYSICS V3731. [cited at p. 42]

[kle06] William Klemperer. Interstellar chemistry. *Proceedings of the National Academy of Sciences*, 103(33):12232–12234, 2006. [cited at p. 17]

[kom92] Andrew Komornicki and David A. Dixon. Accurate proton affinities: Ab initio proton binding energies for N_2, CO, CO_2, and CH_4. *The Journal of Chemical Physics*, 97(2):1087–1094, 1992. [cited at p. 54]

[kre05] H Kreckel, J Mikosch, R Wester, J Glosik, R Plasil, M Motsch, D Gerlich, D Schwalm, D Zajfman, and A Wolf. Towards state selective measurements of the h3+ dissociative recombination rate coefficient. *Journal of Physics: Conference Series*, 4:126–133, 2005. [cited at p. 12]

[lia86] C. L. Liao, R. Xu, and C. Y. Ng. Fine structure effect on the charge transfer reaction of $Ar^+(^2P_{3/2,1/2})$ + $N_2(\tilde{X}^1\Sigma_g^+, \nu = 0)$. *The Journal of Chemical Physics*, 84(3):1948–1950, 1986. [cited at p. 58]

[lid03] David R. Lide. *CRC Handbook of Chemistry and Physics, 84th Edition*. CRC, June 2003. [cited at p. 35, 43]

[lin04] V Linss, H Kupfer, S Peter, and F Richter. Two $N_2^+(B^2\Sigma_u^+)$ populations with different Boltzmann distribution of the rotational levels found in different types of N_2/Ar discharges–improved estimation of the neutral gas temperature. *Journal of Physics D: Applied Physics*, 37(14):1935–1944, 2004. [cited at p. 11, 56, 67]

[lin05] P. J. Linstrom and Eds. W.G. mallard, editors. *NIST Chemistry WebBook, NIST Standard Reference database*. 69. National Institute of Standards and Technology, Gaithersburg MD, 20899, June 2005. (http://webbook.nist.gov). [cited at p. 32, 54, 65, 67]

[lin81] W. Lindinger, F. Howorka, P. Lukac, S. Kuhn, H. Villinger, E. Alge, and H. Ramler. Charge transfer of $Ar^+ + N_2 \rightleftarrows N_2^+ + Ar$ at near thermal energies. *Phys. Rev. A*, 23(5):2319–2326, May 1981. [cited at p. 58, 59, 60, 61, 62, 75, 76]

[luc01] A. Luca, S. Schlemmer, I. Cermak, and D. Gerlich. On the combination of a linear field free trap with a time-of-flight mass spectrometer. *Review of Scientific Instruments*, 72(7):2900–2908, 2001. [cited at p. 27]

[luc05] A. Luca, G. Borodi, and D. Gerlich. Interactions of ions with hydrogen atoms. In FD Colavecchia, PD Fainstein, J Fiol, MAP Lima, JE Miraglia, EC Montenegro, and RD. Rivarola, editors, *Progress report in XXIV ICPEAC 2005*, Rosario, Argentina,, July 2005. ICPEAC 2005. [cited at p. 15, 42, 43]

[lui85] J. A. Luine and G. H. Dunn. Ion-molecule reaction probabilities near 10 K. *Astrophysical Journal*, 299:L67–L70, December 1985. [cited at p. 12, 19]

[mar89] R. E. March and R. J. Hughes. *Quadrupole Storage Mass Spectrometry*. John Wiley, New York, 1989. [cited at p. 24]

[mar98] Christopher L. Hendrickson George S. Jackson Alan G. Marshall. Fourier transform ion cyclotron resonance mass spectrometry: A primer. *Mass Spectrometry Reviews*, 17(1):1–35, 1998. [cited at p. 12, 19]

[mau78] G. Mauclaire, R. Derai, and R. Marx. ICR determination of kinetically excited ions produced in water and methane by charge transfer from thermal rare gas ions. *International Journal or Mass Spectrometry and Ion Physics*, 26(3):289–301, 1978. [cited at p. 68]

[mce89] M.J. McEwan, A.B. Denison, W.T. Huntress, Anicich V.G., J. Snodgrass, and M.T. Bowers. Association reactions at low pressure. 2. The CH_3^+/CH_3CN system. *Journal of Physical Chemistry*, 93(10):4064–4068, 1989. cited By (since 1996) 8. [cited at p. 12]

[meh09] T. Mehner. Experimente mit und an kalten atomstrahlen. Master's thesis, Technische Universität Chemnitz, 2009. [cited at p. 19, 64]

[meo07] M. Meot-Ner and A. Somogyi. A thermal extrapolation method for the effective temperatures and internal energies of activated ions. *International Journal of Mass Spectrometry*, 267(1-3):346–356, 2007. Meot-Ner, Michael (Mautner) Somogyi, Arpad 62 ELSEVIER SCIENCE BV 224UY. [cited at p. 53]

[meo77] M. Meot-Ner and F. H. Field. Proton affinities and cluster ion stabilities in CO_2 and CS_2 - Applications in martian ionospheric chemistry. *Journal of Chemical Physics*, 66(10):4527–4531, 1977. 10 AMER INST PHYSICS DG114. [cited at p. 44, 52, 53]

[mik06] J. Mikosch, U. Frühling, S. Trippel, D. Schwalm, M. Weidemüller, and R. Wester. Velocity map imaging of ion-molecule reactive scattering: The $Ar^+ + N_2$ charge transfer reaction. *Physical Chemistry Chemical Physics*, 8(25):2990–2999, 2006. [cited at p. 56, 63]

[moh05] Peter J. Mohr and Barry N. Taylor. Codata recommended values of the fundamental physical constants: 2002. *Rev. Mod. Phys.*, 77(1):1–107, Mar 2005. [cited at p. 13]

[mun63] M. S. B. Munson, J. L. Franklin, and F. H. Field. Reactions of gaseous ions .13. System methane-hydrogen. *Journal of the American Chemical Society*, 85(22):3584, 1963. 10 AMER CHEMICAL SOC 3110B. [cited at p. 42]

[ng92] C. Y. Ng. State-Selected and State-to-State Ion-Molecular Reaction Dynamics by Photoionization and Differential Reactivity Methods. In C. Y. Ng and M. Baer, editors, *Advances in Chemical Physics: State-Selected and State-To-State Ion-Molecule Reaction Dynamics, Part 1. Experiment*, page 401. Wiley, New York, 1992. [cited at p. 56, 57]

[nor66] R. B. Norton, E. E. Ferguson, F. C. Fehsenfeld, and A. L. Schmeltekopf. Ion-neutral reactions in the martian ionosphere. *Planetary and Space Science*, 14(10):969–978, 1966. [cited at p. 12]

[par88] Gérard Parlant and Eric A. Gislason. Theoretical state-to-state inelastic cross sections for collisions of $Ar^+(^2P_{3/2},^2P_{1/2})$ with N_2. *The Journal of Chemical Physics*, 88(3):1633–1637, 1988. [cited at p. 58]

[par89] Gérard Parlant and Eric A. Gislason. Theoretical state-to-state cross sections for collisions of $N_2^+(\nu)$ + Ar. II. Results at higher energies. *The Journal of Chemical Physics*, 91(9):5359–5364, 1989. [cited at p. 58]

[pau53] W. Paul and H. Steinwedel. A new mass spectrometer without magnetic field. *Zeitschrift für Naturforschung*, pages 448–450, 1953. [cited at p. 19]

[pau88] H. Pauly. *Other low-energy beam sources*, volume 1. G. Scoles, 1988. [cited at p. 35]

[pau93] W. Paul and D. Gerlich. Temperature of trapped ions mesured with spectroscopic methods. In T. Anderson *et al.*, editor, *ICPEAC 1993, Book of Contributed Papers*, pages 807–808, 1993. [cited at p. 16]

[pau94] W. Pauli and D. Gerlich. The problem of cooling ions in a low density ion trap. In R. Schrittwieser T. Märk and D. Smith, editors, *Symposium on Atomic, Cluster and Surface Physics*, 1994. [cited at p. 14, 16, 18]

[pop87] John A. Pople and Larry A. Curtiss. Theoretical thermochemistry. 2. Ionization energies and proton affinities of AHn species (A = C to F and Si to Cl); heats of formation of their cations. *The Journal of Physical Chemistry*, 91(1):155–162, 1987. [cited at p. 54]

[reb89] C. Rebrion, B. R. Rowe, and J. B. Marquette. Reactions of Ar^+ with H_2, N_2, O_2, and CO at 20, 30, and 70 K. *The Journal of Chemical Physics*, 91(10):6142–6147, 1989. [cited at p. 56, 63, 64, 74]

[rot06] B. Roth, P. Blythe, H. Wenz, H. Daerr, and S. Schiller. Ion-neutral chemical reactions between ultracold localized ions and neutral molecules with single-particle resolution. *Physical Review A (Atomic, Molecular, and Optical Physics)*, 73(4):042712, 2006. [cited at p. 13]

[row08] B. R. Rowe. Low Temperature Reactions involving Neutral and Charged Species. In Ian W. M. Smith, editor, *Low temperatures and cold molecules*. Imperial College Press, UK, 2008. [cited at p. 14]

[row85] B. R. Rowe, J. B. Marquette, G. Dupeyrat, and E. E. Ferguson. Reactions of He^+ and N^+ ions with several molecules at 8 K. *Chemical Physics Letters*, 113(4):403–406, 1985. [cited at p. 32, 33]

[row87] B. R. Rowe and J. B. Marquette. Cresu studies of ion/molecule reactions. *International Journal of Mass Spectrometry and Ion Processes*, 80:239–254, 1987. [cited at p. 12]

[sav05b] I. Savic and D. Gerlich. Temperature variable ion trap studies of $C_3H_n^+$ with H_2 and *HD*. *Phys . Chem. Chem. Phys .*, 7:1026–1035, 2005. [cited at p. 19]

[sch00] J. P. Schiffer, M. Drewsen, J. S. Hangst, and L. Hornekær. Temperature, ordering, and equilibrium with time-dependent confining forces. *Proceedings of the National Academy of Sciences of the United States of America*, 97(20):10697–10700, 2000. [cited at p. 13]

[sch05] Schlemmer S., Asvany O., Hugo E., and Gerlich. Deuterium fractionation and ion-molecule reaction at low temperatures. In Blake GA Herbst E. Lis DC, editor, *Proceedings IAU Symp.*, pages 125–134, 2005. [cited at p. 12]

[sch99] S. Schlemmer, T. Kuhn, E. Lescop, and D. Gerlich. Laser excited N_2^+ in a 22-pole ion trap: Experimental studies of rotational relaxation processes. *International Journal of Mass Spectrometry*, 185-187:589–602, 1999. [cited at p. 11, 16, 56, 57, 58, 60, 78]

[scu91] R. Schultz and P. Armentrout. The charge-transfer reaction $N_2^+(X, \nu = 0) + Ar \rightarrow Ar^+ + N_2$ from thermal to 20 eV c.m. *Chemical Physics Letters*, 179(5-6):429–434, 1991. 51 ELSEVIER SCIENCE BV FL741. [cited at p. 58, 61]

[sha87] J.-D. Shao, Y.-G. Li, G. D. Flesch, and C. Y. Ng. Absolute state-to-state total cross sections for the reactions $N_2^+(\tilde{X}, \nu = 0-2)$+Ar($^1S_0$) $\rightarrow N_2(X, \nu)$+ $Ar^+(^2P_{3/2,1/2})$. *The Journal of Chemical Physics*, 86(1):170–175, 1987. [cited at p. 58]

[sin89] D Singy, P Schmelzbach, W Gruebler, and W Zhang. Production of intense polarized hydrogen atomic-beams by cooling the atoms to low-temperature. *Nuclear Instruments & Methods in Physics Research Section A*, 278(2):349–367, Jun 1 1989. [cited at p. 35]

[smi81] D. Smith and N. G. Adams. Charge-transfer reaction $Ar^+ + N_2 \rightleftarrows N_2^+ + Ar$ at thermal energies. *Phys. Rev. A*, 23(5):2327–2330, May 1981. [cited at p. 56, 57, 59, 60, 62, 63, 64, 74, 76]

[smi94] M. A. Smith. Ion Molecule Reaction Dynamics at Very Low Temperatures. In M. Baer C. Y. Ng and I. Powis, editors, *Unimolecular and Bimolecular Reacrion Dynantics*, pages 182–251. Wiley, New York, 1994. [cited at p. 12, 56, 57, 63, 64, 74]

[smi98] Smith M. A. Low-temperature rate studies of ions and radicals in supersonic flows. *International Reviews in Physical Chemistry*, 17:35–63(29), 1 January 1998. [cited at p. 12]

[szu93] J. E. Szulejko and T. B. McMahon. Progress toward an absolute gas-phase proton affinity scale. *Journal of the American Chemical Society*, 115(17):7839–7848, 1993. [cited at p. 43, 44, 52, 53, 54]

[tho11] J. J. Thomson. Rays of positive electricity. *Philos. Mag.*, 21, 1911. [cited at p. 11]

[tie05] A. Tielens. *The physics and chemistry of the interstellar medium*, chapter The galactic ecosystem, pages 1–24. Cambridge Univ Pr, 2005. [cited at p. 17]

[tos92] Paolo Tosi, Oleg Dmitrijev, and Davide Bassi. The charge transfer reaction Ar^++$N_2 \rightarrow N_2^+$ + Ar. Crossed-beam measurements of the integral cross

section as a function of the collision energy. *Chemical Physics Letters*, 200(5):483 – 487, 1992. [cited at p. 58]

[tra91] J. Traeger and M. Kompe. Determination of the proton affinity of carbon dioxide by photoionization mass spectrometry. *Organic mass spectrometry*, 26(4):209–214, 1991. [cited at p. 54]

[tro09] N. Troscompt, A. Faure, S. Maret, C. Ceccarelli, P. Hily-Blant, and L. Wiesenfeld. Constraining the ortho-to-para ratio of H_2 with anomalous H_2CO absorption. *Astronomy and Astrophysics*, 506:1243–1247, November 2009. [cited at p. 17]

[ved91] Fernande Vedel. On the dynamics and energy of ion clouds stored in an r.f. quadrupole trap. *International Journal of Mass Spectrometry and Ion Processes*, 106:33–61, 1991. [cited at p. 12]

[vig93] A. Viggiano and A. Morris. Rate constants for the reaction of $Ar^+(^2P_{3/2})$ with N_2 as a function of N_2 vibrational temperature and energy level. *J. Chem. Phys.*, 99:3526–3530, 1993. [cited at p. 56, 62, 63, 64, 74]

[wal80] R. Walder and J. L. Franklin. Proton affinities of neutral molecules. *Int. J. of Mass Spectrometry and Ion Processes*, 36(1):85–112, 1980. [cited at p. 42, 43]

[wan05] B. S. Wang and H. Hou. Computational study of the ion-molecule reactions involving fluxional cations: $CH_4^+ + H_2 \rightarrow CH_5^+ + H$ and isotope effect. *Journal of Physical Chemistry A*, 109(38):8537–8547, 2005. 56 AMER CHEMICAL SOC 967WG. [cited at p. 42, 43]

[wan05b] Xue-Bin Wang, Hin-Koon Woo, and Lai-Sheng Wang. Vibrational cooling in a cold ion trap: Vibrationally resolved photoelectron spectroscopy of cold c[sub 60][sup -] anions. *The Journal of Chemical Physics*, 123(5):051106, 2005. [cited at p. 15]

[wic94] O. Wick. *Untersuchung von Ionen-Molekülreaktionen bei extrem niedrigen Energien mit zustandsselektiv präparierten Reaktanden*. PhD thesis, Alert-Ludwigs-Universität Freiburg, 1994. [cited at p. 56, 57, 63, 64]

[woo07] J. Woodall, M. Agúndez, A. J. Markwick-Kemper, and T. J. Millar. The UMIST database for astrochemistry 2007. http://www.udfa.net, 2007. [cited at p. 32, 45, 50, 68]

[zar98] Richard N. Zare. Laser Control of Chemical Reactions. *Science*, 279(5358):1875–1879, 1998. [cited at p. 57]

List of publications and conference contributions

C. Mogo, D. Gerlich, M. Smith, *Measurements of the* $(Ar - N_2)^+$ *system in a 22PT*, article in preparation

G. Borodi, C. Mogo, D. Gerlich, *Reactions of ions with H or D atoms under interstellar conditions*, Poster, TU-Chemnitz 2008, Germany

G. Borodi, D. Kunte, C. Mogo, D. Gerlich *ITS LEIF: Ion Technology and Spectroscopy at Low Energy Ion Beam Facilities*, Poster, TU-Chemnitz 2008, Germany

C. Mogo, S. Decker, D. Gerlich *Experimental determination of thermochemical data in temperature variable ion traps*, Poster, TU-Chemnitz 2008, Germany

G. Borodi, A. Luca, C. Mogo, D. Gerlich, *Combination of a cold rf-ion trap with a slow H atom beam for investigating ion-atom collisions*, Poster, Symposium organized by the FOR 388, Schloss Hotel Pillnitz, Dresden June 2005, Germany

A. Luca, G. Borodi, C. Mogo, D. Gerlich, *Reactions of small hydrocarbon ions* CH_n^+ *with H and D atoms at low temperatures*, Poster, Symposium organized by the FOR 388, Schloss Hotel Pillnitz, Dresden June 2005, Germany

J. Brandão, C. Mogo, and B. C. Silva, *Potential energy surface for H2O(3A") from accurate ab initio data with inclusion of long-range interactions*, Poster, Molec XV - International Conference on Dynamics of Molecular Systems, Conference Center Dennenhoeve, September 5/10 2004, Nunspeet, The Netherlands

J. Brandão, C. Mogo, B. C. Silva, *Potential energy surface for H2O(3A") from accurate ab initio data with inclusion of long-range interactions*, J. Chem. Phys. 121 (2004) 8861.

J. Brandão, C. Mogo, B. C. Silva *Dynamic calculations on a* H_2O *surface*, Poster, Coimbra's 2004 - 2th Portuguese Conference on Chemical Physics, Universidade de Coimbra, June 26/27 2004, Coimbra, Portugal

Selbstständigkeitserklärung

Ich erkläre, dass ich die vorliegende Arbeit selbstständig und nur unter Verwendung der angegebenen Literatur und Hilfsmittel angefertigt habe.
Ich erkläre, nicht bereits früher oder gleichzeitig bei anderen Hochschulen oder an dieser Universität ein Promotionsverfahren beantragt zu haben.
Falls diese Erklärung nicht zutrifft, füge ich eine Stellungnahme diesem Antrag bei. Ich erkläre, obige Angaben wahrheitsgemäß gemacht zu haben und erkenne die Promotionsordnung der Fakultät für Naturwissenschaften der Technischen Universität Chemnitz vom 03.12.2010 an.

César Mogo

Curriculum Vitae

Personal

name:	César Mogo
birth date :	31.01.1976
place:	Faro, Portugal
Citizenship:	Portuguese

Education

School:	1993 - 1996	High school Escola Sec. Fonseca Benevides Lisbon
University:	1996 - 2003	Degree in physical engeneering Universidade do Algarve, Portugal
	Feb. 2003	Diploma thesis: ”Brain lesions volume measurements by method of discreet integration”
Traineeships:	2003 - 2004	Environmental Chemistry Multidiscilinary Center (CMQA) University of Algarve
PhD studies:	2004 - 2009	Ion trap studies in the group of D. Gerlich Chemnitz, Germany

Acknowledgements

At this point I would like to express my gratitude to some of the people who have contributed to the results of this dissertation.
Thanks to Dr. Alfonz Luca for his invitation and initial support.
Prof. Dr. Dieter Gerlich for conceding me the opportunity to study in Germany and introducing me to this field of research. Dr. Gheorghe Borodi, with whom I shared a lot of good discussions.
Thanks to engineers Doreen Kunte, Angelika Hiller and Gunter Vales for the excellent technical support and good atmosphere.
Dr. Radek Plasil for his support in the last writing stages.
Thanks to the administrative personal, namely Ivonne Schubert and Annet Kurasch.
I also would like to thank the present and some of the former group members, namely Silvio Decker, Mirko Kämpf, and Thomas Mehner and for their help and support, as for the enlightening discussions.
To Dr. Hans Jörgen Deyerl which gave a big contribute to the writting of the proton affinity chapter.
Financial support by the Deutsche Forschungsgemeinschaft (DFG), as well from the ITS LEIF project, is gratefully acknowledged.
On a personal level, I would like to thank Nadine Steinhardt, for bearing with me since the beginning of this adventure, I owe you a BIG dinner!
Finally, I would like to thank someone, who was able to bring me the warmth of the African Sun in to the middle of Germany, Cynthia Kazi.